IMPROVEMENT IN EFFECTIVENESS OF DIAMOND AS REINFORCEMENT IN STRENGTHENING THE POROUS ALUMINIUM COMPOSITE

BY

BISMA PARVEEZ

A thesis submitted in fulfilment of the requirement for the degree of Doctor of Philosophy (Engineering)

Kulliyyah of Engineering
International Islamic University Malaysia

MARCH 2024

ABSTRACT

The growing demand for lightweight structures in automotive and aerospace fields has attracted enormous attention to further reduction in weight of aluminium (Al) alloys and composites, that are mostly preferred for such applications. This urge resulted in the development of porous Al. Porous Al is a lightweight material that inherits high strength and stiffness to weight ratio, energy saving and excellent impact energy absorption during collision. However, these are often associated with low density resulting in low mechanical and thermal performance, which might limit its efficiency, design flexibility as well as potential applications. The aim of this research is to improve the strength of porous Al by the inclusion of alloying elements and Ti-coated diamond particles as reinforcements. In this study the powder metallurgy technique was applied due to its near net shape production, flexibility in terms of constituent addition and material conservation capabilities. The alloying elements such as magnesium (Mg), copper (Cu), boron (B), and tin (Sn) were added to the Al matrix to strengthen it and further reinforced with titanium (Ti)-coated diamond particles. The porosities in such composites were achieved by using polymethylmethacrylate (PMMA) particles as space holders. The porous Al composites were developed at varying processing parameters such as sintering temperature, compaction pressure, and sintering time, followed by varying Ti-coated diamond content, PMMA particle content, and PMMA particle size. Further, the compressive properties (plateau strength, and energy absorption capacity) of the resultant porous Al composites were optimized using experimental methodology, Design of experiments (L_9 orthogonal array) as well as statistical methodology, analysis of variance (ANOVA). Finally based on the optimum process parameters, PMMA content and PMMA particle size, the porous Al composite with various content (0, 6, 9, 12, 15 and 20 wt.%) of uncoated and Ti-coated diamond particles were studied. Thus, the optimum content of diamond required to enhance the performance of porous Al composite was evaluated. The microstructure of the resultant porous Al composite revealed that the PMMA space holders contributed to well-defined macro pores with good interfacial integrity. In addition to this, the XRD analysis confirmed the presence of strengthening phases as a result of addition of alloying elements. Additionally, Ti-coating improved the interfacial bonding of diamond particles with Al alloy matrix. The results of parameters optimization revealed that the sintering temperature significantly impacted the compressive properties, and the maximum values could be achieved at sintering temperature of 590°C, compaction pressure of 350 MPa, and sintering time of 90 min. On the other hand, the compositional optimization revealed that the diamond content had a major impact on the compressive properties and the enhanced values could be achieved at diamond content of 12 wt. %, PMMA particle size of 150 μm, and PMMA content of 25 wt. %. The stress strain curves also showed a significant improvement in the compressive properties with nearly ductile behavior. Moreover, the maximum values of plateau strength and energy absorption capacity in the range of (40-45 MPa) and (11.20-13.68 MJ/m^3) respectively were achieved for porous composite reinforced with 9-12 wt.% of Ti-coated diamond particles. The results reflected an increment of 61-82% in plateau strength and 54-88% in energy absorption capacity as compared to the unreinforced porous Al. This shows a significant improvement in the strength and energy absorption capacity of porous Al composites on addition of Ti-coated diamond as a reinforcement. This material can be potentially applied as cores material in the sandwich structures to lighten the weight of structures without compromising their strength especially in automotives and aerospace applications.

خلاصة البحث

وقد جذب الطلب المتزايد على الهياكل خفيفة الوزن في مجالات السيارات والفضاء اهتماما هائلا لمزيد من الانخفاض في وزن سبائك الألومنيوم)أل (والمواد المركبة، التي يفضل معظمها لمثل هذه التطبيقات .نتج عن هذه الرغبة تطوير آل مسامي .المسامية آل هي مادة خفيفة الوزن ترث قوة عالية وصلابة لنسبة الوزن، وتوفير الطاقة وممتازة امتصاص الطاقة تأثير أثناء الاصطدام .ومع ذلك، غالبًا ما ترتبط هذه مع انخفاض الكثافة مما يؤدي إلى .انخفاض الأداء الميكانيكي والحراري، مما قد يحد من كفاءتها ومرونة التصميم بالإضافة إلى التطبيقات المحتملة الهدف من هذا البحث هو تحسين قوة ال المسامية عن طريق إدراج عناصر السبائك وجزيئات الماس المغلفة بالتي كتعزيزات .في هذه الدراسة تم تطبيق تقنية تعدين المسحوق بسبب إنتاجها شبه الصافي للشكل والمرونة من حيث البورون ،(Cu) النحاس ،(Mg) إضافة المكونات وقدرات الحفاظ على المواد .العناصر السبائكية مثل المغنيسيوم .(Ti) لتقويتها وزيادة تعزيزها بجزيئات الماس المغلفة بالتيتانيوم Al إلى المصفوفة (Sn) وأضيف القصدير ,(B) .كحاملات للفضاء (PMMA) تم تحقيق المسامية في مثل هذه المركبات باستخدام جزيئات بولي ميثيل ميثاكريلات ،تم تطوير مركبات آل المسامية عند معلمات معالجة مختلفة مثل درجة حرارة التلبيد وضغط الضغط ووقت التلبيد .PMMA و ,وحجم الجسيمات ،PMMA ومحتوى الجسيمات ،Ti تليها محتوى الماس المتفاوت المغلف بـ وعلاوة على ذلك، تم تحسين خصائص الضغط)قوة الصفيحة، وقدرة امتصاص الطاقة (من المركبات آل التي وكذلك المنهجية (L9 صفيف متعامد) يسهل اختراقها الناتجة باستخدام منهجية تجريبية ,تصميم التجارب وأخيرا استنادا إلى معلمات العملية المثلى، ومحتوى بمما وحجم .(ANOVA) الإحصائية، وتحليل التباين الجسيمات بمما، مركب آل مسامي مع محتوى مختلف)0 و 6 و 9 و 12 و 15 و 20 واط% . تمت دراسة جزيئات .المغلفة .وهكذا، تم تقييم المحتوى الأمثل للماس اللازم لتعزيز أداء المركب المسامي Ti الماس غير المغلفة و ساهموا في وجود مسامٍ كلية PMMA كشفت البنية المجهرية لمركب آل المسامي الناتج عن ذلك أن حاملي فضاء وجود أطوار التقوية نتيجة إضافة عناصر XRD محددة جيدًا مع سلامة بينية جيدة .بالإضافة إلى ذلك، أكد تحليل .Al السبائك .بالإضافة إلى ذلك، أدى طلاء تي إلى تحسين الترابط البيني لجزيئات الماس مع مصفوفة سبائك كشفت نتائج تحسين المعلمات أن درجة حرارة التلبيد أثرت بشكل كبير على خصائص الضغط، ويمكن تحقيق القيم ،ضغط ضغط 350 ميجا باسكال ,ووقت تلبيد 90 دقيقة .من ناحية أخرى ،°Cالقصوى عند درجة حرارة تلبد 590 كشف التحسين التركيبي أن محتوى الماس كان له تأثير كبير على خصائص الضغط ويمكن تحقيق القيم المحسنة .% .في محتوى الماس من 12 واط ,% .حجم الجسيمات بمما من 150 ميكرون، ومحتوى بمما من 25 واط أظهرت منحنيات إجهاد الإجهاد أيضًا تحسنًا كبيرًا في خصائص الانضغاط مع سلوك الدكتايل تقريبًا .علاوة على ذلك، فإن القيم القصوى لقوة الهضبة وقدرة امتصاص الطاقة في نطاق)40-45 ميجا باسكال (و)11.20-13.68 على التوالي تم تحقيقها للمركب المسامي المقوى بـ 9-12 واط %.من جزيئات الماس المغلفة بـ (m3/ميجا جول عكست النتائج زيادة بنسبة 61-82 %في قوة الهضبة و 54-88 %في قدرة امتصاص الطاقة بالمقارنة مع .Ti آل المسامي غير المقوى

APPROVAL PAGE

The thesis of Bisma Parveez has been approved by the following:

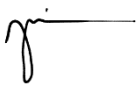

Nur Ayuni Jamal
Supervisor

Md. Abdul Maleque
Chairman Supervisor

Prof. Ir. Dr. Zuraida Bt. Ahmad
Internal Examiner

Prof. Dr. Md. Md Mustafizur Rahman
External Examiner

Prof. Dr. Akram M Z M Khedher
Chairman

DECLARATION

I hereby declare that this thesis is the result of my own investigations, except where otherwise stated. I also declare that it has not been previously or concurrently submitted as a whole for any other degrees at IIUM or other institutions.

Bisma Parveez

Signature ..... Bisma ..... Date .....26/02/2024.....

INTERNATIONAL ISLAMIC UNIVERSITY MALAYSIA

DECLARATION OF COPYRIGHT AND AFFIRMATION OF FAIR USE OF UNPUBLISHED RESEARCH

INVESTIGATION OF COMPRESSIVE PROPERTIES OF DIAMOND REINFORCED POROUS ALUMINIUM COMPOSITE BY PARAMETRIC AND COMPOSITIONAL OPTIMIZATION

I declare that the copyright holders of this thesis are jointly owned by the student and IIUM.

No part of this unpublished research may be reproduced, stored in a retrieval system, or transmitted, in any form or by any means, electronic, mechanical, photocopying, recording or otherwise without prior written permission of the copyright holder except as provided below

1. Any material contained in or derived from this unpublished research may be used by others in their writing with due acknowledgement.

2. IIUM or its library will have the right to make and transmit copies (print or electronic) for institutional and academic purposes.

3. The IIUM library will have the right to make, store in a retrieved system and supply copies of this unpublished research if requested by other universities and research libraries.

By signing this form, I acknowledged that I have read and understand the IIUM Intellectual Property Right and Commercialization policy.

Affirmed by Bisma Parveez

Bisma

…….. ……..26/02/2024……

Signature Date

To Almighty Allah for his bountiful favors upon me; and to my beloved parents and family, for their endless love, support, and encouragement

AKNOWLEDGEMENTS

In the Name of Allah, the Most Compassionate, the Most Merciful

Allah - beginning with the name of the Most Gracious, the Most Merciful Most Auspicious is he in whose control is the entire kingship; and he is able to do all things [67:1]. All Praise to Allah, the Lord of the creation, and countless blessings and peace upon our Master Mohammed (PBUH).

I am most indebted to my supervisor, Asst. Prof. Dr, Ayuni Jamal whose enduring disposition, kindness, promptitude, thoroughness and friendship have facilitated the successful completion of my work. Her brilliant grasp of the aim and content of this work led to his insightful comments, suggestions and queries which helped me a great deal. Despite her commitments, she took time to listen and attend to me whenever requested. The moral support she extended to me is in no doubt a boost that helped in building and writing the draft of this research work. I am also grateful to my chairman supervisor, Prof. Dr. Md Abdul Maleque, whose support and cooperation contributed to the outcome of this work. He was always there to solve any problem I faced in my research. I also want to extend my thanks to my co-supervisors Asst. Prof. Dr. Ahmad Zahirani Ahmad Azhar and Asst. Prof. Dr. Hafizah Hanim Mohd Zaki and field supervisor, Assoc. Prof. Dr. Farazila Yosuf for their support and guidance during my study period. Similar appreciation is extended to all the academic staff especially Prof. Dr. Sher Khan, Ex staff Prof. Dr. Abdi O. Shuriye and technical stall of International Islamic University Malaysia for their support and affections towards me throughout my programme in the department.

I also express my appreciation to the Research Management Center sand center for postgraduate studies, International Islamic university for their support in providing funds through research grants and scholarship. It is a great pleasure to express my sincere thanks and gratitude to my fellow friends who supported me and encouraged me to complete my experimental work and thesis. A special thanks to my dear friends Masrat Rasheed, Shufaq Ayesha, Abida Khaliq and Sumera Irfan for their encouragement and appreciations throughout my research journey. I also want to thank Dr. Abdul Aabid for his guidance on simulations and supporting my research publications.

My profound thanks go to my beloved mother, Mubeena Akhter and father, Parveez Ahmad mir, without their support and belief in me this all seemed to be difficult. May Allah(swt) reward them abundantly for providing me with the privilege of acquiring knowledge. Also, I am blessed to have a sister, namely Uzma Parveez by my side, who always guides me through, supports me and at times saves me from making wrong decisions. May Allah (swt) reward her.

Once again, I glorify Allah for His endless mercy on me, one of which is enabling me to successfully round off the efforts of writing this thesis. Alhamdulillah

TABLE OF CONTENTS

Abstract ..... **ii**
Abstract in Arabic ..... **iii**
Approval Page ..... **iv**
Declaration ..... **v**
Copyright Page ..... **vi**
Dedication ..... **vii**
Aknowledgements ..... **viii**
Table of Contents ..... **ix**
List of Tables ..... **xii**
List of Figures ..... **xiv**
List of Symbols ..... **xivx**
List of Abbreviations ..... **xix**

CHAPTER ONE: INTRODUCTION **1**
1.1 Background 1
1.2 Problem Statement 6
1.3 Research Philosophy 8
1.4 Research Objectives 9
1.5 Research Scope 10
1.6 Research Methodology 10
1.7 Thesis Outline 13

CHAPTER TWO: LITERATURE REVIEW **15**
2.1 Introduction 15
2.2 Porous composites 16
2.3 Pore forming agents 22
2.4 Processing techniques 23
2.4.1 Melt Route 23
2.4.2 Powder Metallurgy Technique 24
2.5 Process parameter and compositional optimization 26
2.6 Application of porous metals and their composite 29
2.7 Summary 31

CHAPTER THREE: EXPERIMENTAL PROCEDURE **33**
3.1 Introduction 33
3.2 Experimental design plan 33
3.3 Selection of input variables 36
3.4 Selection of response variables 38
3.5 Experimnental set up 38
3.5.1 Matrix alloy 38
3.5.2 Reinforcement material 39
3.5.3 Space holder material 40
3.5.4 Experimental equipment's used 41
3.6 Preparation of porous Al composite 41
3.6.1 Mixing 43

3.6.2 Compaction 43
3.6.3 Sintering 44
3.7 Characterization And Testing 45
3.7.1 Characterization 45
3.7.1.1 Morphological analysis 46
3.7.1.2 Phase analysis 47
3.7.1.3 Density and porosity measurement 48
3.7.2 Compression testing 49
3.8 Summary 50

CHAPTER FOUR: RESULTS AND DISCUSSION 52
4.1 Overview 52
4.2 Effect of processing parameters on compressive properties of porous Al composites 53
4.2.1 Morphology 55
4.2.2 Effect of process parameters (Experimental) 57
4.2.2.1 Effect of sintering temperature 57
4.2.2.2 Effect of compaction pressure 61
4.2.2.3 Effect of sintering time 64
4.2.3 Effect of process parameters (Analytic) 65
4.2.3.1 Analysis of Signal to Noise Ratio 65
4.2.3.2 Analysis of variance 66
4.2.3.3 Regression analysis 69
4.2.3.4 Response optimization 71
4.2.3.5 Contour plots 72
4.2.3.6 Confirmation test 74
4.3 Effect of diamond content, PMMA content and PMMA particle size on compressive properties of porous Al composites 76
4.3.1 Morphology of porous Al composites 77
4.3.2 Effect of varying composition (Experimental) 79
4.3.2.1 Effect of diamond particle content 79
4.3.2.2 Effect of PMMA particle size 81
4.3.2.3 Effect of PMMA content 83
4.3.3 Effect of varying composition (Analytic) 84
4.3.3.1 Analysis of Means 84
4.3.3.2 Analysis of variance 86
4.3.3.3 Regression analysis 89
4.3.3.4 Response optimization 91
4.3.3.5 Interaction plots 92
4.3.3.6 Contour plots 94
4.3.3.7 Confirmation test 97
4.4 Effect of uncoated and coated diamond in improving compressive properties of porous Al composite 98
4.4.1 Morphological analysis 98
4.4.1.1 Microstructure 98
4.4.1.2 Porosity and Density 101
4.4.1.3 X-ray Diffraction analysis 103
4.4.1.4 Compressive properties 106

4.4.1.5 Effect of alloying elements in improving strength.....108
4.4.1.6 Effect of Ti-coated diamond in improving strength...109
4.5 Summary.....111

CHAPTER FIVE: CONCLUSION AND RECOMMENDATIONS 114
5.1 Conclusions.....114
5.2 Contributions to knowledge.....116
5.3 Recommendations.....117

REFERENCES.....119

PUBLICATIONS AND CONFERENCES 137

LIST OF TABLES

Table 3.1	Factors and levels in L9 Taguchi orthogonal array experimental design plan for parameter optimization	35
Table 3.2	Factors and levels in L9 Taguchi orthogonal array experimental design plan for composition optimization adhesive	35
Table 3.3	Taguchi's orthogonal array showing experimental design	36
Table 3.4	Taguchi's orthogonal array showing experimental design for compositional optimization	36
Table 3.5	Composition of Alloy matrix	39
Table 3.6	L9 Orthogonal array with design factors for parameter optimization	39
Table 3.7	L9 Orthogonal array with design factors for composition optimization	42
Table 4.1	Control factors (process parameters) and their levels	54
Table 4.2	L9 orthogonal array layout with design factors	55
Table 4.3	Density and porosity of porous Al composite for nine sets of parameters	59
Table 4.4	ANOVA Variance table for plateau stress	67
Table 4.5	ANOVA Variance table for energy absorption capacity	67
Table 4.6	Fits and diagnostics for all observations for plateau stress	70
Table 4.7	Fits and Diagnostics for All Observations for Energy absorption capacity	70
Table 4.8	Response optimization: processing parameters	72
Table 4.9	Confirmation test comparisons with predicted values	75
Table 4.10	Control factors (Process Parameters) and their levels	76
Table 4.11	L9 Orthogonal array layout with design factors	77
Table 4.12	Densities and porosities of porous Al composite for 9 sets of parameters	79
Table 4.13	ANOVA Variance table for Plateau strength	87
Table 4.14	ANOVA Variance table for energy absorption capacity	88

Table 4.15	Fits and diagnostics for all observations for plateau strength	89
Table 4.16	Fits and diagnostics for all observations for energy absorption capacity	90
Table 4.17	Comparison of confirmation test with predicted values	91
Table 4.18	Comparison of confirmation test with predicted values	98
Table 4.19	Compressive properties of uncoated and Ti-coated diamond composite	106

LIST OF FIGURES

Figure 1.1	The micrograph of scanning electron microscopy (a) open-cell porous composite and (b) closed-cell porous composite (Kennedy, 2012)	1
Figure 1.2	Properties and various applications of porous composite	2
Figure 1.3	Melt route for the production of porous composite	3
Figure 1.4	Schematic diagram of powder metallurgy technique for porous metal composite	4
Figure 1.5	Schematic representation of processing technique	11
Figure 1.6	Overview of Research Methodology Flowchart	13
Figure 2.1	(a) Plateau strength (MPa), (b) energy absorption (MJ/m3) and (c) microhardness (HV) of porous Al/SiO2 composite (Salehi et al., 2015))	18
Figure 2.2	Optical images showing macrostructure of (a) A359, (b) A359/5vol%Al2O3, (c) A359/10vol%Al2O3 and (d) A359/15vol%Al2O3 composite foams (Daoud, 2009)	18
Figure 2.3	Optical micrographs showing the morphological characteristics of (a) Al foam and (b) 10% SiCp/Al foam (Guden & Yüksel, 2006)	19
Figure 2.4	Optical microscopy showing the cell structure of AlSi9Mg/SiCp composite foams	20
Figure 2.5	(a) Yield strength (MPa) and (b) energy absorption (MJ/m3) of nanocomposite Al-B4C foams (Moradi et al., 2015)	20
Figure 2.6	SEM images of Cu-coated carbon fibers in the composite: (a) carbon fibers dispersed in the Al matrix; (b) and (c) interface between carbon and Al matrix (Mu et al., 2011)	21
Figure 2.7	Powder metallurgy (space holder technique) for the fabrication of Al/CNT foams	25
Figure 2.8	(a) Products with cores of porous Al (Stöbener & Rausch, 2009); (b) prototype of the engine mounting bracket of BMW and (c) crossbeam of a machine tool with an porous Al core (foam core)	30

Figure 3.1	Metallic powders for matrix alloy, (a) Aluminium (Al), (b) Magnesium (Mg), (c) tin (Sn), (d) Copper (Cu), and (e) Boron (B)	39
Figure 3.2	Ti coated diamond powder as reinforcement material	40
Figure 3.3	Various sizes of PMMA particles, (a) 75 µm, (b) 125 µm, and (c) 150 µm	40
Figure 3.4	Schematic diagram of fabrication of porous Al composite	42
Figure 3.5	Compaction process of final powder mixture using hydraulic press	44
Figure 3.6	Sintered samples of size 10×10mm	45
Figure 3.7	Sectioned samples from porous Al composite	46
Figure 3.8	Schematic overview of scanning electron microscope with EDX	47
Figure 3.9	X-ray Diffraction set up	48
Figure 3.10	Desiccator with pump (right) and Densimeter (left)	49
Figure 3.11	Compression testing machine with 30 kN load	50
Figure 4.1	SEM micrography of a) Elemental powder mixture, b) PMMA particle and c) Ti-coated diamond particle	56
Figure 4.2	SEM micrograph of (a) PMMA particles, and (b) Cross section of sintered porous Al composite	57
Figure 4.3	SEM morphology of porous Al composite developed at, (a) 580 °C, 350 MPa and 60 min, (b) 590 °C, 350 MPa and 120 min, and (c) 600 °C, 350 MPa and 120 min	58
Figure 4.4	SEM images and EDX analysis of porous Al composite showing wetting action near the vicinity of diamond particles at different sintering temperatures, (a, d) 580 °C (b, e) 590 °C, and (c, f, g) 600 °C	61
Figure 4.5	Samples compacted at (a) 300 and 450 MPa, and (b) at 350, 380, and 400 MPa	62
Figure 4.6	Effect of compaction pressure on relative density and porosity of Al compacts	63
Figure 4.7	SEM micrography of porous Al composite at sintering temperature of 590°C and at varying sintering time (a) 120 min, (b) 90 min and (c) 60 min	65

Figure 4.8	S/N ratio response curve of plateau stress	66
Figure 4.9	S/N ratio response curve of energy absorption capacity	66
Figure 4.10	Percentage of the contribution of processing parameters on the (a) plateau strength and (c) energy absorption capacity	69
Figure 4.11	Comparison of experimental and modal predicted plateau stress and energy absorption capacity	71
Figure 4.12	Contour plot of plateau stress in diamond-reinforced porous Al composite	73
Figure 4.13	Contour plot of energy absorption capacity of diamond-reinforced porous Al composite	74
Figure 4.14	Compressive stress- strain diagram of confirmation test at optimum parameters	75
Figure 4.15	Microstructure of porous Al composite, (a) Pore distribution and shape, (b) EDX of composite cross section, (c) Pore cell and pore connectivity, and (d) Well bonded diamond particle	78
Figure 4.16	SEM images of (a, b) cell wall of sintered porous Al composite near the vicinity of diamond particle, and (c) EDX of the Al alloy matrix and Ti-coated diamond interface	81
Figure 4.17	Pore size and wall thickness of pores in porous Al composite with varying PMMA particle size, (a) 75 µm, (b) 130 µm and (c) 150 µm	82
Figure 4.18	SEM microstructure of porous Al composite with varying PMMA particle content, (a, d, g) 20 wt.%, (b, e, h) 25 wt. %, and (c, f, i) 30 wt. %.	84
Figure 4.19	Mean response curve of plateau strength	85
Figure 4.20	Mean response curve of energy absorption capacity	86
Figure 4.21	Percentage of the contribution of input factors on, (a) plateau strength, and (b) energy absorption capacity	88
Figure 4.22	Evaluation of experimental and modal predicted (a) Plateau strength, and (b) Energy absorption capacity	90
Figure 4.23	Interaction plots for plateau strength	93
Figure 4.24	Interaction plots for energy absorption capacity	94

Figure 4.25	Contour plot of energy absorption capacity of, (a) PMMA size vs diamond content (b) PMMA vs diamond content and (c) PMMA size vs PMMA content	96
Figure 4.26	Contour plot of energy absorption capacity of, (a) PMMA size vs diamond content (b) PMMA vs diamond content and (c) PMMA size vs PMMA content	96
Figure 4.27	Comparison of confirmation test result at optimal input factors and maximum value obtained from Taguchi L9 runs	97
Figure 4.28	SEM micrography of porous Al with no reinforcement, (a) magnification of 33x, (b) magnification of 100x, and their (c) EDX	99
Figure 4.29	Morphology and elemental analysis of porous Al composite reinforced with, (a) 6 wt. %, (b) 9 wt. %, (c) 12 wt. %, (g) 15 wt. %, (e) 20 wt. % of uncoated diamond particles, and (f) EDX of porous Al composite	100
Figure 4.30	Morphology and elemental analysis of porous Al composite reinforced with, (a) 6, (a) 9, (a) 12, (a) 15, (a) 20 wt.% of Ti-coated diamond particles and (f) EDX of porous al composite	101
Figure 4.31	Percentage of (a) porosity and (b) relative densities of porous Al composite reinforced with uncoated and Ti-coated diamond	102
Figure 4.32	XRD patterns of porous Al composite reinforced with uncoated diamond	105
Figure 4.33	XRD patterns of porous Al composite reinforced with Ti-coated diamond particles	105
Figure 4.34	Compressive stress-strain diagram of Ti-coated and uncoated porous Al composite	107
Figure 4.35	Morphology and elemental analysis of (a) 6 wt. %, (b) 9 wt. %, (c) 12 wt. %, (d) 15 wt. %, (e) 20 wt. % of uncoated and (f) 6 wt. %, (g) 9 wt. %, (h) 12 wt. %, (i) 15 wt. % and (j) 20 wt. % of Ti-coated diamond particle reinforced porous Al composite	111

LIST OF SYMBOLS

P	Density
Mm	Micrometer
MPa	Mega Pascal
MJ	Mega Joule
kN	Kilo Newton
%	Percentage
Wt	Weight
Rpm	Revolutions per minute
˚C	Degree Celsius

LIST OF ABBREVIATIONS

Al	Aluminium
Al_2O_3	Alumina
ANOVA	Analysis of variance
ASTM	American society for testing and materials
B	Boron
B_4C	Boron carbide
CBN	Boron nitride
Cu	Copper
CNT	Carbon nanotubes
DOE	Design of experiment
EDX	Energy dispersive x-ray
Fe	Iron
Mg	Magnesium
Mn	Manganese
MS	Mean square
NaCl	Sodium chloride
Ni	Nickel
O	Oxygen
P	Phosphorus
PM	Powder metallurgy
PMMA	Polymethylmethacrylate

RSM	Response surface methodology
SDP	Sintering dissolution process
SEM	Scanning electron microscopy
SiC	Silicon carbide
SS	Sum of square
Sn	Tin
TEM	Tunneling electron microscopy
Ti	Titanium
TiC	Titanium carbide
XRD	X-ray diffraction
Zn	Zinc

CHAPTER ONE

INTRODUCTION

1.1 BACKGROUND

Porous composites are low density materials with unique properties, suitable for lightweight structures, thermal management, and energy absorption applications. Due to the broader accessibility of practical technologies and a better understanding of their physiological, chemical, and mechanical characteristics, these materials have gained increasing attention in recent decades. Conceptually, cell connectivity categorizes porous composites as closed or open-celled structure. In open-cell structure, pores are connected to allow matter to pass through them. Moreover, open-cell structure prevents film from occurring between adjacent cells in the matrix material. They have sponge-like interconnected pores as shown in Figure 1.1 (a) (Kennedy, 2012). By contrast, pores are isolated in closed-cell structure. Cells in the closed-cell porous metals and its composite are separated by a thin film of matrix material as shown in Figure 1.1 (b) (Kennedy, 2012). Due to their remarkable energy absorption capabilities with high plateau stress values and damping capacity, these are used in several applications as mentioned in Figure 1.2 (Wang et al., 2011).

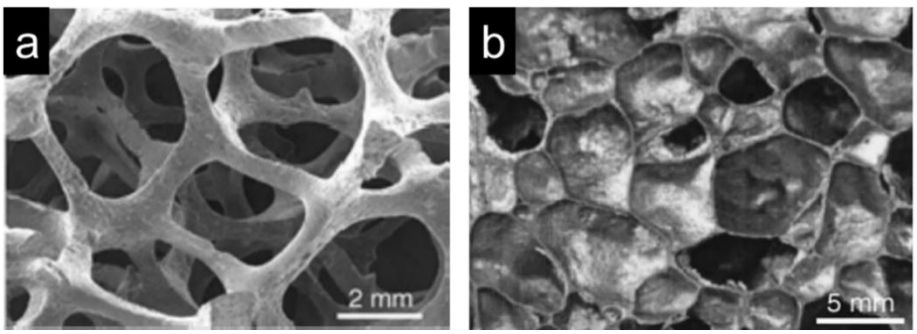

Figure 1.1 The micrograph of scanning electron microscopy (a) open-cell porous composite and (b) closed-cell porous composite (Kennedy, 2012)

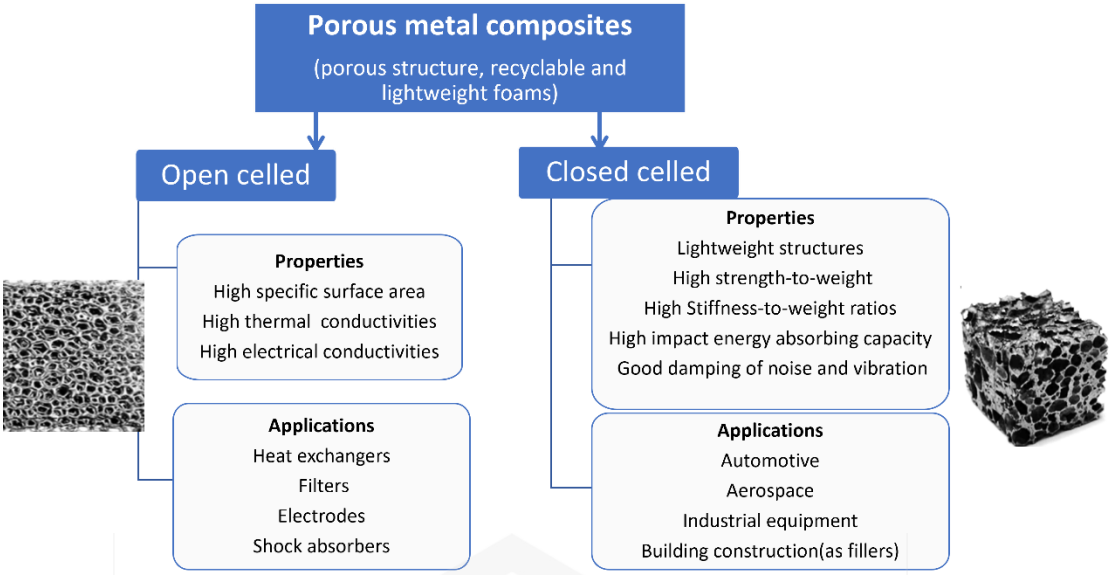

Figure 1.2 Properties and various applications of porous composite

Various techniques have been employed to develop such porous composites, mostly melt route, and space holder technique (powder metallurgy). In the melt route method, metal is melted in graphite crucible, and the melt is stirred at some stirring speed with the help of a mechanical stirrer, reinforcements are added to the melt during stirring. Afterwards, a foaming agent is added to the melt. After the foaming process is completed, a foam-containing metallic die is taken out from the furnace and cooled in compressed air as demonstrated in Figure 1.3 (Aldoshan & Khanna, 2017; Das et al., 2020). However, the melt route exhibited the inability to develop near net shape parts, high casting temperature requirements and non-uniform distribution of reinforcements. To overcome such problems, the powder metallurgy route (PM) was mostly preferred due to their production of parts with high dimensional accuracy and high productivity by involving limited use of materials and energy as a result there occurs minimal waste of raw materials (Hassan, 2019).

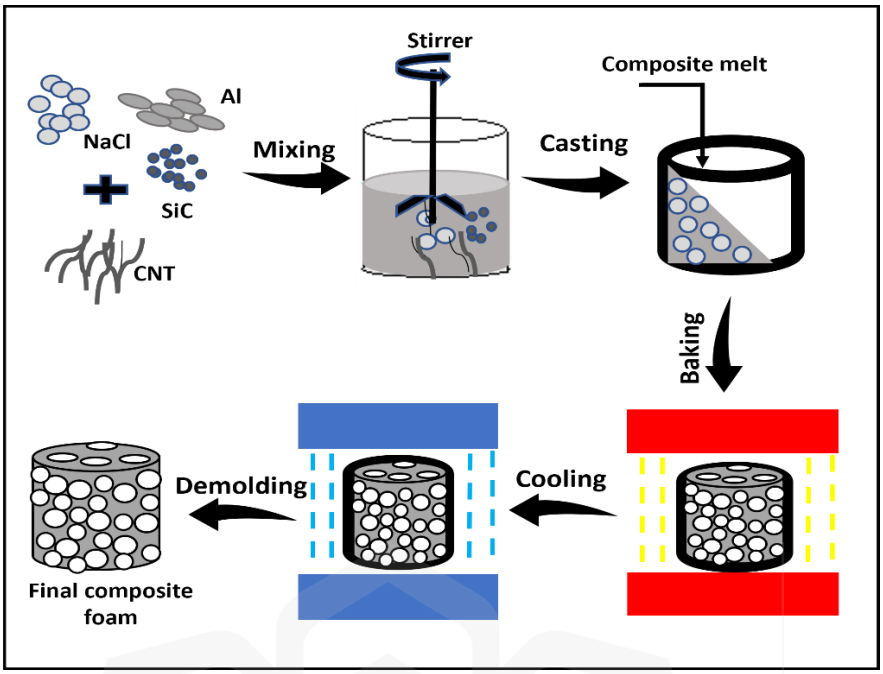

Figure 1.3 Melt route for the production of porous composite

The key processes include mixing, compaction, and sintering as demonstrated by Figure 1.4. Sintering temperatures are important in determining the mechanical properties of porous composite as it affects the bonding of metal matrix particles the reinforcements (Kumar and Madurai, 2020). This technique is frequently used in the production of iron (Fe)-based porous metals and composites that are almost free from impurities and inclusions. It also allows the fabrication of porous composites near-net shape with an interconnected pore structure and the required properties. (Capek et al., 2015).

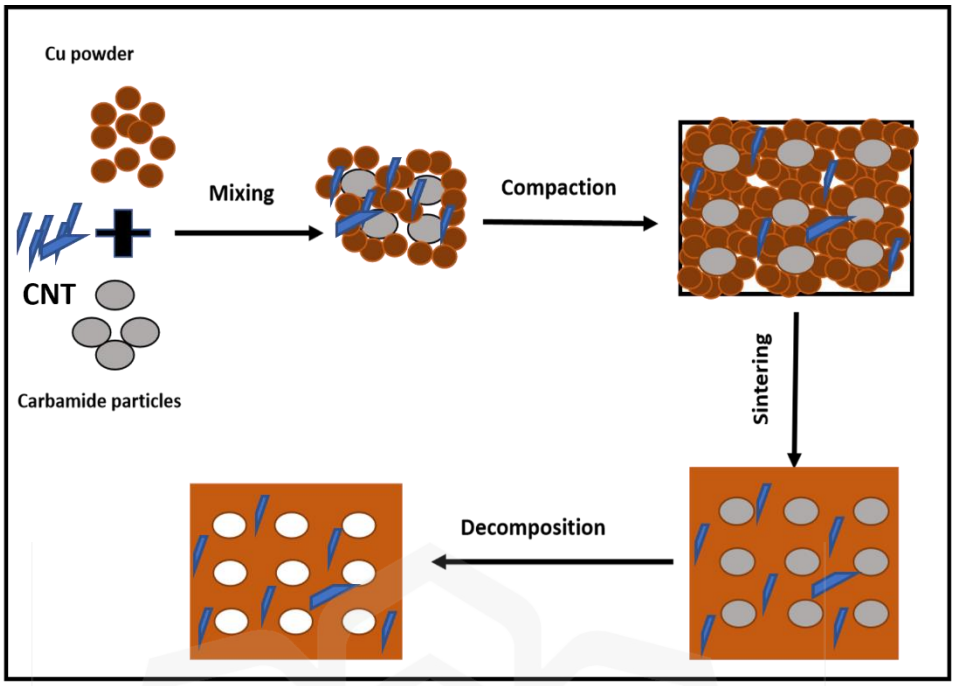

Figure 1.4 Schematic diagram of powder metallurgy technique for porous metal composite

Moreover, the porosities in porous composite have been achieved by researchers using blowing agents such as calcium carbonates ($CaCO_3$) (Aboraia et al., 2011), and titanium hydride (TiH_2) (Mukherjee et al., 2017) or space holders such as sodium chloride (NaCl) (Jiang et al., 2007; Razali et al., 2013), carbamide (Yang et al., 2017;Yang et al., 2019). The space holders efficiently tailor the shape and size of porosities When added to porous composites, the resultant pores mimic the shape and size of space holders. But, in case any reaction occurs between the residue of space-holders and the metal matrix, it may impair the properties of the resulting composite. To prevent this, a space holder material is required with least affinity with metals, such as poly (methyl methacrylate) (PMMA) (French, 2014). The closed cell structured porous Al with different porosities and densities were developed using varying PMMA content, as a result the porosities were efficiently regulated (Jamal et al., 2016; Tan et al., 2018).

Many porous composite, using lightweight metal such as aluminum (Al), magnesium (Mg) (Aida et al., 2017; Shunmugasamy & Mansoor, 2015), and titanium (Ti), have been developed. Among all, porous Al composites have immense prospect in applications requiring lighter weight, higher-strength, and higher-energy absorption capacity, particularly in structural and automobile manufacturing. But their lower strength limits their usage and capabilities. To overcome this, researchers have added zinc (Zn), tin (Sn), boron (B) and Mg as alloying elements to aid Al matrix (Farahani et al., 2022; Hamdi, 2018). The addition of Mg was found to decrease the wetting angle and allows the liquid melt to flow into micropores by capillary action. This liquid fills the pores resulting in a high-density foam framework (Jamal et al., 2018). Also, boron when added to stainless steel improved their microstructure thus their mechanical properties. At temperatures higher than the eutectic transformation temperature, the eutectic reaction occurs between metals and boron, resulting in liquid phase formation, which helps to sinter the composite (Ali et al., 2018). When dispersed in the stainless-steel matrix, boron can form metal-boride complexes and separate at grain boundaries (Kontis et al., 2016).

Further to enhance the strength of porous Al composites, researchers have added silicon carbide (SiC) (Chung et al., 2014; Y. Luo et al., 2010), alumina (Al_2O_3) (Alizadeh and Aliabadi, 2012), and carbon nanotube (CNT) (Yang et al., 2017; Yang et al., 2020) to porous Al composite. However, there exists challenges in preparing high-quality composite include their clustering tendency, poor wettability, and large discrepancy in density and size between CNTs and metal matrix composite (Yang et al., 2011). Considering the extraordinary properties including high hardness, higher strength, and thermal conductivity of diamond, the properties of porous Al composite can potentially improve. Several researchers have used diamond as reinforcement in

solid composite (Aliyi, 2019; Yin et al., 2017). One of the biggest challenges associated with the use of diamond particles as reinforcement is their poor wettability resulting in weak interface between diamond and metal matrix. Several methods for improving diamond wettability have been investigated. The interfacial bonding of diamonds with metal matrix have been improved by surface treating or by applying coating or functionalized with high thermal conductivity metals or alloys such as copper (Cu), silver (Ag), and Al (Chung et al., 2014; Wu et al., 2012). Another technique is to form a carbide layer between the diamond and metal interfaces to improve diamond wettability, for example, by using tungsten (W) or titanium (Ti) coating (Chung et al., 2014).

Despite research on the development of porous Al composite using PM, the study on optimizing composite properties based on processing parameters in still limited (Küçük et al., 2017). Also, the PMMA content and size is found to affect the properties of porous composites, thus the effect of their variation on the properties of porous composite needs to be further examined. Moreover, the possibility of employing Ti-coated diamond as reinforcement in the porous composites to enhance their strength requires extensive studies since it is not explored yet in porous composites. Therefore, the present work was dedicated to studying the effect of varying PM process parameters, different PMMA particle content and size and Ti-coated diamond particles content on the microstructure and compressive properties of porous Al composite.

1.2 PROBLEM STATEMENT

Until now, most of the car segments are made of dense metals and polymers, there exists a requirement of lightweight material that can further upgrade the vehicles' design

flexibility, efficiency, and performance. In addition, the reduction in weight of automotives can result in reducing fuel consumption, increase the fuel economy and minimize the carbon dioxide (CO_2) release to the environment. However, such lightweight materials are also required to improve the impact energy absorption during collision, hence preserving the passenger's safety. Although the porous Al composites have potential to offer lightweight property in combination with high strength and stiffness to weight ratio, energy saving and excellent impact energy absorption during collision. But these are often associated with low density and strength thus low mechanical and thermal performance which limits their efficiency, design flexibility as well as potential applications. Even though the strengthening effect could be achieved by selecting a strong based of metal matrix, for example Al alloy as well as by applying traditional heat treatment processes. Still their desirable level of strength could not be obtained due to the formation of cracks in the cell wall because of thermal stresses (Maiorano et al., 2023). Further, the strengthening of porous composites by the addition of reinforcements reveals the clustering tendency, poor wettability, and large discrepancy in density and size of reinforcement and Al matrix. Also, poor wettability due to the formation of brittle intermediate product is often the main challenge faced in combining Al matrix and carbonaceous reinforcement that results in deteriorated properties of composite. Also, the porosities in such composites are mostly acquired using blowing agents however they require high decomposition temperature, and uncontrolled porosities. Further, using salts as space holders no doubt allows control over porosities but due to high saline concentration during dissolution process causes corrosion of metals and alloys and insufficient dissolution of salts from small pores.

In view of all these drawbacks, PMMA particles were used as space holders in the current research, these particles decompose at low temperature leaving no residue

behind and allow tailoring of porosities. Further, PM technique was employed as fabrication technique that allows the production of complex parts near to net shape, provides flexibility in terms of constituent addition in composites to strengthen them and promotes material conservation by discarding the wastage of material during machining processes. Further the usage of alloying elements and Ti-coated diamond particles as reinforcements to strengthen the porous Al composite was initiated in the current study. The introduction of such an alloying element is anticipated to improve the interfacial bonding between Al matrix and diamond reinforcement. Moreover, to prevent the formation of brittle carbide intermediate product, Ti-coated diamond particles were employed. Thus, the combination of efficient processing technique and excellent physical and mechanical properties are foreseen to contribute a major improvement in many sectors and industries including automotive industry.

1.3 RESEARCH PHILOSOPHY

This research focused on strengthening of porous Al composite by inclusion of alloying additives, that assist in strengthening of Al matrix by forming alloy phases. Further by adding Ti-coated diamond particles as reinforcement to enhance the overall strength of the porous composites by improving their compressive properties. The addition of alloying elements and Ti coating on diamonds improves the interfacial bonding between Al matrix and diamond reinforcement. The development of these composites using powder metallurgy technique enables near net shape and low temperature production of the resultant composites. The properly planned experiments required to find the effect of process parameters, Ti-coated diamond content, PMMA content and PMMA size on the compressive properties of porous Al composites were carried and optimum values were acquired.

Based on these optimum values, uncoated and Ti coated diamond reinforced composites with varying diamond content were examined to analyze the effect of Ti-coated diamond in strengthening porous composites and to find the optimum content required to get best results for compressive properties. Thus, the philosophy of this research is to enhance the strength of porous composite by improving the strength of matrix and improve the wettability and stability of diamond particles in porous Al composite thereby increasing their overall performance for filler material application in automotives and aerospace structures.

1.4 RESEARCH OBJECTIVES

The aim of this research is to enhance the strength of porous Al composite. In relation to this, the specific objectives are:

1. To determine the effect of processing parameters (compaction pressure, sintering time and sintering temperature) on the microstructure and compressive properties porous Al composite and find the optimum value of process parameters.
2. To explore the influence of diamond particle content, PMMA content and PMMA particle size on the structural and compressive properties of porous composite and find their optimum values.
3. To examine the effect of addition of varying content of uncoated and coated diamond reinforced porous Al composites by comparing their structural and compressive properties developed under optimum conditions.

1.5 RESEARCH SCOPE

The existing works on porous Al composites revealed their immense potential in improving the performance and safety of automotives. However, enhancing their strength by improving bonding, and wettability of reinforcement material with Al matrix and preventing the formation of reaction products has always remained a challenge. Thus, the scope of this study was to improve the bonding strength between Al matrix and reinforcement by the addition of alloying elements in Al matrix and using coated diamond particles as reinforcement. In this context, Ti-coating prevents the formation of undesirable phases due to the reaction between diamond particles and Al matrix during sintering whereas alloying elements forming low temperature phases, thereby leading to strengthening of porous Al composite. Therefore, this study is expected to broaden the understanding related to the achievement of good interfacial bonding of diamond particles with the matrix material as well as the effective employment of diamond particles in enhancing the strength of Al matrix in developing light weight and high strength material.

1.6 RESEARCH METHODOLOGY

The overall aim of this research is to enhance the strength of porous Al composite by incorporating Ti-coated diamond, using powder metallurgy technique as demonstrated in Figure 1.5.

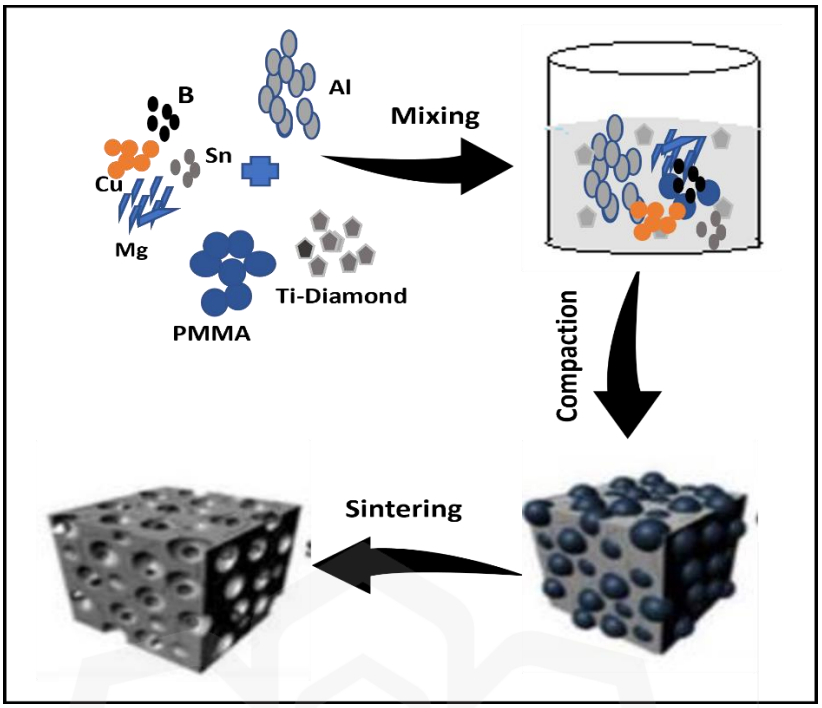

Figure 1.5 Schematic representation of processing technique

Moreover, the morphology, porosity, density, compressive strength, and energy absorption capacity of porous Al composite were evaluated accordingly. Therefore, the following plan was followed to achieve the objectives of this study:

1. Literature review: Initially, a review of the current state-of-the-art technologies on the potential application of carbonaceous material as reinforcement in improving the properties of porous Al composite was conducted. This gave an overview and review of the research that has been carried out in this area.
2. Evaluating the effect of the processing parameters on the properties of porous Al composite reinforced with Ti-coated diamond using Design of experiment (DOE) Taguchi's orthogonal array for efficient planning of the experiments and further analyzing the data by analysis of variance (ANOVA) to find the optimum values of parameters.
3. Evaluating the compressive properties of porous Al composite at varying percentages of Ti-coated diamond particles, PMMA content and PMMA size.

The composites were fabricated at the optimized parameters using powder metallurgy technique and planning the experimental runs by applying DOE based Taguchi's orthogonal array and ANOVA to reveal the statistical relationship between the factors and the optimum values.

4. Comparing the microstructure and compressive properties of uncoated and coated diamond reinforced porous composite developed at optimized parameters with optimum size and content of PMMA particles via powder metallurgy method. The alloying elements such as Mg, Sn, Cu and B powder were mixed with the Al matrix along with the Ti-coated diamond particles and space holder to obtain a homogeneous composition, followed by compaction at optimized pressure to develop a high strength compact specimen prior to sintering at optimized temperature under a controlled atmosphere to attain a pure porous composite body.
5. Characterization of starting materials, green specimens and porous Al composite using different analyses of SEM, EDX, XRD and density and porosity measurement by Archimedes principle.
6. Conducting compressive testing of porous Al composite.
7. Identifying the effect of processing parameters and the influence of Ti-coated diamond particles, PMMA and alloying elements on the experimental results for the development of porous Al compositive with effective energy absorption capacity.

The highlights of the systematic methodology that were adopted to achieve the aim and scope of this research work are presented in the workflow and experimental design in Figure 1.6.

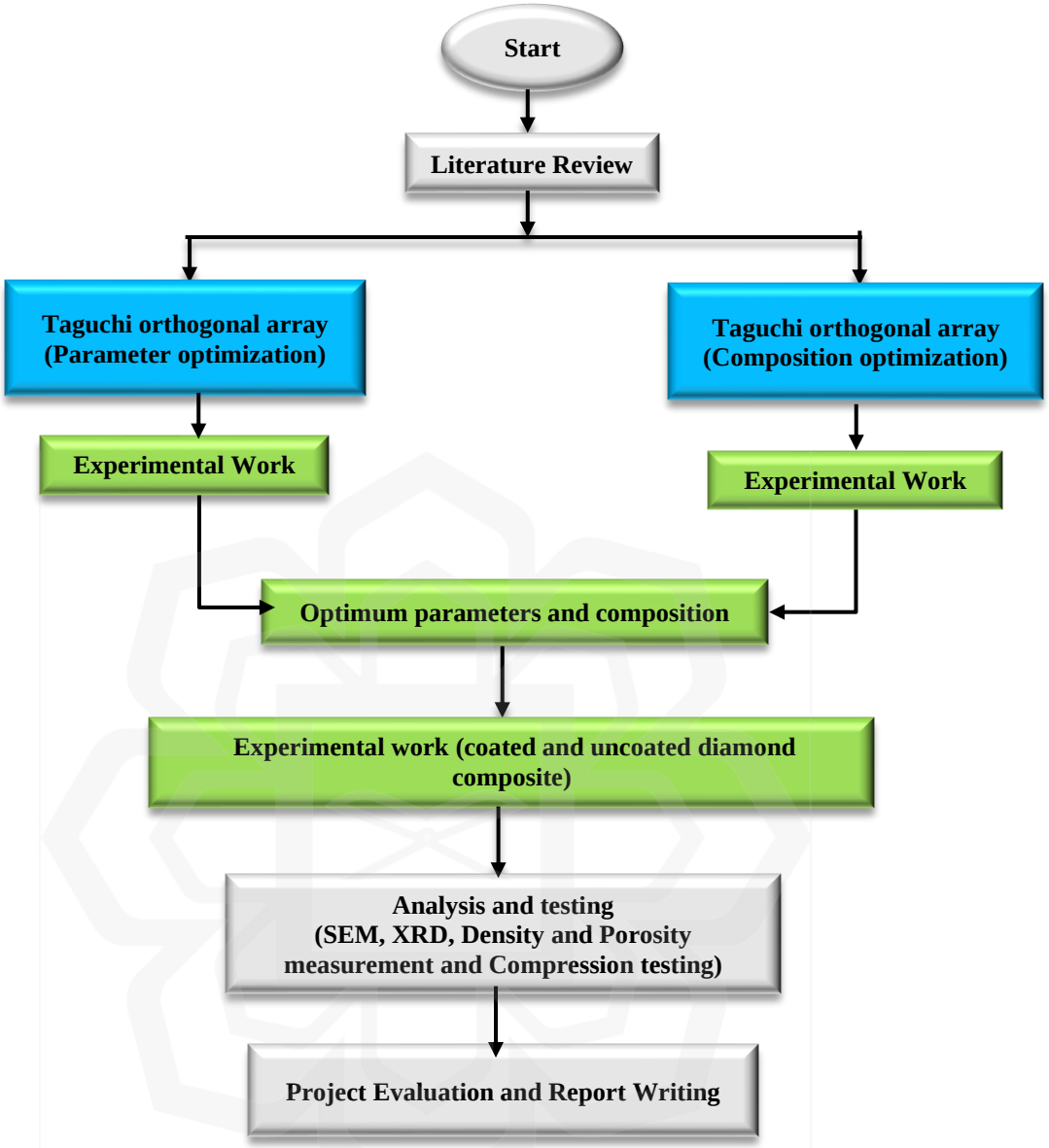

Figure 1.6 Overview of Research Methodology Flowchart

1.7 THESIS OUTLINE

This thesis has been organized into chapters. The summary of thesis structure according to each chapter.

Chapter one gives an idea about the introduction of porous composites. The various techniques, their microstructures, properties and applications are also presented.

Chapter two presents the current state of art on this thesis topic. The properties of porous Al composite influenced by several reinforcement additions and their resultant effect has been elucidated.

Chapter three explains the methodology adopted in this study. The fabrication technique involving various processes along with the parameters has been explained. It also mentions the objectives of the present work, research scope and the flow diagram to achieve them.

Chapter four presents the result and discussion of the research outcome achieved from the three objectives. It is divided into three subtitles as per the objectives and the simulations and experimental outcomes of the objectives have been discussed involving characterization analysis and mechanical testing.

Finally, Chapter five concludes the outcomes from the research objectives in three sections. Each section mentions the conclusion of each objective. Further, recommendations for future considerations are also provided in this chapter.

CHAPTER TWO

LITERATURE REVIEW

2.1 INTRODUCTION

The motivation of the current research was to enhance the compressive properties of the resultant porous Al composite by incorporating alloying additives and Ti-coated diamond particle. This was achieved by carrying out the parameter optimization followed by the optimization of Ti-coated diamond content, PMMA content and size. Finally, the microstructure, densities and percentage of porosity, and compressive properties of porous Al composite reinforced with uncoated and Ti-coated diamond particles were studied and compared to investigate the effectiveness of Ti-coating on improving the interfacial bonding between the Al alloy matrix and diamond particle as well as on the strength of porous Al composite. In general, diamond is an inert material with exceptional properties such as hardness, high strength, and thermal conductivity. Considering the high strength, thermal conductivity, hardness, and low thermal expansion coefficient of diamond particles, it can potentially improve the overall properties of porous metal composite. One of the biggest challenges associated with the use of diamond particles as a reinforcement is its poor wettability that often results in weak interface or bonding between diamond and metal matrix. Several methods for improving diamond wettability have been investigated by previous researchers including surface treating or by applying coating on the diamond particles (Chung et al., 2014). Another technique is to form a carbide layer for example titanium carbide (TiC) between the diamond and metal interface to improve the diamond wettability (Chung et al., 2014). Therefore, this chapter reviews about the development of porous

Al and porous Al composite with respect to various reinforcements, techniques and space holders employed in its production to improve its performance.

2.2 POROUS COMPOSITES

Porous metals are lightweight, non-flammable and recyclable materials with excellent thermal properties, high conductivity, and good damping capacity. Among all porous metals, porous Al are considered as ideal material due to their light weight, high strength-to-weight ratio, high stiffness. etc. thus are preferably used in aerospace, automotive, building construction and industrial equipment (Byakova et al., 2014; Navacerrada et al., 2013). Efforts have been devoted for developing porous Al with increased strength. Ideas are mostly based on research focusing on the fabrication of high-strength solid metal. One approach for strengthening porous Al is inclusion of alloying elements (e.g. Mg, Ni) that promote intermetallic formation (Ebhota & Jen, 2018). In addition, an Al alloy powders of higher strength or their ingots can be used to fabricate high-strength porous Al. Alloyed porous Al, such as AlZn5Mg1, AlSc0.24 (Huang et al., 2012, 2013), and AlZn10Mg0.3 are stronger than pure porous Al prepared via a similar technique (Karuppasamy & Dennison, 2018).

Magnesium (Mg), nickel (Ni), iron (Fe), silicon (Si), manganese (Mn), cobalt (Co) and scandium (Sc) are some of the most investigated alloying elements used to enhance the mechanical properties of existing porous Al (Moreno et al., 2020). Various mechanisms for strengthening have been claimed. Some authors suggested that the formation of intermetallic phases is essentially required for stabilization of foam, but others proposed that oxide formation plays an important role (Banhart, 2013). Perales et al., (2012) studied the influence on the compression behavior and energy absorption capability of Al-3 wt.% Sn alloy on addition oof various alloying elements (Mg, Co,

Ni, Mn and Ti). The energy absorption of Al foams increased with an increase in the contents of these alloying elements due to formation of intermetallic phases, confirming the general results of previous related reports.

Also, Xia et al., (2013) explored the closed-cell structured porous Al with various percentages of Mn resulted into even distribution of Mn particles in porous Al in the form of oxides and intermetallic materials leading to improvement in the microhardness, compressive strength and energy absorption capacities as compared to commercially available porous Al. Moreover, a closed-cell porous material with 5% Zn and 1% Mg inclusions was found to have increased compressive strength twice as compared with that of conventional foams. Thus, the addition of alloying elements also influences the foaming process thereby affecting their properties.

Another approach to improving the properties of porous Al is the addition of hard reinforcing materials (ceramics and carbonaceous). The incorporation of micro- or nano-sized reinforcement into a metal matrix has resulted in improvement in the properties of a ductile metal. For example, ceramic particles, such as silicon carbide (SiC), alumina (Al_2O_3) (Islam et al., 2016), TiB_2 (Atturan et al., 2016) and ceramic nanoparticles (Casati & Vedani, 2014), are some of the most studied reinforcing materials. (Salehi et al., 2015) examined the microstructure and mechanical properties of Al/SiO_2 composite foam and observed an increase in plateau strength and energy absorption with the addition of SiO_2 up to a certain limit; beyond this limit, its value decreases, but the SiO_2 content increases as hardness values increase (Figure 2.1). This finding explains the capability of nanoparticles to prevent dislocation and strengthen the matrix by creating high-density dislocations; however, plateau strength and energy absorption follow the density and degree of the fluctuation of stress in the plateau region.

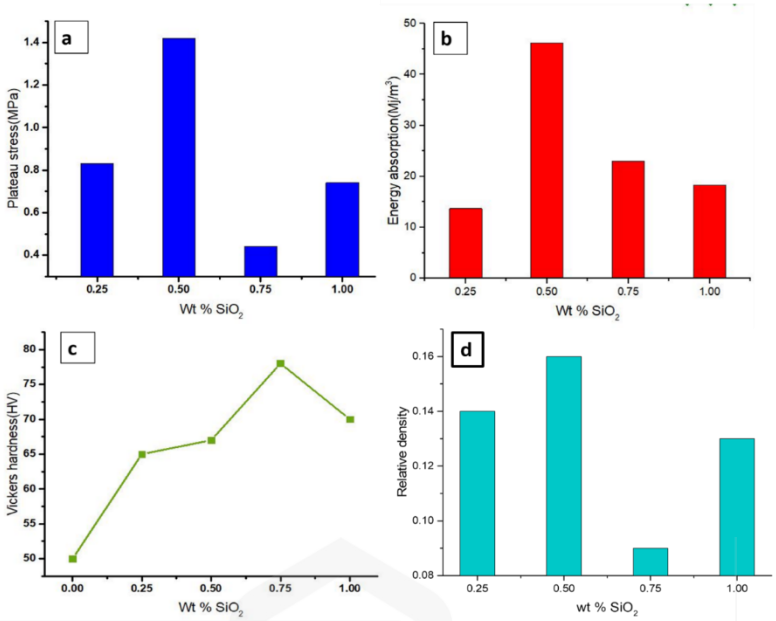

Figure 2.1 (a) Plateau strength (MPa), (b) energy absorption (MJ/m^3) and (c) microhardness (HV) of porous Al/SiO_2 composite (Salehi et al., 2015)

Also, (Daoud, 2009) reinforced A359 alloy matrix with Al_2O_3 particles and revealed the formation of roughly equiaxed polyhedral cell structures, and the cell structure is more uniform in A359 with Al_2O_3 reinforcement compared with that of pure A359 foam as evident from Figure 2.2. This can be attributed to the uniform distribution of Al_2O_3, resulting in an increase in plateau strength, yield stress, plastic stress, young's modulus, and energy absorption as the alumina content increased.

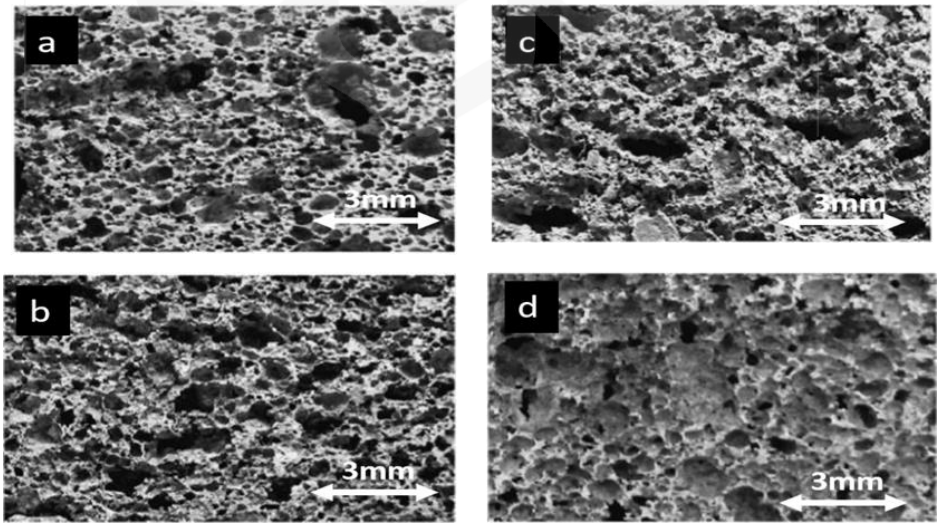

Figure 2.2 Optical images showing macrostructure of (a) A359, (b) A359/5vol%Al_2O_3, (c) A359/10vol%Al_2O_3 and (d) A359/15vol%Al_2O_3 composite foams (Daoud, 2009)

Further, Guden & Yüksel, (2006) employed SiC as reinforcement in porous Al composite Figure 2.3 and revealed the brittle compression behavior of fabricated composite. Yu et al., (2008) fabricated SiC-reinforced porous AlSi9Mg composite Figure 2.4 exhibiting a uniform cell structure and the influence of the strain rate on compressive properties revealed an increase in the yield stress with increase in the relative density, strain rate and SiC content. Furthermore, Moradi et al., (2015) studied the microstructure and compressive properties of B_4C-reinforced porous Al. The yield strength and energy absorption increased with the addition of B4C reinforcement as demonstrated by Figure 2.5.

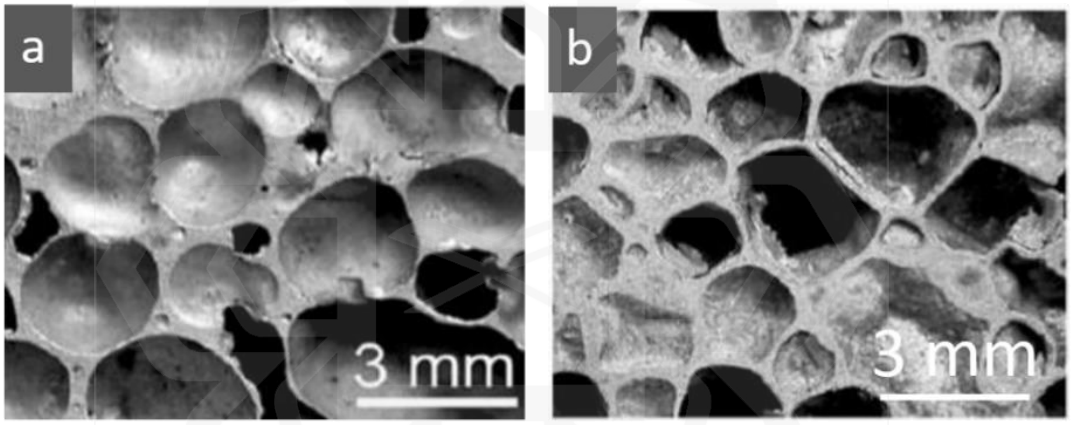

Figure 2.3 Optical micrographs showing the morphological characteristics of (a) Al foam and (b) 10% SiCp/Al foam (Guden & Yüksel, 2006)

The wettability of ceramic particles is often an issue faced in such composite. To prevent that, Mg has found to improve the microstructure, compression properties of porous Al composites (Lin et al., 2019).Guo et al., (2016) explored the effect of Mg addition on AlSi7 based alloys reinforced with Al_2O_3 and results showed that the Mg reacts with Al_2O_3 phase and Si element forming $MgAl_2O_4$ phase having good wettability with Al melt and Mg_2Si phase. Also, Alfonso et al., (2017) characterized porous (Al-6Si-3Cu-xMg (x = 7, 9 and 11 wt.%)) developed by in-situ process. The results showed strong dependence of microstructures of the porous composite on the

fabrication temperature and the Mg content. However, the porous Al composites reinforced with ceramics showed more brittle behavior than the porous Al (Jiang et al., 2012; Li et al., 2012).

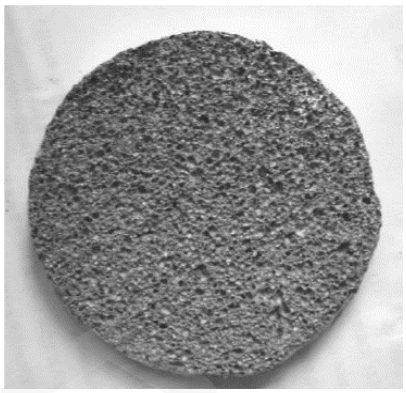

Figure 2.4 Optical microscopy showing the cell structure of AlSi9Mg/SiCp composite foams (Yu et al., 2008)

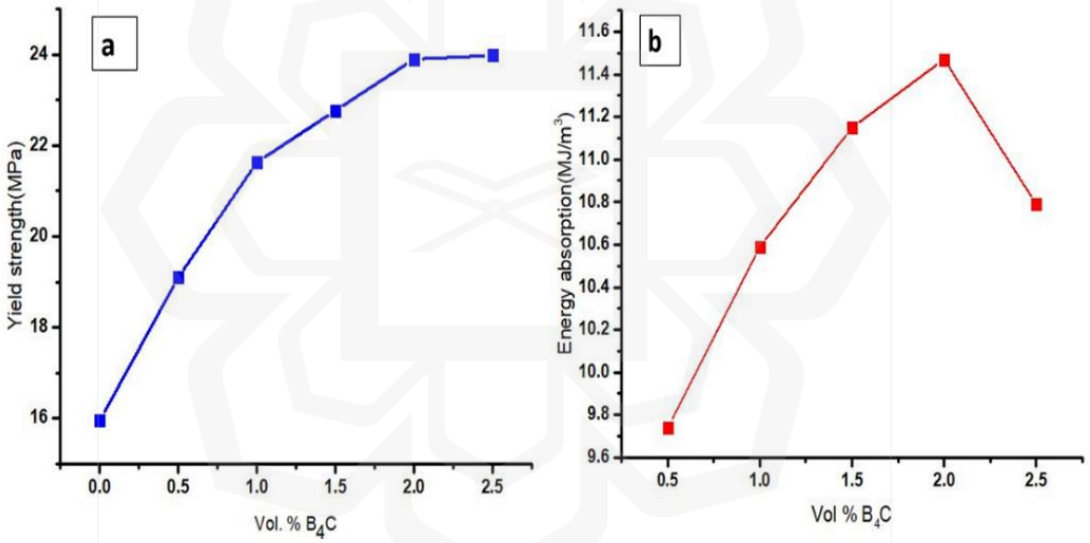

Figure 2.5 (a) Yield strength (MPa) and (b) energy absorption (MJ/m^3) of nanocomposite Al-B_4C foams (Moradi et al., 2015)

The thickness of the cell walls is the crucial factor that determines the strength of porous Al composites. Thinner cell walls have weaker strength and thus lower compressive properties. The strength of the cells walls of porous Al composites was found to be improved by the inclusion of carbon nanotubes (CNTs). CNTs possess a high mechanical strength, a high elastic modulus, a high aspect ratio (i.e. length-to-thickness or length-to-diameter ratios) and excellent thermal and electrical conductivities (Jiang

et al., 2012; Tjong, 2013) Therefore, they are regarded as the most efficient reinforcing materials for developing composite materials for functional and structural engineering applications (Choudhary et al., 2022). However, the addition of CNT's result into the formation of brittle and low-strength interfacial reaction products (Al_4C_3) (Che et al., 2016). However, this problem has been addressed by researchers by applying metal coating on CNT particles, to prevent the formation of interfacial reaction products (Al_4C_3) and enhance the strength of interfacial bonding between carbonaceous particles and Al matrix reinforced Cu-coated CNTs in porous Al composites resulting into good wettability and uniform distribution of coated CNT particles, thus collapse stress values improved (Mu et al., 2011). Further, Damanik et al., (2019) fabricated Ni-coated carbon fiber-reinforced porous Al and observed an effective distribution of the coated CNT in the Al matrix with enhanced wettability at their interfaces.

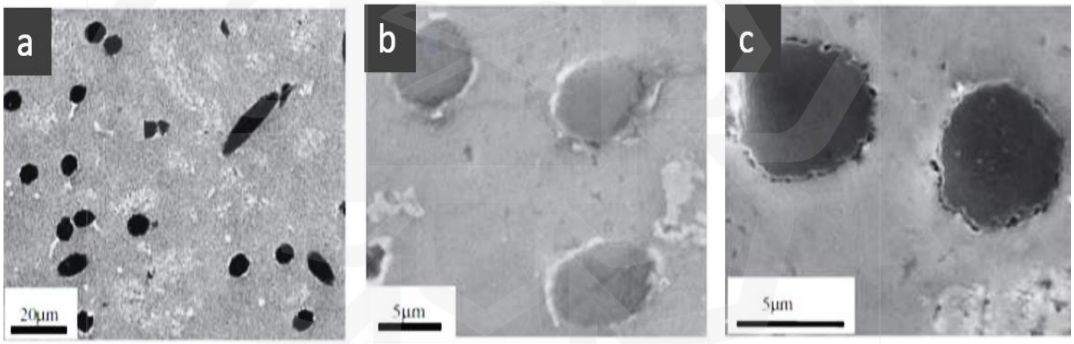

Figure 2.6 SEM images of Cu-coated carbon fibers in the composite: (a) carbon fibers dispersed in the Al matrix; (b) and (c) interface between carbon and Al matrix (Mu et al., 2011)

Even though outcomes are amazing, the addition of CNTs in metal matrices is still an unexplained problem because of their poor dispersion, high capability to agglomerate, and poor wettability in a molten metal matrix.

2.3 PORE FORMING AGENTS

The porosities in the composites are formed by mixing pore forming agents with the matrix powder. These foaming agents decompose at high sintering temperatures into a solid component and gas component causes foaming of material matrix or acting as space holders that after sintering process are leached out by dissolution method. The foaming agent that solidifies on decomposition and evolves gases are called blowing agents such as titanium hydride (TiH_2), calcium carbonate ($CaCO_3$), zirconium hydride (ZrH_2), etc (Behymer & Morsi, 2023). Also, the ones that are either leached out by dissolution method or decompose during sintering process are called space holders. Typically, sodium chloride (NaCl), carbonate particles, carbamide, and various polymers have been employed as space-holder materials for fabrication of porous composites especially through powder sintering process (Luo et al., 2022; Contreras et al., 2021).

Paulin (Paulin, 2014) studied the foaming effect of different foaming agents on the porous Al and revealed that expensive foaming agent TIH_2 can be replaced by $CaCo_3$, CaMg $(CaCO_3)_2$ (dolomite). However, these can be used at high compaction pressures and high temperature due to their high temperature requirement for their decomposition process to take place. Also, Li et al., (2018) compared the effect of $CuSO_4$ an TiH_2 as foaming agent, the compressive stress and energy absorption of porous Al using $cuso_4$ was higher as compared to porous Al/TiH_2. to overcome the problems associated with the usage of blowing agents as pore forming materials, space holders were applied by researchers. Razali et al., (2013b) employed NaCl particles as space holders and studied their effect on the mechanical properties of porous Al and observed that the compressive strength decreases with increase in size due to presence of thin walls. However, their porosity increment increased their energy absorption

capacity as well. Conversely NaCl particles result in the formation of irregular pores and also take a long time to leach out of sintered composite sample (Salvo et al., 2018). Further the usage of carbamide (ammonium bicarbonate) as space holders in porous Al resulted into better and controlled porosities (shape and size), enhanced compressive strength and it increased with increasing sintering temperature and time (Bafti & Habibolahzadeh, 2010). Yet the salt-based space holders have limitation of withstanding higher temperatures and causes corrosion of metals and alloys during dissolution process as a result of higher salt concentration.

Polymers that are water-soluble such as PMMA particles have proved to be promising when used as space holders. PMMA particles have been used as space holders in porous composites, resulting in efficient control over porosities, pore shape and pore size thus controlling densities. Moreover, decomposing at lower temperature 350˚- 400˚C, and leaving almost negligible residue behind (Bi et al., 2015; Tatt et al., 2021).

2.4 PROCESSING TECHNIQUES

Several techniques have been employed by researchers to develop Porous Al composites, mainly melt route, and powder metallurgy route.

2.4.1 Melt Route

In this method, the metal powder mixture is melted in graphite crucible and the melt is stirred at some stirring speed using the mechanical stirrer, the reinforcements are added to the melt during stirring. Followed by adding foaming agent to the melt that decomposes and releases gases. The uniform gas bubbles are formed by stirring resulting in formation of porous composite. Finally, after the foaming process, the metallic die containing the porous composite withdrawn from the furnace and cooled in

compressed air. Aldoshan & Khanna, (2017) fabricated CNT and SiC reinforced Al foams through melt route. This process resulted in an increase in the plateau stress, peak stress and energy absorption in addition increased their relative density; though, there was a decrease in densification strain with the increase in relative density. Also, with increased strain rate values dynamic compressive properties improved. Further, Das et al., (2020) developed porous Al composite via melt route by adding SiC as thickening agent and calcium hydride as foaming agent, moreover graphene was added to strengthen the cell walls of the foam. The plateau stress and energy absorption were found to have sensitivity towards strain rate. With increased strain rate values plateau stress of foams increased. Karuppasamy & Dennison, (2018) fabricated porous Al composites through melt route and were found to have better porosity and good mechanical properties. Although, the melt route is the most applied technique for the development of porous composites due to their ease in manufacturing. Since it requires lesser fabrication processes. But their high temperature requirement to melt the metal matrix limits their usage. Further, the uniform distribution of reinforcements is difficult to achieve resulting into non uniform distribution and agglomeration of micro and nano sized reinforcements, furthermore this process requires the ceramic addition to stabilize the melt mixture and does not allow control over porosities during foaming process. It also requires machining of parts developed for finishing due to their inability to develop composites near to net shape and complex geometries.

2.4.2 Powder Metallurgy Technique

The development of porous metals via powder metallurgy (PM) technique employing space holder as pore forming agents is one of the most diversified and constantly evolving metalworking methodologies for fabricating various shapes and sizes. The

main benefit of PM involves producing parts near to net shape with high dimensional accuracy and high productivity by involving limited use of materials and energy as a result there occurs minimal waste of raw materials (Hassan, 2019). It allows proper control over porosities, pore shape as well as pore size and uniform distribution of reinforcements in porous composites. The key processes include mixing, compaction, and sintering. Sintering temperatures are important in determining the mechanical properties of porous composite by affecting the bonding between metal matrix and reinforcements (Vairamuthu et al., 2010).

Yang et al., (2020) prepared CNT-reinforced porous Al composite using PM technique, as demonstrated in Figure 2.7. In this technique, composite powders were ball milled, mixed with carbamide particles (space holder) based on volume fraction and cold pressed. Then, the specimens were introduced to a water bath at 80 °C for several hours and sintered. This technique resulted in the uniform distribution of CNT and good interfacial bonding, leading to an improved fatigue strength of composite.

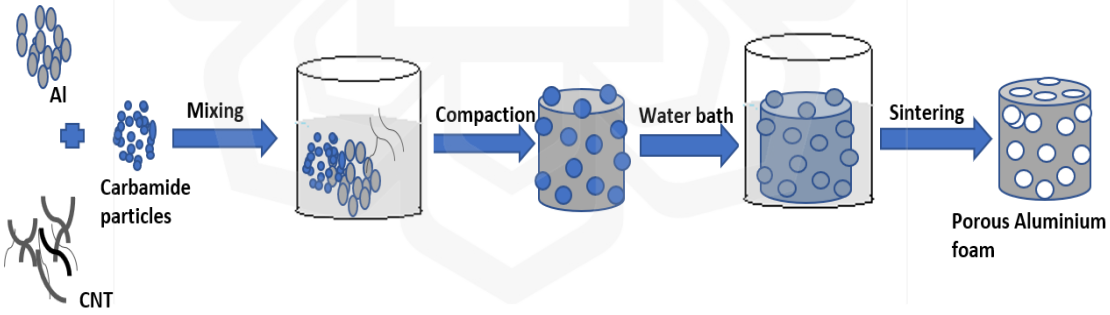

Figure 2.7 Powder metallurgy (space holder technique) for the fabrication of Al/CNT foams

The PM technique also allows the control over pore shape and size, that in turn affects the density and mechanical properties of porous Al composites. Jiang et al., (2007) observed that the increase in pore size and relative density improved the compressive stress–strain. Also, Ma et al., (2018) developed the CNT-reinforced porous Al matrix

composite via PM route and observed an improved pore uniformity and pore size resulting into improved compressive properties. Duarte et al., (2015) also developed an Al-CNT-based porous composite by employing the PM technique and found well dispersed, non-agglomerated, directionally aligned and stretched CNTs in the Al matrix resulting into improved Vickers microhardness value of the porous composite.

2.5 PROCESS PARAMETER AND COMPOSITIONAL OPTIMIZATION

The properties of the resultant porous composites developed depend on the process parameters as well as composition of the composite (Begum et al., 2020; Surace et al., 2009b). The porous composites developed using PM technique are greatly influenced by the process parameters such as (compaction pressure, sintering temperature and time). The importance of adequate compaction pressure is to mechanically destroy the oxide film present on the surface of metal surface and bring the fresh metallic surface in contact for effective bonding between metal particles and with other constituents of composites. The formation of fresh metal–metal contacts during compaction are also required to fuse the constituents together in the subsequent sintering process to get better bonded and an interconnected metallic framework (Manohar et al., 2020). Researchers have extensively studied their influence by optimizing them and evaluating the most important parameters and their values to develop composites with better properties (Küçük et al., 2017; Madgule et al., 2022).

If the cost and time allow, a Design of Experiments (DOE) based Taguchi's L_9 orthogonal array is preferred because more parameters of each level can be tested. DOE is a statistical analytic tool that helps to detect the relevant factors for the fabrication process involving planning and experimentation. Taguchi's L_9 orthogonal array is a planning and organizing tool for the selected parameters and their levels. The

experiments are conducted based on the nine sets of parameters acquired from the L_9 orthogonal array to acquire potential response factors influencing the input variables. Such methods allow the designer to control the changes by analyzing the responses through limited test runs. Researchers have applied this concept and demonstrated its effectiveness in optimizing the properties of composites. Further, the statistical analysis is carried out using Analysis of variance (ANOVA). It is a statistical procedure that is commonly used to calculate the percentage effect of each factor on experimental data. The ANOVA table aids in determining which variables need to be controlled for an analysis. Using this statistical analysis, the results are predicted and compared with experimental results to find the deviations, followed by finding the optimum processing parameters. Further, a verification experiment is conducted, and it is an effective tool for detecting any possibility of interactions between control parameters. Under optimal conditions, if the predicted response is different from the observed response, it indicates that the interactions are significant. However, in case the predicted and observed responses match, the interactions are unlikely to be significant, and the additive model reflects good estimation. Further, the orthogonal factorial Taguchi experimental design has been applied by researchers to determine the optimum process parameters and composition to produce Mg matrix carbide-reinforced composites using PM technique. Accordingly the parameter and reinforcement levels maximizing relative density and microhardness values were evaluated (Kumar et al., 2023). In another study the parameters such as composition (Al fraction), compaction pressure and the sintering time for the development of porous Al were considered for optimization. The response results (relative density and plateau stress) obtained using DOE were further evaluated using ANOVA to recognize the most influential variables. on the quality of the porous material. It was observed that the Al content affects the relative density and compressive

stress significantly. (Surace et al., 2009b). A similar technique has been applied to optimize the process parameters for the development of Al based composite developed via powder metallurgy (PM) route. Sintering time, sintering temperature and compaction pressure were the three main input factors and density, Vickers hardness and compression strength were the response factors. The influence of individual input parameters has been analyzed using Taguchi based S/N ratio and ANOVA. Finally, the parameter levels that produced the best composite material were acquired (Vairamuthu et al., 2010). Moreover, the process parameters and composition optimization for Al–graphite composite to improve their fracture toughness was carried out using a similar technique. The study considered the a/W ratios, composite composition and testing methods as input parameters. The analysis revealed that the material's fracture toughness was primarily influenced by the a/W ratio and composition, while the testing methods affected insignificantly (Begum et al., 2020).

This design is primarily used in industrial applications to investigate the impact of various control factors. This method differs from other statistical experimental design methods in dividing the experiment's effective parameters into two categories: controllable and uncontrollable. It also enables us to study the whole space of parameters by conducting few experiments only. Thereby requiring less energy and material for the analysis. Considering these benefits, design of experiments (Taguchi's L_9 orthogonal array) followed by ANOVA was considered in this study to evaluate the effect of process parameters and composition on the compressive properties of porous Al composites.

2.6 APPLICATION OF POROUS METALS AND THEIR COMPOSITE

The lightweight porous metals and composites have been used to reduce the weight of mechanical and building structures such as an European distributor (Shinko) replaced developed the entire Al part of the tool with porous Al resulting into reduction in weight from 82 kg to 32 kg (Schäffler et al., 2008). Also, a composite beam was fabricated by embedding porous Al alloy (AlZn10Si8Mg) in the AlZn10Si8Mg alloy. The transverse beam was found to dampen up to 370 Hz of vibration frequencies by means of interface slipping or internal friction between the core and the skin. In this frequency range, sound attenuation of up to 60% was achieved (Banhart, 2007). Moreover, an Austrian manufacturer manufactures closed-cell Al foams annually as a crash absorber element through automated production technology for Audi cars. On the other hand, as a result of flexibility in terms of tailoring structure and properties, a porous Ti have been developed for bone implant application using PM technique, where ammonium bicarbonate was used as space-holder (Torres et al., 2012).

Also, the Al-10wt.% SiC porous composite has been used as permanent cores in bicycle rods. Such bicycle rods, with an Al-composite based foam core resulted into 35% weight reduction as compared to the dense metallic component without a foamed core and produced by the same technology (Vicario et al., 2016). The energy absorption characteristics of Al composite foams need to be assessed as they can be used for the absorption of crash energy in high-speed vehicles during impacts. These energy-absorbing materials are employed for the crashworthiness design of vehicles for ensuring their safety (Lukaszewicz, 2014). The crash boxes made of thin-wall metal columns primarily composed of mild steel and Al are used in the automobile body of white (BIW) to absorb crash energy during an impact. These thin-wall metal columns are economical and conventional materials for energy absorption used in ships, trains,

high-load factory products and automobile (Baroutaji et al., 2017). Li et al., (2019) developed low-cost and lightweight porous Al alloy (Al lSi$_7$Mg alloy) composite with MnO_2 as reinforcements and oyster shell particles as foaming agents for railway transportation via the melt route.

Casting porous Al cores with Al shells can be used to form low-density and lightweight components, as shown in Figure 2.8 (a). Figure 2.8 (b) also illustrates a prototype of an automobile engine mounting bracket of BMW manufactured by LKR Ranshofen, Austria. This part is made of a porous Al (foam core) (Metcomb) with a cast shell. The length of the 25 cm part is strong enough to bear the full weight load of an automobile engine (Banhart, 2014). Also, the porous material-based cores made of Al for machine tools as shown in Figure 2.8 (c) absorb the vibrations produced by the motion of parts that was also observed in case of machine tools increasing their accuracies.

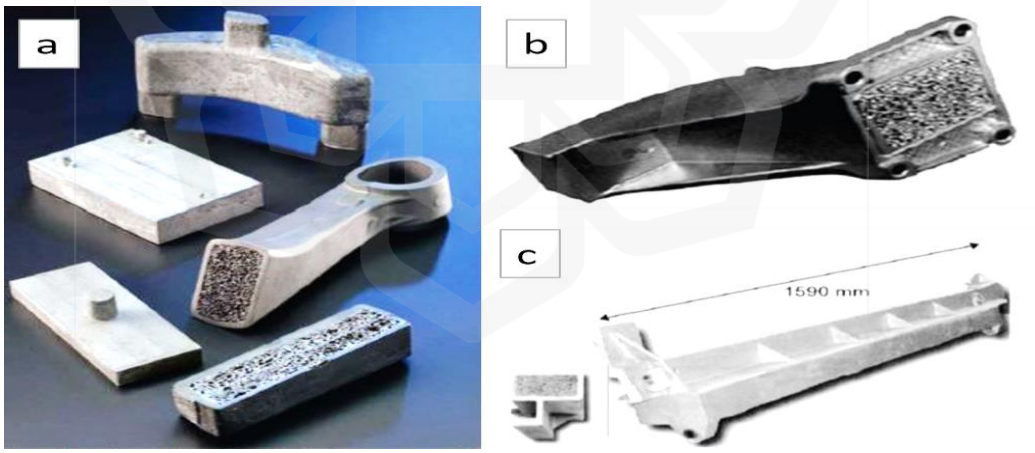

Figure 2.8 (a) Products with cores of porous Al (Stöbener & Rausch, 2009); (b) prototype of the engine mounting bracket of BMW and (c) crossbeam of a machine tool with an porous Al core (foam core) (Banhart, 2014)

The porous Al alloy (AlSi-alloy) reinforced filled in the A-pillar of a Ford passenger car filled provided an improvement of 30% in crash energy absorption and the weight increase was only 3%. Valeo and Cymat in their joint program developed a crash box

for Valeo's front-end module systems (Banhart, 2010). Since porous composites especially porous Al composites have been used as lightweight materials in various applications mostly as cores in the structures. Thus, they have a great prospect in reducing weight as well as enhancing the strength of machines and automotive structures if applied as cores and fillers. Therefore, more extensive research is required to enhance the properties of porous Al composites.

2.7 SUMMARY

This chapter provides an overview of the research conducted to enhanced properties and performance of porous composite. It summarises the efforts of many researchers aiming to enhance the characteristics of these materials by adding various alloying elements and hard reinforcements in metal matrix. The inclusion of alloying elements strengthens the matrix while as reinforcements such as ceramic and carbonaceous materials improve the overall strength of the porous composites. So far carbonaceous reinforcements have proved to improve the properties of porous composites remarkable, but these are associated with challenges such as clustering tendency, non-uniform dispersion resulting into non uniform stress concentration during loading. Also, their bonding and wettability with Al matrices have some limitations. Further, to attain tailored porosities the usage of blowing agents and salts high decomposition temperature requirements and cause corrosion of metals due to saline concentration during dissolution respectively. While the usage of space holders was beneficial as compared to other pore forming agents, because of their ease of control over the porosities of porous materials, their strengths and low decomposition temperature requirement. Moreover, PM technique was found to be beneficial in tailoring the distribution of reinforcements and porosity in porous composites.

Considering the fact that carbonaceous reinforcements can improve the properties of porous composites remarkable and to prevent the problem of clustering, diamond particles were used as reinforcements in porous Al composites and the wettability between Al matrix and diamond was improved by using coated diamond. The coating material bonds metallurgically with diamond and also wets the Al matrix, resulting into better interfacial bonding. Further, the high temperature requirement for decomposition of space holder particles can be avoided by using PMMA particles as space holders, that decompose at low temperature leaving almost no residue behind. Finally, PM was employed to develop porous composites in order to tailor porosities and compressive properties for energy absorption applications.

As from the existing literature the properties of porous composites were found be influenced by the process parameters of production technique and composition of porous composites. Thus, in the present work the efforts to seek improved performance especially in terms of processing parameters and materials optimization were explored. Such porous composites can be potentially applied as core or fillers in lightweight automobile parts to absorb energy during impact and in other structural and functional systems.

CHAPTER THREE

EXPERIMENTAL PROCEDURE

3.1 INTRODUCTION

This chapter describes the experimental procedures, methodological design plan and data optimization analysis utilized to develop and analyse porous aluminium (Al) composites in this research study. It presents both experimental as well as statistical approach in conducting the research. The powder metallurgy techniques were applied to fabricate the porous Al composite. and based on the design plan developed by Design of experiments (DOE) (L_9 Taguchi orthogonal array), experiments were conducted. Then, the optimization of processing parameters and PMMA content, PMMA particle size and Ti-coated diamond content was carried out.

For parametric optimization, the parameters of powder metallurgy technique including sintering temperature, compaction pressure and sintering time were considered as input factors while the plateau strength and energy absorption capacity were considered as output responses. Further using experimental and statistical analysis, the morphological, porosities, densities and compressive properties of the resultant porous composite were evaluated. To find the optimum values of process parameters, PMMA size and content and diamond content required to get the porous composites of better properties.

3.2 EXPERIMENTAL DESIGN PLAN

Experimental design plan is a process of properly planning the input variable factors to determine the impact on response variables. A design plan is an effective procedure for planning experiments for evaluating the data obtained in order to yield

desirable outcomes. In the present study the experimental design plan was developed via DOE using L_9 Taguchi orthogonal array. he 9-run array is more effective, as for each level of any chosen parameter all three levels of the other parameters are also tested. Orthogonal arrays are the best and most common type of Taguchi array for optimization of parameters. These are also a special standard of experimental design that only requires a small number of experimental trials to be run in finding the effects of main factors on the output. The experimental design proposed by Taguchi involves the utilization of orthogonal arrays in organizing the input factors that affect the responses and the levels at which they should be varied. Instead of testing all possible combinations (time consuming and ineffective cost), the Taguchi method involves testing pairs of combinations. This allows the collection of the necessary data to determine the effects of input factors on the output performance.

Considering these benefits, DOE (Taguchi's L_9 orthogonal array) was considered in this study to evaluate the effect of process parameters and composition on the compressive properties of porous Al composites. According to the Taguchi L9 Taguchi orthogonal array, the experimental design plan consists of three factors at three levels, (parameter (P) = 3 and Level (L) = 3) as mentioned in Table 3.1 and Table 3.2. Before opting for an orthogonal array, the least number of experiments to be carried out was calculated using the Equation. (3.1) as mentioned below:

$$N = 1 + N_V(L - 1) \qquad 3.1$$

Where, N = Number of experiments to be conducted, N_v = Number of parameters, L = Number of levels. In this work, N_v = 3 and L = 3, Hence, N=9.

Table 3.1 Factors and levels in L_9 Taguchi orthogonal array experimental design plan for parameter optimization

Process parameters		**Levels**		
		Level 1	Level 2	Level 3
(a)	Sintering Temperature (˚C)	580	590	600
(b)	Sintering Time (min)	60	90	120
(c)	Compaction pressure (MPa)	350	380	400

Table 3.2 Factors and levels in L9 Taguchi orthogonal array experimental design plan for composition optimization adhesive

Composition		**Levels**		
		Level 1	Level 2	Level 3
(a)	Ti-coated diamond (wt.%)	4	8	12
(b)	PMMA content (wt.%)	20	25	30
(c)	PMMA size (μm)	75	125	150

Table 3.3 and Table 3.4 demonstrate the Taguchi orthogonal arrays when values of P and L were set as three which were specifically designed to achieve objective one and objective two, respectively. In this Taguchi method a, b and c were set as the parameters and 1, 2 and 3 as the levels. After conducting experiments as per orthogonal array and observing the change in critical properties, optimizing the level of processing parameters using data analysis was done based on the analysis of variance (ANOVA). A statistical analysis of ANOVA was performed to investigate the contribution of each input factor in attaining the process outcome.

Table 3.3 Taguchi's orthogonal array showing experimental design for parameter optimization

Taguchi, P=3, L=3							
Run	**a**	**b**	**C**	**X**	**a**	**b**	**c**
1	1	1	1	X_1	580	1	450
2	1	2	2	X_2	580	2	500
3	1	3	3	X_3	580	3	600
4	2	1	2	X_4	630	1	500
5	2	2	3	X_5	630	2	600
6	2	3	1	X_6	630	3	450
7	3	1	3	X_7	650	1	600
8	3	2	1	X_8	650	2	450
9	3	3	2	X_9	650	3	500

Table 3.4 Taguchi's orthogonal array showing experimental design for compositional optimization

Taguchi, P=3, L=3							
Run	**A**	**b**	**C**	**X**	**a**	**b**	**c**
1	1	1	1	X_1	4	20	75
2	1	2	2	X_2	4	25	125
3	1	3	3	X_3	4	30	150
4	2	1	2	X_4	8	20	150
5	2	2	3	X_5	8	25	125
6	2	3	1	X_6	8	30	75
7	3	1	3	X_7	12	20	150
8	3	2	1	X_8	12	25	75
9	3	3	2	X_9	12	30	125

3.3 SELECTION OF INPUT VARIABLES

The strength of the composite can be increased by forming a strong interface bond between the matrix and the reinforcements. This can be accomplished by selecting the appropriate processing parameters. As per studies the most important parameters of PM technique influencing the properties of resultant composites are compaction pressure,

sintering temperature, and sintering time (Küçük et al., 2017; Madgule et al., 2022). Thus, based on previous studies, the following parameters (sintering temperature (°C), compaction pressure (MPa) and sintering time (min)) were chosen as the input factors to optimize the compressive properties (plateau strength and energy absorption capacity) as stated in the first objective.

The compaction process is crucial as this process holds together the neighboring powder particles by forming cold welds, which impart enough green strength to the compacts for handling further processes. The sintering time on the other hand affects the diffusion rate and grain growth of the composite. Additionally, the temperature selection for the sintering process should be below the melting point of the major component of the composite to ensure the optimum grain growth that sufficiently fills the voids and hence strengthens the composite. Moreover, the sintering temperatures also play a major role in controlling the microporosities formed in the porous composite that have a significant impact on its strength (Manohar et al., 2020). Moreover, some studies also revealed that the composition of composites also influence their properties (Begum et al., 2020; Surace et al., 2009b).

Thus, in the present study compositional optimization was also carried out to analyse the effect of input factors such as diamond particle content (wt.%), PMMA content (wt.%) and PMMA particle size (µm) on the response factors (plateau strength (MPa) and energy absorption capacity (MJ/m^3)) as stated in the second objective. Furthermore, based on the results or responses obtained from the first and second objective, porous Al composite with various content of uncoated and Ti-coated diamond were developed to study the effect of varying content of uncoated and Ti-coated diamond on the plateau strength (MPa) and energy absorption capacity (MJ/m^3) of porous composites and to find the composite of better compressive properties.

3.4 SELECTION OF RESPONSE VARIABLES

Porous Al composite are recently known to have excellent compressive properties due to their peculiar porous structure (Salehi et al., 2015). This property allows them to have good energy and impact absorption capabilities that is critical for the design of building or automotive structures. Therefore, in this study, the plateau strength and energy absorption capacity were chosen as the response variable to investigate the effect of input factors on the performance of porous composite.

3.5 EXPERIMNENTAL SET UP

The raw materials used in this present study included the pure Al powder mixed with magnesium (Mg), copper (Cu), Boron (B) and tin (Sn). The matrix material was selected based on the requirement of lightweight and high strength material.

3.5.1 Matrix alloy

The Al alloy matrix was formed by mixing Al powder with magnesium (Mg), copper (Cu), Boron (B) and tin (Sn) powders as presented in Figure 3.1. These alloying elements were added to the Al powder in fixed amount as tabulated in Table 3.5, to facilitate liquid phase sintering and disrupt the oxide layer present on the surface of the Al particles and to strengthen the Al matrix by forming low temperature strengthening phases. The quality of these powders was controlled by using powders of higher purity approximately 99.5 %.

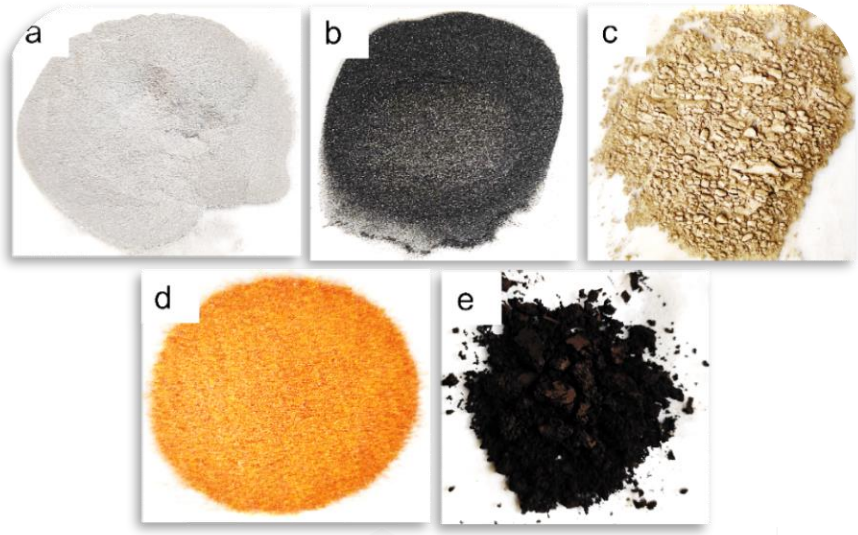

Figure 3.1 Metallic powders for matrix alloy, (a) Aluminium (Al), (b) Magnesium (Mg), (c) tin (Sn), (d) Copper (Cu), and (e) Boron (B)

Table 3.5 Composition of Alloy matrix

Composition Alloy matrix	**wt.%**	**Average particle size (µm)**	**Purity (%)**
Al	94	45	99.7
Mg	1	10	99.9
Sn	2	45	99.5
Cu	2	10	99.5
B	1	75	99.4

3.5.2 Reinforcement material

Titanium coated diamond was used as reinforcement material as shown in Figure 3.2. Ti coating prevents the formation of undesirable carbides and improves the strength of interfacial bonding between Al matrix and diamond particles (Zhang et al., 2017a). It is found that the Ti coating could significantly improve the wetting property that led to the improvement of the relative density and strength of the composite (Yang et al., 2009). In the current study, Ti-coated diamond particles with an average particle size of 45 µm served as the reinforcement material.

Figure 3.2 Ti coated diamond powder as reinforcement material

3.5.3 Space holder material

On the other hand, polymethylmethacrylate (PMMA) particles was introduced because of their superior formability, strong biocompatibility, and lower decomposition temperature (between 360 and 400 °C), which results in complete decomposition with no residue left behind (Bi et al., 2015; Tatt et al., 2021).The weight percentage of Ti-coated diamond particles, PMMA content and PMMA particle size in achieving the objective number one were fixed at 5 wt.%, 30 wt.% and 150 µm in which the input processing parameters including compaction pressure, sintering temperature, and sintering time were varied accordingly. To achieve objective number two, the optimum values of processing parameters that were successfully obtained from objective number one were fixed whereas Ti-coated diamond content, PMMA particle content and PMMA particle size were varied accordingly. The PMMA space holder at different particle size of 75 µm, 125 µm, and 150 µm are shown in Figure 3.3.

Figure 3.3 Various sizes of PMMA particles, (a) 75 µm, (b) 125 µm, and (c) 150 µm

3.5.4 Experimental equipment's used

The porous Al composite was developed using PM technique involving three steps: mixing, compaction, and sintering. The powders were thoroughly mixed using horizontal lab roll ball mill (Model: QM-5) followed by the orbital shaker. The compaction process was then carried out using cylindrical die with a diameter of 10 mm in a hydraulic tablet press of pressure range 0-24 tons. Compacted specimens were then sintered in a mini tube furnace (Model:CY-O1200501CS) in argon gas atmosphere. The morphological analysis of the starting powder and metallic powder mixture was executed via a scanning electron microscope equipment (SEM) (JEOL JSM-6300F). The X-ray diffraction (XRD) patterns were acquired via XRD equipment (XRD, PAN analytical empyrean 1032) using Cu Kα radiation to identify their possible phase transformations. The XRD patterns were documented for 2θ, ranging from 20° to 80°. The compressive properties were measured using uniaxial compression testing machine with a cross head speed of 0.5 mm/min at room temperature and load cell of 30 kN (Dartec model3500 universal testing machine). Finally, the experimental and optimization procedure were carried out using analysis of variance (ANOVA).

3.6 PREPARATION OF POROUS AL COMPOSITE

The fabrication of porous Al composites was carried out using powder metallurgy (PM) technique as shown in Figure 3.4, due to their ability to develop samples near to net shape with high dimensional accuracy and high productivity with limited use of materials and energy as a result there occurs minimal waste of raw materials (Hassan, 2019). It also allows proper control over porosities, pore shape as well as pore size and uniform distribution of reinforcements in porous composites. This technique involved three stages of process including powder mixing, compaction and sintering. Initially

each powder was weighed according to their proportions required for a particular composition in preparing porous composite. Then, these powders were mixed accordingly. In the current research work, mixing was done in four steps. Then, a suitable amount of final powder mixture was compacted followed by two steps sintering.

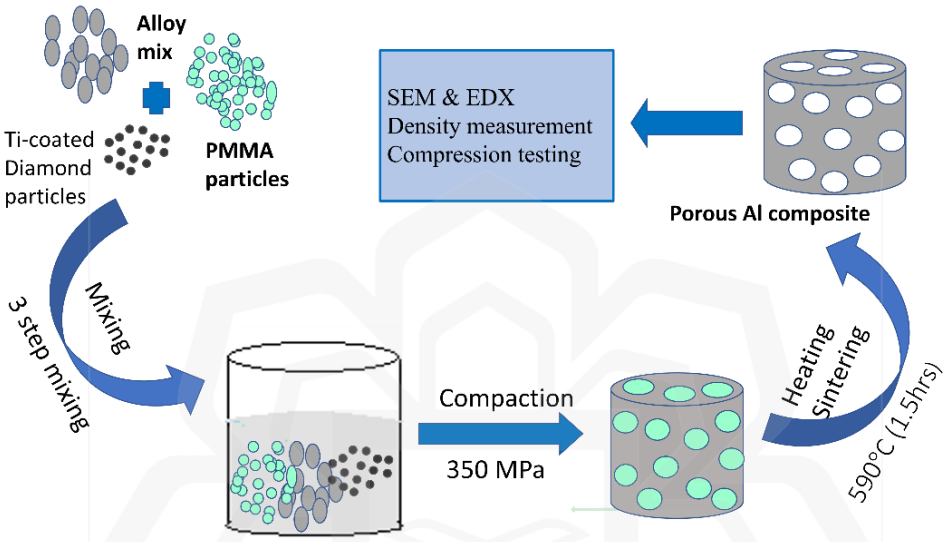

Figure 3.4 Schematic diagram of fabrication of porous Al composite

According to Taguchi orthogonal array, nine set of samples with varying input factors and output factors were developed as demonstrated in Table 3.6 and Table 3.7 respectively.

Table 3.6 L9 Orthogonal array with design factors for parameter optimization

S.no	Sintering temperature (°C)	Compaction pressure (MPa)	Sintering time (min)	Plateau strength (MPa)	Energy Absorption capacity (MJ/m^3)
1	580	350	60	-	-
2	580	380	90	-	-
3	580	400	120	-	-
4	590	350	120	-	-
5	590	380	90	-	-
6	590	400	60	-	-
7	600	350	120	-	-
8	600	380	60	-	-
9	600	400	90	-	-

Table 3.7 L9 Orthogonal array with design factors for composition optimization

S.no	Ti-coated diamond content (wt.%)	PMMA content (wt.%)	PMMA size (µm)	Plateau strength (MPa)	Energy Absorption capacity (MJ/m^3)
1	4	20	75		
2	4	25	125	-	-
3	4	30	150	-	-
4	8	20	150	-	-
5	8	25	125	-	-
6	8	30	75	-	-
7	12	20	150	-	-
8	12	25	75	-	-
9	12	30	125	-	-

3.6.1 Mixing

The metallic powders were mixed in four steps. Initially alloy matrix mix was prepared by mixing metallic powders in a ball mill with a ball to powder ratio of 10:1 for 24 h at a fixed speed of 300 rpm. Then, Ti-coated diamond particles were mixed with the metallic mixture known as elemental powder mixture using oscillating mixer for 2 h at the speed of 800 rpm. The resultant powder was then mixed with PMMA particles for 2 h using oscillating mixer at a fixed speed of 800 rpm. Before mixing PMMA particles with the matrix-reinforcement mix, a bit of low sulfur content (CLE) safe oil was added as a binder to minimize the powder mixture segregation during processing. The resultant powder mixture was then known as final powder mixture.

3.6.2 Compaction

After mixing process was completed, the compaction of the final powder mixture was carried out at three different compaction pressures of 350 MPa, 380 MPa and 400 MPa to serve objective number one using hydraulic compaction machine as shown in Figure 3.5. It is important to note that once the optimal compaction pressure was successfully determined, the resultant compaction pressure was used and fixed to serve objective

number two and objective number three. The final powder mixture was then compressed in a cylindrical die having diameter of 10 mm as shown in Figure 3.5.

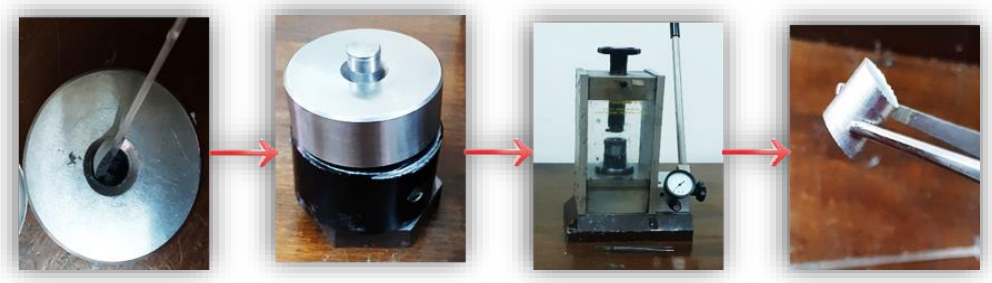

Figure 3.5 Compaction process of final powder mixture using hydraulic press

3.6.3 Sintering

The compacted specimens undergo sintering for adding strength and integrity to them. The cylindrical specimens were sintered at three different sintering temperatures (580 °C, 590 °C and 600 °C) and three different sintering time (60 min, 90 min and 120 min). A tubular furnace was utilized to perform the sintering process under controlled Argon (Ag) gas atmosphere. It is important to note that once these processing parameters had been optimized, the resultant sintering time and sintering temperature were used and fixed to achieve objective number two and objective number three. In this process, two steps sintering technique were implemented in which the specimens were initially heated at 450 °C for 10 minutes under the heating rate of 2 °C/min to ensure complete decomposition of PMMA space holder particles in the composite body followed by sintering at various temperatures and times as shown in Figure 3.4. The resultant sintered specimens having size of 10 mm ×10 mm (1 cm x1 cm) developed in this study are shown in Figure 3.6.

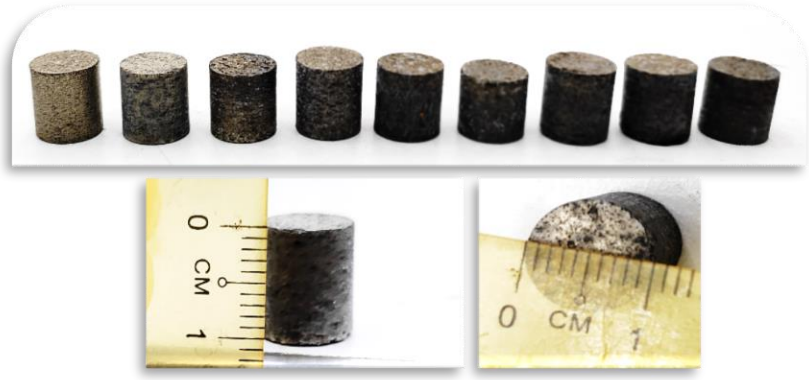

Figure 3.6 Sintered samples of size 10×10mm

3.7 CHARACTERIZATION AND TESTING

The resultant porous Al composite specimens were then undergone further analyses including morphological examination, density, and porosity determination by Scanning electron microscopy (SEM), Electron dispersive X-ray (EDX), Thermogravimetric analysis (TGA), X-ray diffraction (XRD) analysis and Archimedes principle respectively followed by compressive properties analysis.

3.7.1 Characterization

Metallography involved the study of the physical structure and components of the porous Al composite samples developed from the experimental runs. Samples from each of the experimental run were sectioned out from the larger piece of the composite using diamond cutter as shown in Figure 3.7.

Careful steps were taken to ensure that the sectioned sample still represents the feature of the larger piece, and preserves the information required to be further investigated. During the cutting process, coolant was introduced to avoid unnecessary changes in the feature of the resultant composite specimens.

Figure 3.7 Sectioned samples from porous Al composite

Microstructural procedure involved the preparation of porous Al composite specimens that required in obtaining an appropriate microstructure or at least microstructure in a condition that presented a clear and satisfactory surface examination. In this process, the samples were immersed in an acetone for the duration of two minutes after sintering to remove the impurities followed by cutting the specimens in a small portion for microstructural analysis.

3.7.1.1 Morphological analysis

The cross section of the resultant porous Al composite specimens was examined using SEM and EDX. These analyses were used to observe the surface morphology, topography and elemental composition of raw materials, powder mixtures and the resultant composite. Moreover, JEOL JSM-6300F type equipment was used to determine the nature of the particle distribution, particle size variation and morphological structure of the raw materials, elementary powder mixture, final powder mixture and the resultant porous composite.

This analysis was performed by scanning specimens with a focused beam of electrons. These electrons interacted with atoms in the specimens producing various signals that could be detected and contained information about the sample's topography

and composition. Moreover, an EDX incorporated with SEM was then utilized to determine the analytical composition of the specimens as shown in Figure 3.8. It entailed producing an X-ray spectrum from the SEM's whole scan area.

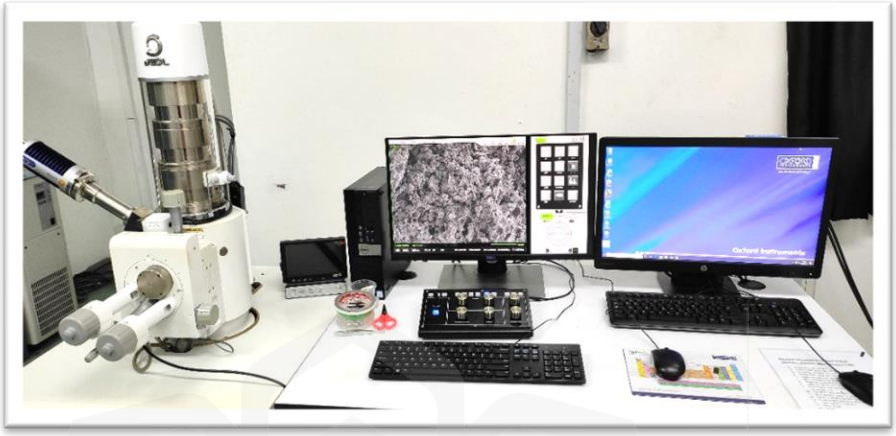

Figure 3.8 Schematic overview of scanning electron microscope with EDX

3.7.1.2 Phase analysis

The XRD analysis is carried out for phase identification of crystalline material. In this this analysis, PAN analytical empyrean 1032 XRD diffractometer was used to analyze the raw materials, powder mixture as well as the resultant porous Al composite for phases identification and the presence of any possible compounds based on the input process parameter variation. The equipment step scanning mode was set at 3°/min at the scanning range of 20°-80°. The specimens were then scanned through the range of 2θ angles and all possible diffraction directions of the lattice were detected and recorded as demonstrated in XRD set up in Figure 3.9. Conversion of the diffraction peaks to d-spacing allows the identification of the specimen’s peaks, as each peak has a set of unique d-spacing which was then compared with the standard reference patterns in the International Center for Diffraction data (ICDD) database.

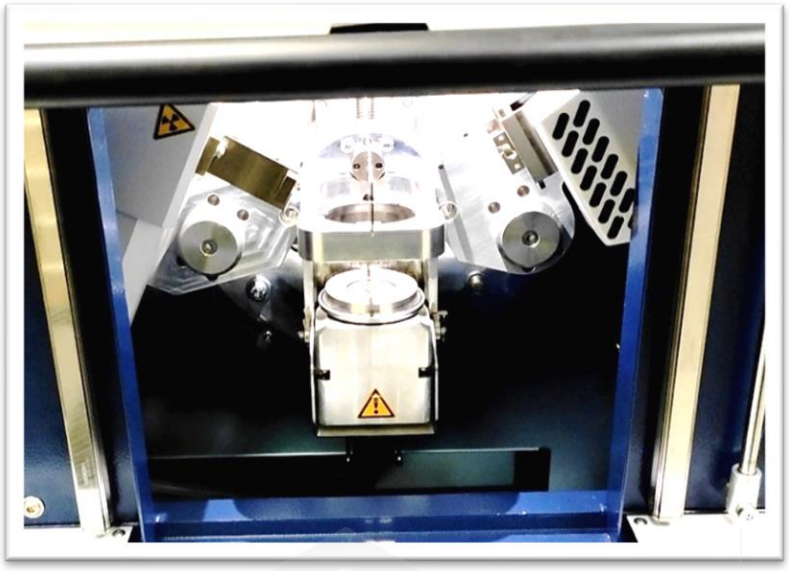

Figure 3.9 X-ray Diffraction set up

3.7.1.3 Density and porosity measurement

The density and porosity of the compacted and sintered composite were measured using the Archimedes principle. The sintered samples were weighed using an electronic balance to determine the dry weight (W_d). The specimens were then submerged in deionized water and vacuumed for two hours in a desiccator, as shown in Figure 3.10.. This allowed water to fill the open pores of specimens. The samples were then taken out of the deionized water, weighed, and the result was noted as saturated weight (W_{ss}). A densimeter, as shown in Figure 3.10, was used to determine the mass of the sintered samples submerged in liquid reading was recorded as the weight of saturated specimens, W_s. Finally the porosity of the sintered samples was calculated using the following equation (Jamal et al., 2016):

$$Porosity, P = \frac{W_{ss} - W_d}{W_{ss} - W_s} \times \rho l \qquad (3.2)$$

where saturated weight is denoted by W_{ss}, dry weight is denoted by W_d, weight of saturated sample submerged in liquid is indicated by W_s and ρl represents the density

of water. The density of the porous specimens was further calculated using the following equation:

$$Density, \rho = \frac{W_d}{W_d - W_s} \times \rho l \tag{3.3}$$

where ρ indicates the density of sample, W_d as dry weight of sample, W_s as weight of saturated sample submerged in liquid and ρl as the density of water which is equal to 1.

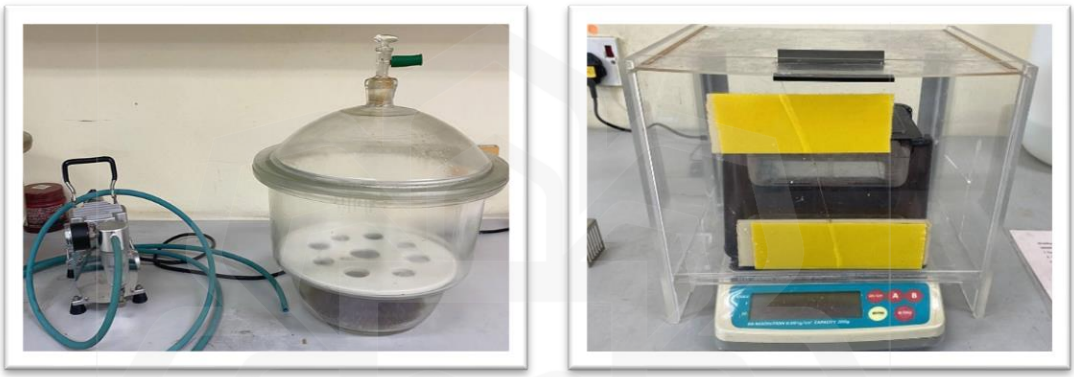

Figure 3.10 Desiccator with pump (right) and Densimeter (left)

3.7.2 Compression testing

: In this study, the compressive strength of porous Al composites with varying diamond content has been measured at room temperature using a universal testing machine, as shown in Figure 3.11. The load cell and crosshead speed were set at 30 kN and 0.5 mm/min, respectively. To reduce errors, tests were repeated, and the average compressive strength of a porous composite was used for further analysis. The compressive strength of the sample was determined employing the following equation:

$$Compressive\ strength, \sigma_c = \frac{F}{A} \tag{3.4}$$

where F denotes the applied force and A denotes the cross-sectional area of the sample.

Further, the energy absorption capacity of porous Al composite was determined was determined using the following equation. (Jamal et al., 2016):

$$W = \int_0^{\varepsilon} \sigma \, d\varepsilon \tag{3.5}$$

where W indicates the energy absorption capacity, σ indicates the compression stress and ε is the compression strain.

Figure 3.11 Compression testing machine with 30 kN load

3.8 SUMMARY

In this chapter, the experimental design, materials and procedure used in this research were explained in detail. Moreover, the sample preparation technique including the testing procedures were also described. The Taguchi orthogonal array was adopted for the systematic planning of experimental design followed by statistical analysis using analysis of variance (ANOVA). Powder metallurgy technique was employed to fabricate porous composite at varying input processing parameter including sintering temperature (°C), compaction pressure (MPa), sintering time (min), Ti-coated diamond content, PMMA content and PMMA particle size. The plateau strength (MPa) and energy absorption capacity (MJ/m^3) were evaluated as output responses. These responses were measured using universal compressive testing machine. Finally, the analysis of surface morphology of the raw materials, powder mixtures and the resultant

porous Al composite was performed using of SEM/EDX and XRD equipment as presented in detail in this chapter.

CHAPTER FOUR

RESULTS AND DISCUSSION

4.1 OVERVIEW

This chapter discusses the effect of processing parameters of the powder metallurgy (PM) technique on the morphology, porosity, and compressive properties of porous Al composites. The processing parameters including sintering temperature, compaction pressure, and sintering time were taken into consideration. Followed by discussion on the effect of titanium (Ti)-coated diamond content, PMMA particle content, and PMMA particle size morphology, porosity, and compressive properties of composites. In both cases the optimum values of the variables based on the compressive property's responses were acquired. The experimental runs were executed using experimental design formulated by Taguchi L_9 orthogonal array by employing these three parameters at three levels and nine sets of experimental runs were acquired. The analysis of variance and Taguchi-based S/N ratio were used to assess the effects of each individual input parameter. The optimal parameter levels to reach the maximum values for compressive properties (plateau strength and energy absorption capacity) were shown in the main effect plots. Furthermore, confirmation tests on the optimized parameters were conducted to confirm that the selected parameters were vital for controlling the compressive properties of the porous Al composite.

Further, the effect of varying content of uncoated and coated diamond on the microstructure, density, and compressive properties of porous composites that were developed at optimum processing parameters and at optimum PMMA size and content has been discussed. Finally, the optimum content of Ti coated diamond and the benefit

of using coated diamond in improving the compressive properties and performance of porous Al composite as compared to uncoated ones had also been discussed.

4.2 EFFECT OF PROCESSING PARAMETERS ON COMPRESSIVE PROPERTIES OF POROUS AL COMPOSITES

The processing techniques and processing parameters significantly influence the performance of porous composite (Daoud et al., 2021). It has been recorded that the sintering temperature, compaction pressure and sintering time contributed more impact on the properties of resultant porous composite when processing via powder metallurgy technique (Kumar and Madurai, 2020). Since compressive properties of porous composites are mainly by virtue of their porous structure and this porous structure is designed by the processes in the fabrication technique. Especially in the case of PM, where compaction process enables tailoring of uniform porosities by compacting homogeneous mixture of composite powder and space holders. Further, in the sintering process the bonding between the composite constituent particles occurs, thereby deciding the strength of resultant composite. Thus, in the current study, the investigation of the effect of different compaction pressure, sintering temperatures, and sintering time on the microstructural, density, porosity and compressive properties was carried out. The DOE based statistical analytic tool was applied to detect the relevant factors for the fabrication process involving planning and experimentation (Jankovic et al., 2021). Such method also allows to control the changes by analyzing the responses through limited test runs. Researchers have applied this concept and demonstrated its effectiveness in optimizing the properties of composite (Weissman & Anderson, 2015). Therefore, the DOE method was chosen to analyze the effect of processing parameters on compressive properties and obtain their optimum values for achieving better results. Among all DOE tools, the Taguchi's L_9 orthogonal array was applied to get the

experimental runs required to acquire potential response factors that influence the input variables.

Taguchi's L_9 orthogonal array is considered as one of the most efficient planning and organizing tools for optimizing multifactor conditions, requiring only a few experiments. This technique is mostly preferred where experiments involve use of expensive material and fabrication process. Thus, the robust L_9 orthogonal array design variables were applied in this study to evaluate how sintering temperature, compaction pressure, and sintering time affects the compressive properties of porous Al composites. As shown in Table 4.1, the various input factors, and their levels. Also, Table 4.2 shows a well-organized typical L_9 orthogonal array with all possible combinations. Nine experiments were carried out based on the selected parameters and their levels. Following the tests, the two-response factors, plateau strength and energy absorption capacity, were obtained, as shown in Table 4.2. However, the current investigation assumed that the problem was linear and thus, carried out statistical analysis using ANOVA, based on the linear regression model described in Equation (4.1) as follows:

$$Y = b_0 + AX_1 + BX_2 + CX_3 \quad 4.1$$

where Y represents the dependent variable (plateau strength and energy absorption capacity), b_0 is the intercepts or reaction variable, and A, B, and C are the sintering temperature, compaction pressure, and sintering time, respectively.

Table 4.1 Control factors (process parameters) and their levels

Factors	Symbol	Unit	Level 1	Level 2	Level 3
Sintering temperature	**A**	**°C**	**580**	**590**	**600**
Compaction pressure	**B**	**MPa**	**350**	**380**	**400**
Sintering time	**C**	**min**	**60**	**90**	**120**

In terms of cost, this approach meets the demands of solving problems in process optimization and significantly lowers the amount of time needed for experimental research and production expenses.

Table 4.2 L_9 orthogonal array layout with design factors

Runs	A	B	C	Plateau strength (MPa)	Energy Absorption capacity (MJ/m^3)
1	**580**	**350**	**60**	**21.34**	**5.33**
2	**580**	**380**	**90**	**22.02**	**5.78**
3	**580**	**400**	**120**	**21.30**	**4.65**
4	**590**	**350**	**120**	**26.72**	**8.32**
5	**590**	**380**	**90**	**31.06**	**9.23**
6	**590**	**400**	**60**	**25.46**	**7.38**
7	**600**	**350**	**120**	**24.78**	**7.25**
8	**600**	**380**	**60**	**21.63**	**6.50**
9	**600**	**400**	**90**	**30.02**	**8.32**

4.2.1 Morphology

Figure 4.1 (a) shows the SEM images of elemental powders and their mixture obtained on mixing the constituents of porous composite via three step mixing process. The mixing process resulted in the strain hardening of powder particles that caused brittleness, fragmentation, and formation of more equiaxed and finer particles. Moreover, mixing of PMMA particles with the CLE safe oil binder prior to mixing with metallic powder mixture was found to result in sticking of metallic powder mixture to the PMMA surface as shown in Figure 4.1 (b) Also, the metallic particles were observed to adhere on the surface of diamond particles as shown in Figure 4.1 (b). Also, metallic particles were observed to adhere on the surface of diamond particles as shown in Figure 4.1 (c). The adhesion of metallic particles on their surfaces is beneficial in terms of improving the bonding of PMMA and Ti-coated diamond with the alloy matrix during sintering process.

In the current study, Sn, Mg, Cu and B were incorporated in Al matrix to improve their wettability with the reinforcement particles. Sn enhances the fluidity and sintering properties of Al during the sintering process. While, Mg was added to improve the wettability of Al, by breaking down the stable oxide film present on the surface of the Al particles (Showaiter & Youseffi, 2008). Furthermore, Cu and B were

added to improve the strength of Al matrix (Ali et al., 2018; Dixit & Srivastava, 2019; Kang et al., 2021). Additionally, it has been reported that these elements impact the various characteristics of molten Al, such as the melting point during the formation of a porous structure, surface tension, and viscosity. The melting point and surface tension greatly influence the relative density and the cell size of porous structure (Kumar et al., 2023).

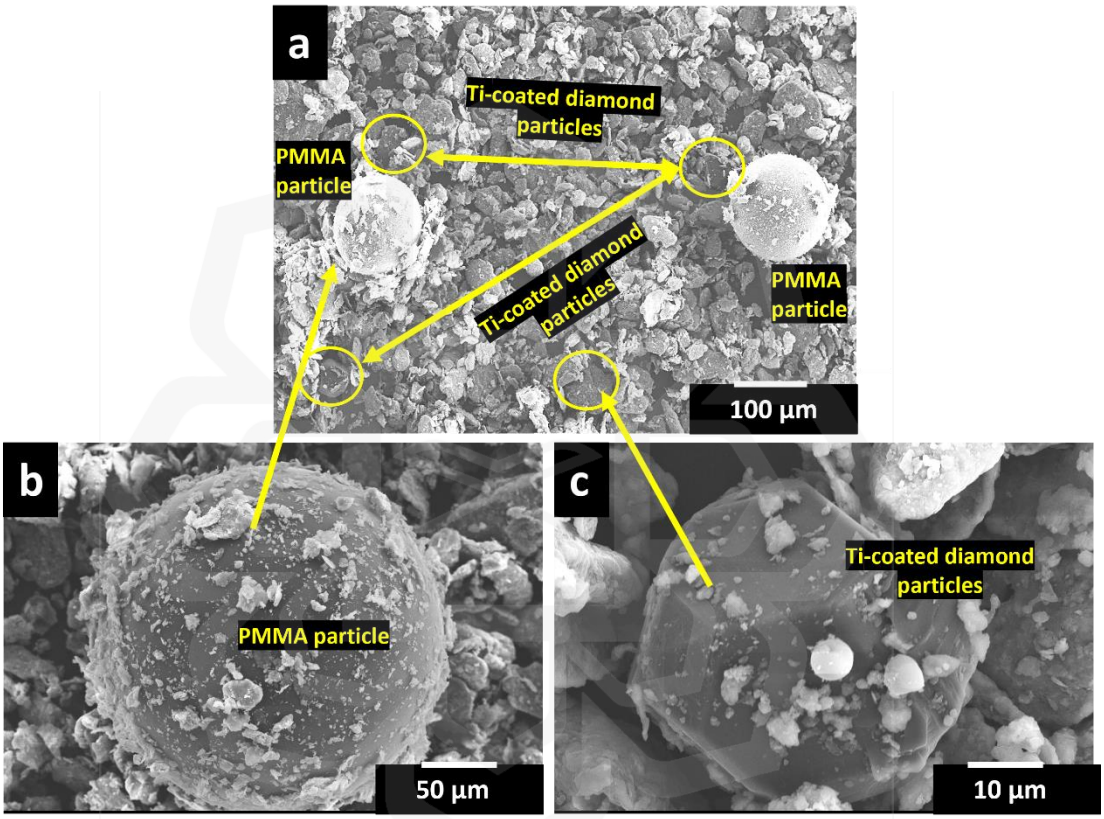

Figure 4.1 SEM micrography of a) Elemental powder mixture, b) PMMA particle and c) Ti-coated diamond particle

The porous structure in porous Al composite were formed using spherical PMMA particles as space holders as shown in Figure 4.2 (a). These spherical PMMA particles result in formation of closed macropores that replicated the shape and size (153-178 µm) of PMMA particles as shown in Figure 4.2 (b). This implies that the morphology of the resultant porous structure could be controlled by careful selection of PMMA in terms of sizes and proportions. It is important to note that the control of the porosity

and pore size distribution in the resultant porous composite is essential for tailor-made materials with properties suited to particular applications (Michailidis et al., 2014). Similar pore structures were obtained in the study of involving porous Mg composite fabrication using PMMA particles as space holder material (Tan et al., 2018). Further, the macropores in the porous Al composite were regularly distributed and separated by a unique cell wall, as shown in Figure 4.2(b).

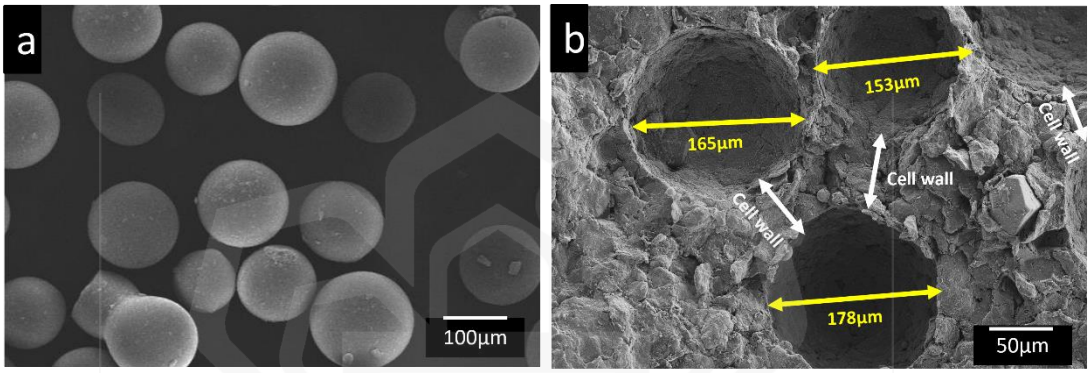

Figure 4.2 SEM micrograph of (a) PMMA particles, and (b) Cross section of sintered porous Al composite

4.2.2 Effect of process parameters (Experimental)

4.2.2.1 Effect of sintering temperature

An adequate sintering temperature is required to promote mass transfer and diffusion process during sintering process resulting in filling of micropores formed during compaction process. Microporosities are the undesirable microcavities formed during fabrication process especially in compaction and sintering process. Some of these microporosities are present in composites after compaction, because of friction between their constituent particles leaving small gaps behind. Such microporosities can thus be reduced by using appropriate sintering temperature. Also, complete removal of space holder particles is essential to prevent crack formation in the resultant porous composite body during sintering (Esen & Bor, 2011). During the sintering process, the vaporization of PMMA bulges the sample resulting in crack formations. To prevent this,

in the current study the compacted samples were first heated at 450 °C to remove PMMA particles. followed by sintering at various temperatures to investigate its effects on the microstructure, plateau strength and energy absorption capacity. As previously investigated by the researchers that the enhanced performance of porous Al can be achieved beyond the sintering temperature of 580 °C (Jamal et al., 2018). In view of this, the effects of various sintering temperatures (580 °C, 590 °C and 600 °C) on the performance of porous Al composite were investigated.

Additionally, the porosity and density of the porous composite are also influenced by the sintering temperature (Küçük et al., 2017). Although the amount of PMMA particles was fixed at 30 wt.%, the resultant percentage of porosity at various sintering temperatures exceeded 30% as tabulated in Table 4.3. This could be due to the presence of microporosity in the porous composite as evident from Figure 4.3 (a-c).

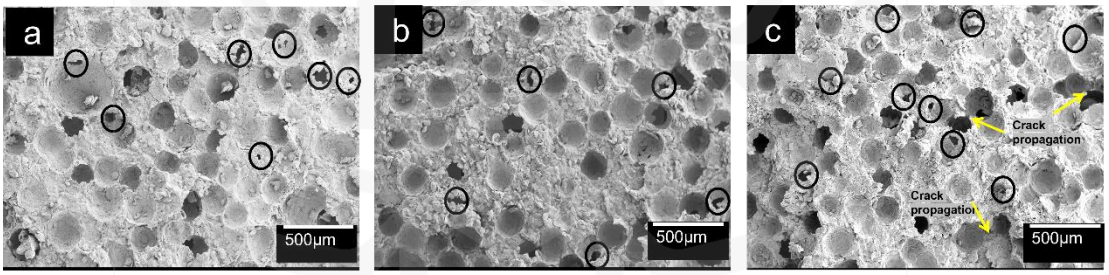

Figure 4.3 SEM morphology of porous Al composite developed at, (a) 580 °C, 350 MPa and 60 min, (b) 590 °C, 350 MPa and 120 min, and (c) 600 °C, 350 MPa and 120 min

When sintered is carried out at low temperature (580 °C), few of these micro pores get filled with liquid matrix, and on further increment in temperature around 590 °C, most of these micro pores get filled with liquid matrix. However, on further increase in sintering temperature to 600 °C, these micro pores increase due to oxidation taking place at high temperature. This can be attributed to detrimental effect of sintering porous

Al at high temperature that often lead to partial melting, oxidation and evaporation of alloying or additive elements (Arifvianto & Zhou, 2014; Mukherjee et al., 2017).

The argon gas that controlled the atmosphere during sintering process leaks at high temperature and introduces atmospheric oxygen into the furnace leading to oxidation of porous composite. These oxides form porosities in the composites during sintering process. This phenomenon was seen to insignificantly affect the porosity, as increase in sintering temperature from 580 °C to 600 °C, the increased porosity from 41% to 43% only as evidenced from Figure 0.3 (a-c) and Table 0.3. However, it had detrimental effect on the bonding strength between the constituents of composites thus effecting their compressive properties.

Table 4.3 Density and porosity of porous Al composite for nine sets of parameters

S.no	**1**	**2**	**3**	**4**	**5**	**6**	**7**	**8**	**9**
Porosity (%)	**40**	**40**	**41**	**41**	**42**	**41**	**43**	**44**	**43**
Relative density	**0.83**	**0.81**	**0.80**	**0.86**	**0.84**	**0.86**	**0.84**	**0.83**	**0.84**

The compressive properties, including the plateau strength and energy absorption capacity of porous Al composites as shown in Table 4.2 increased from 22.02 MPa to 31.06 MPa and 5.77 MJ/m^3 to 9.19 MJ/m^3 when the sintering temperature increased from 580 °C to 590 °C, respectively. However, the plateau strength and energy absorption capacity slightly decreased from 31.06 MPa to 30.02 MPa when the sintering temperature increased from 590 °C to 600 °C, respectively. Figure 4.4 (a-c), respectively. This can be due to the poor wetting behavior between Al matrix and diamond particle at low temperature (580 °C) as evident from Figure 4.4 (a). Also, the oxidation of porous composites at high temperature (600 °C) as evidenced from SEM images and EDX analysis in Figure 4.4 (c) and Figure 4.4 (d-g), respectively. Further, due to the ineffective role of sintering additives of Sn, Mg, Cu and B in providing

sufficient wetting action at 580 °C and 600 °C, respectively. As a result, sufficient wetting action could not be provided by both alloying elements and Ti-coated diamond.

On the contrary, the enhancement in the plateau strength and energy absorption capacity of sintered porous Al composite at 590 °C could be due to the effective role of different alloying elements of Sn, B, and Mg together with the coating of diamond with Ti element at the said temperature that promoted the liquid phase sintering and wetting behavior between Al alloy matrix and diamond particle hence improved the interfacial bonding between the Al alloy matrix and diamond reinforcement as illustrated Figure 4.3 and Figure 4.4, respectively. Additionally, sintering of porous Al composite at 590°C could also be contributed to the partial melting of the alloying elements at this temperature resulting into a strong wetting action between Al alloy matrix and reinforcement particles, thereby improving the bonding strength of Ti-coated diamond in the Al alloy matrix as evident from Figure 4.4 (e). Similar observations were also made in various studies involving porous composite that utilizing the elements of Sn, Mg, and B as sintering additives in assisting the liquid phase sintering of the respective porous composite (Ali et al., 2018; Hamdi, 2018).

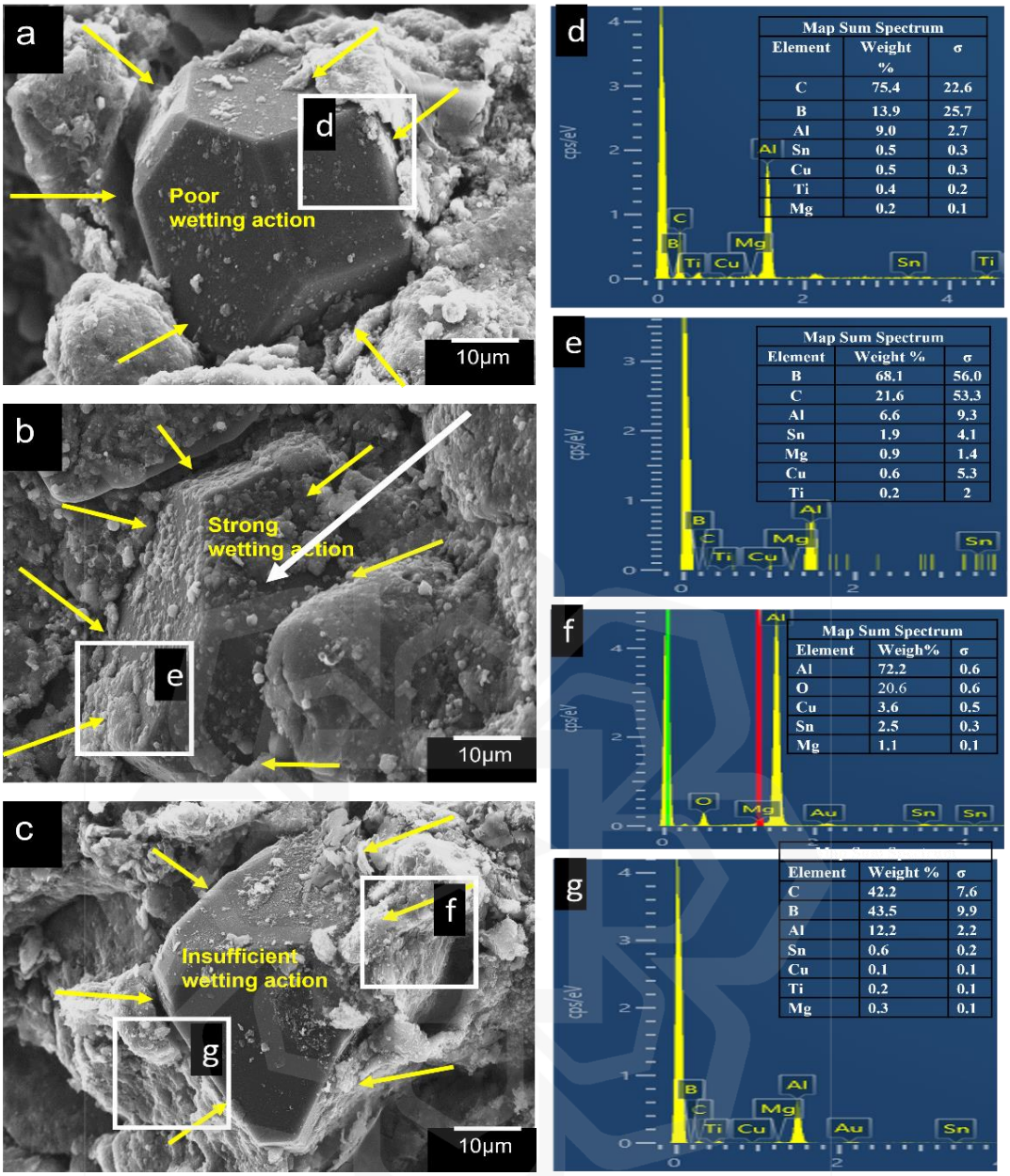

Figure 4.4 SEM images and EDX analysis of porous Al composite showing wetting action near the vicinity of diamond particles at different sintering temperatures, (a, d) 580 °C (b, e) 590 °C, and (c, f, g) 600 °C

4.2.2.2 Effect of compaction pressure

Compaction pressure influences the bonding strength between the Al alloy matrix and reinforcement particles. Since strong binding between Al particles is inhibited by the oxide film that covers their surface, the film needs to be broken down by applying sufficient compacting pressure. During this process, new metallic particle surfaces come into contact with one another for sintering. In the current study, a few preliminary

tests revealed that at compaction pressure less than 350 MPa, defective specimens were obtained together with inadequate green strength to endure additional processes and examinations (Figure 4.5 (a)). On the contrary, when the compaction pressure was above 400 MPa, crack formation was observed due to deformation of PMMA particles that led to the alteration in the final morphology and pore size of the resultant composite as shown in Figure 4.5 (a). Moreover, the compaction pressure between 350-400 MPa produced better samples in terms of physical appearance, retained its original shapes, non-collapsing of PMMA particles, as well as sufficient strength for subsequent processing steps.

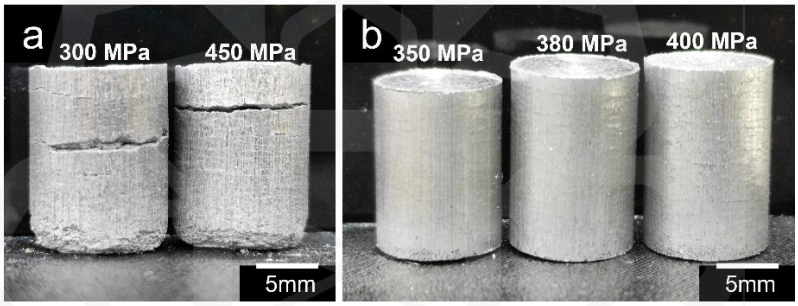

Figure 4.5 Samples compacted at (a) 300 and 450 MPa, and (b) at 350, 380, and 400 MPa

The compaction pressure was also found to influence the relative density and porosity of the compacted specimens insignificantly as shown in Figure 4.6. The relative densities of compacted specimens decreased from 0.762 to 0.753 whereas the percentage of porosity increased from 9 % to 12 % with an increase in compaction pressure from 350 MPa to 400 MPa. Also, the effect of compaction pressure on the compressive properties was least significant as evident from Table 4.2.

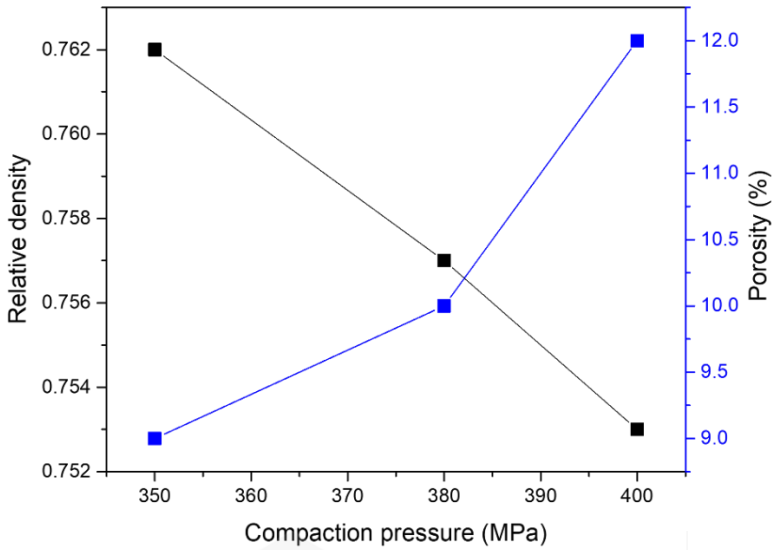

Figure 4.6 Effect of compaction pressure on relative density and porosity of Al compacts

Although the compaction pressures ranging from 300-400 MPa could be considered high as n contrast to the traditional pressures employed in the PM method (Alrebdi et al., 2022). However, in this study Higher compaction pressures are needed to achieve good compacts because the compaction stress is distributed among the components in the porous Al composite, including the diamond and PMMA particles. Moreover, the higher compaction pressures can distort the shape of PMMA particles. Thus to prevent this binders such as CLE-safe oil to the powder mixture before compaction were used to lower the pressure (Li et al., 2013). In addition, the employment of PMMA particles as a space holder allowed easy movement and rearrangement of these particles during the compaction due to their spherical shape. As a result, uniform PMMA particles distribution with improved interconnectivity could be achieved in the green compacts (Manonukul et al., 2010). In fact, when comparing the spherical shape of PMMA particles to other space-holder materials for example non-spherical shape of NaCl (Aida et al., 2016; Surace et al., 2009a), the resultant spherical pores formed by spherical shape of PMMA particles often lead to reduce surface roughness with fewer corners and edges in which aids in reducing the local stress concentrations and non-uniform

deformation during compaction, and thus improves the strength of the porous Al composite (Li et al., 2018).

4.2.2.3 Effect of sintering time

Another important factor that was found to affect the microstructure, plateau strength and energy absorption capacity was sintering time. A sufficient sintering time promotes effective diffusion, easy and fast permeation, as well as improves bonding between the constituents in the porous composite thereby eliminating microporosity. In the current study, the plateau stress and energy absorption capacity were observed to increase by increasing sintering time from 60 min to 90 min and decreased with further increase in sintering time to 120 min as shown in Table 4.2. The increased values of compressive properties can be attributed to the strengthening of porous Al composite due to reduction in void or microporosity formation as a result of diffusion process, hence enhancing the compressive properties and reducing microporosity as evident from Figure 4.7 (a,b). During sintering process, the atoms of composite powder particles get activated thermally, resulting in mass diffusion and fusion between particles (necking) at inter-particle contact points. This diffusion rate increases with increase in the sintering time, and the Al alloy matrix powder particles merged together as a result of necking, leading to a denser structure and closed porosity (Almomani et al., 2014).

However, as the sintering time increased, small pores coalesced, causing larger pores to form as a result (voids) that slowed down the sintering process resulting into the formation of large voids in the resultant porous composite structure as shown in Figure 4.7 (c) thereby reducing its compressive properties. Similar effects were also seen for porous steel composite developed using PM technique as documented in the study of (Tatt et al., 2016). Figure 4.7 (a-c) proves the microstructure of micropores

(voids) at various sintering time of 60 min, 90 min and 120 min in which significant micropores could be observed during sintering time of 120 min (Figure 4.7 (a). Based on these findings, it can be concluded that longer sintering time could adversely affect the porous Al composite's strength (Rahimian et al., 2009).

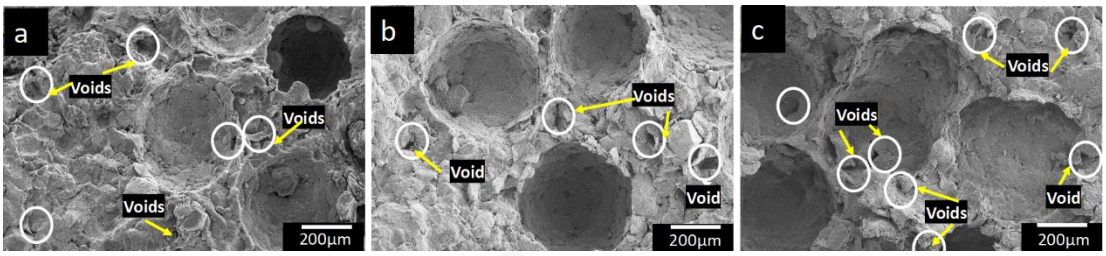

Figure 4.7 SEM micrography of porous Al composite at sintering temperature of 590°C and at varying sintering time (a) 120 min, (b) 90 min and (c) 60 min

4.2.3 Effect of process parameters (Analytic)

4.2.3.1 Analysis of Signal to Noise Ratio

The response variables, including the plateau stress and energy absorption capacity, were considered in the present study to enhance the performance of porous Al composites. In practical application, the plateau stress and energy absorption capacity should be maximized to increase applicability. Therefore, the rule of thumb for determining the S/N ratio for the response factors is "the larger, the better". Figure 4.8 and Figure 4.9 show the plots of the main effect that explain the impact of input process parameters on the plateau stress and energy absorption capacity, respectively. Moreover, Figure 4.8 presents the S/N analysis of plateau stress, in which the sintering temperature set at level 2 (590 °C), compaction pressure at level 3 (400 MPa), and sintering time at level 2 (90 min) results in maximum value of plateau stress. Meanwhile, the maximum energy absorption capacity was achieved at sintering temperature of 590 °C, compaction pressure of 380 MPa, and sintering time of 90 min (level 2), as shown in Figure 4.9.

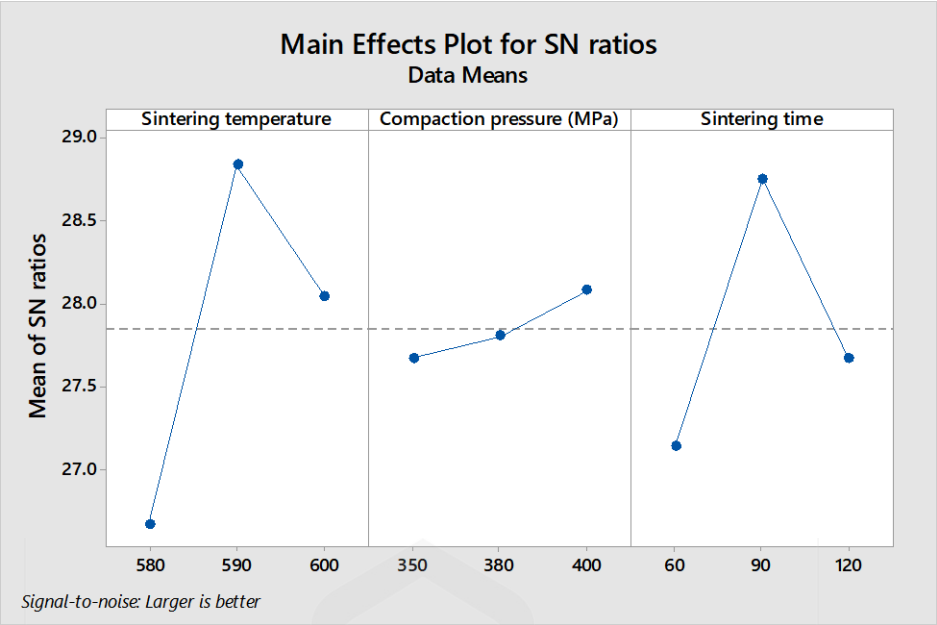

Figure 4.8 S/N ratio response curve of plateau stress

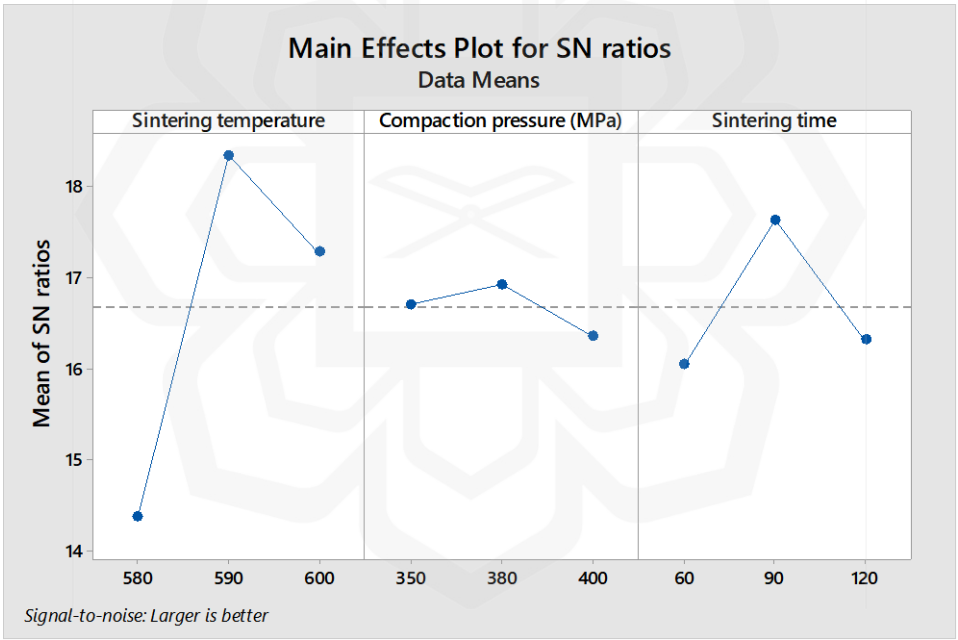

Figure 4.9 S/N ratio response curve of energy absorption capacity

4.2.3.2 Analysis of variance

The effects of processing parameters and their relationships were investigated using ANOVA by comparing the mean square against response errors at predetermined confidence levels. The ANOVA helps to determine the impact of each factor on the overall result variance. Table 4.4 and Table 4.5 demonstrate the ANOVA results for

both response factors (plateau stress and energy absorption capacity). The analysis was conducted with a 10% significance level corresponding to a 90% confidence level. Each ANOVA table includes a percentage contribution of each factor's variable to the total variation. The contribution of each factor that impacts the response factors (plateau stress and energy absorption capacity), as shown in Figure 4.10, were analyzed based on the results from the ANOVA. In this context, the assigned variable is statistically significant if the F-value exceeds 8%. Table 4.4 and Figure 4.10(a) show that sintering temperature is the most significant factor (52.40%), followed by the sintering time (44.729%) and then compaction pressure (2.3%), affecting the value of plateau stress. Similarly, Table 4.5 and Figure 4.10 tabulate that the sintering temperature has the highest significant impact (78.45%) on the energy absorption capacity, followed by the sintering time (19.53%) and compaction pressure (1.2%).

Table 4.4 ANOVA Variance table for plateau stress

Source	DF	Seq SS	Contribution	Adj SS	Adj MS	F-Value	P-Value
Sintering temperature	2	58.903	52.40%	58.903	29.451	9.51	0.095
Compaction pressure	2	2.589	2.30%	9.497	4.748	1.53	0.395
Sintering time	2	44.729	39.79%	44.729	22.364	7.22	0.122
Error	2	6.194	5.51%	6.194	3.097		
Total	8	112.415	100.00%				

Table 4.5 ANOVA Variance table for energy absorption capacity

Source	DF	Seq SS	Contribution	Adj SS	Adj MS	F-Value	P-Value
Sintering temperature	2	14.6761	78.45%	14.6761	7.33803	95.91	0.010
Compaction pressure	2	0.2245	1.20%	0.8049	0.40243	5.26	0.160
Sintering time	2	3.6545	19.53%	3.6545	1.82723	23.88	0.040
Error	2	0.1530	0.82%	0.1530	0.07651		
Total	8	18.7080	100.00%				

The strength of a porous composite could be increased by forming a strong interface bond between the matrix and the reinforcements. Such formation could be accomplished by selecting the appropriate processing parameters, such as compaction pressure, sintering temperature, and sintering time. The compaction process holds together the neighboring powder particles by forming cold welds, which impart

adequate green strength to the compacts for enduring further processes. Meanwhile, the sintering time affects the diffusion rate and the grain growth of the composite. The sintering temperature below the melting point of the major component of the composite resulted into the maximizing the Grain growth and sufficient to fill voids and reinforce the composite. The temperature at which the composite is sintered affects its microporosity, which in turn affects its strength. (Manohar et al., 2020). As evident from Table 4.4 and Table 4.5 the sintering temperature being the most significant factor affecting the plateau stress (52.4%) and energy absorption capacity (78.45%).

On the contrary, the effect of the compaction pressure was minimal and remained at 2.3% and 1.2 % for the outputs of plateau stress and energy absorption capacity, respectively. The plausible explanation could be due to the restriction imposed on the compaction pressure in preventing distortion or cracking of PMMA particles. Therefore, the parameters selected in the current study mainly contributed to the least change in the percentage of porosity of the green compacts as shown in Figure 4.6.

On the other hand, the linear polynomial model as in Figure 4.10 describes the plateau stress and energy absorption capacity as a function of sintering temperature, compaction pressure, and sintering time that had been gathered from the analysis of variance. The greatest R^2 predictions were determined to be 94.49% and 99.18% for plateau stress and energy absorption capacity, indicating that the model could predict new observations nearing or matching the sample data. Furthermore, the current study can be explained well by the regression equation as in the following section.

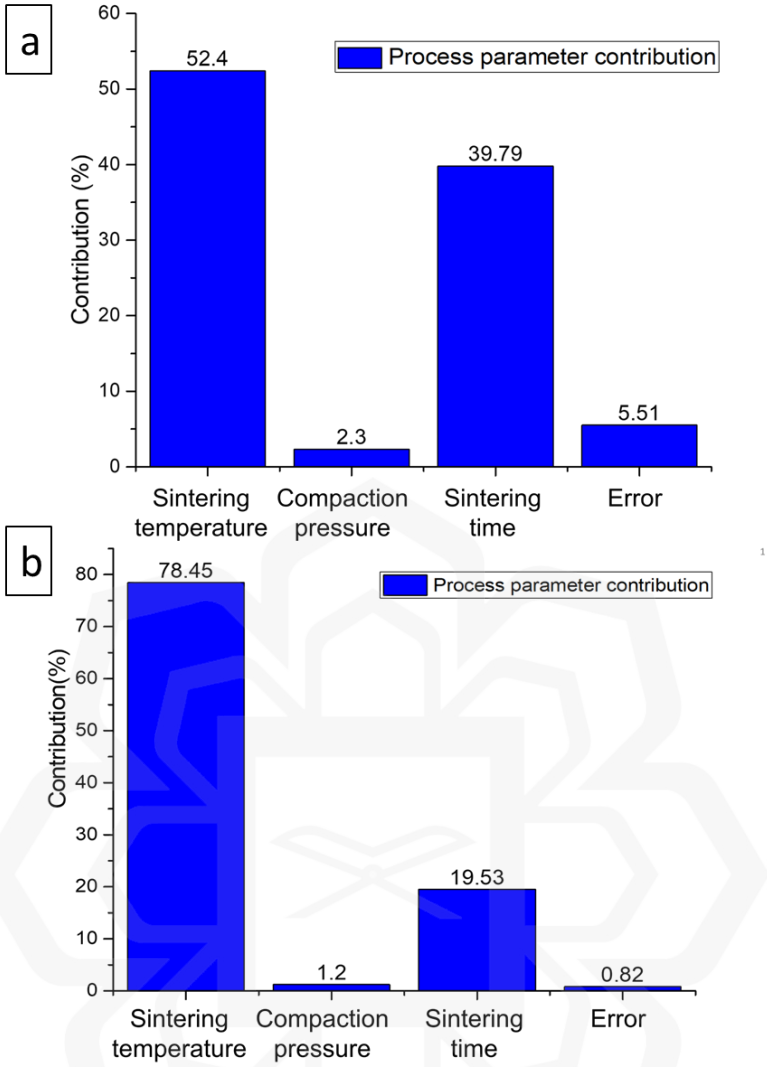

Figure 4.10 Percentage of the contribution of processing parameters on the (a) plateau strength and (c) energy absorption capacity

4.2.3.3 Regression analysis

The L_9 orthogonal array was used together with MINITAB software to recognize a statistical model based on the linear regression equations. A linear polynomial model (regression equations) for plateau stress and energy absorption capacity was selected based on each obtainable factor and presented in the Equations 4.2 and 4.3 as follows:

$$Plateau\ stress \qquad 4.2$$

$$= 24.926 - 3.372A_1 + 2.821A_2 + 0.551A_3 + 1.17B_1 - 1.83B_2 + 0.668B_3 - 2.116C_1 + 3.77C_2 - 1.66C_3$$

Energy absorption capacity **4.3**

$$= 6.9733 - 1.720A_1 + 1.337A_2 + 0.383A_3 + 0.534B_1 - 0.344B_2 + 0.190B_3 - 0.570C_1 + 1.096C_2 - 0.526C_3$$

where A is the sintering temperature, B is the compaction pressure, and C is the sintering time.

Based on the linear regression equations (Equations 4.2 and 4.3), the response of plateau stress and energy absorption values were calculated in finding the percentage deviation. The significant residual errors and the maximum errors of 1.40 and 1.37 (Table 4.6 and Table 4.7) were calculated for plateau stress and energy absorption capacity, respectively.

Table 4.6 Fits and diagnostics for all observations for plateau stress

Runs	Experimental	Model Fit	SE Fit	Resid	Std Resid	Del Resid
1	21.34	20.60	1.68	0.74	1.40	8.65
2	22.02	23.49	1.41	-1.47	-1.40	-8.65
3	21.30	20.56	1.68	0.74	1.40	8.65
4	26.72	27.25	1.41	-0.53	-0.51	-0.39
5	31.06	29.69	1.41	1.37	1.31	2.43
6	25.46	26.30	1.55	-0.84	-1.01	-1.02
7	24.78	24.98	1.41	-0.20	-0.19	-0.14
8	21.63	21.53	1.68	0.10	0.19	0.14

Table 4.7 Fits and Diagnostics for All Observations for Energy absorption capacity

Runs	Experimental	Model Fit	SE Fit	Resid	Std Resid	Del Resid
1	5.330	5.217	0.264	0.113	1.37	3.74
2	5.780	6.005	0.222	-0.225	-1.37	-3.74
3	4.650	4.537	0.264	0.113	1.37	3.74
4	8.320	8.318	0.222	0.002	0.01	0.01
5	9.230	9.062	0.222	0.168	1.02	1.04
6	7.380	7.550	0.244	-0.170	-1.30	-2.38
7	7.250	7.365	0.222	-0.115	-0.70	-0.56
8	6.500	6.443	0.264	0.057	0.70	0.56
9	8.320	8.263	0.264	0.057	0.70	0.56

Moreover, the data for each experiment and model fit were compared as illustrated in Figure 4.11, showing the least discrepancy in their values. Thereby showing the accuracy of model.

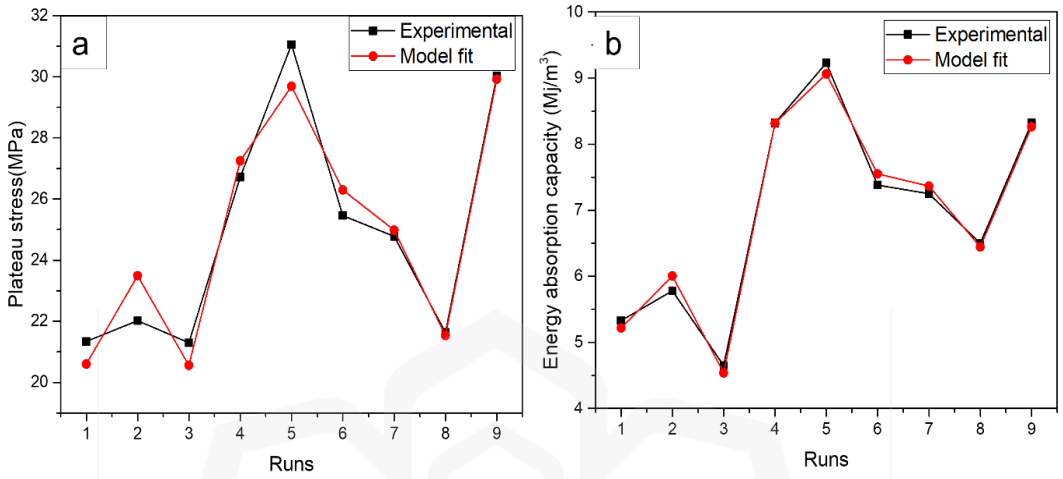

Figure 4.11 Comparison of experimental and modal predicted plateau stress and energy absorption capacity

4.2.3.4 Response optimization

The response optimization study was executed to obtain the optimal results and parameters, as shown in Table 4.8. The goal was to maximize results in optimizing the plateau stress and energy absorption capacity. In this regard, the low plateau stress of 21.3 MPa presented in Table 4.8, can be regarded as the predicted value. Although the maximum and minimum variations exist for the target and lower values, it could be considered impractical. However, this can be due to dependence of the values of compressive properties other factors as well such as composition, mixing parameters, crosshead speed during compression testing, as well as other related parameters. This could result in extremely high or low values. Therefore, a safe and reasonable value for plateau stress and energy absorption capacity could be considered as the fit values as outlined in Table 4.8 which could be attained at a sintering temperature of 590 °C, compaction pressure of 350 MPa, and sintering time of 90 min.

Table 4.8 Response optimization: processing parameters

Response	Goal	Lower	Target	Upper	Weight	Importance
Energy absorption capacity (MJ/m^3)	Maximum	4.65	9.23		1	1
Plateau stress (MPa)	Maximum	21.30	31.06	------	1	1

Solution

Solution	Sintering temperature (°C)	Compaction pressure (MPa)	Sintering time (min)	Energy absorption capacity Fit	Plateau stress Fit	Composite Desirability
1	590	350	90	9.94	32.6856	1

Response	Fit	SE Fit	95% CI	95% PI
Energy absorption capacity (MJ/m^3)	9.940	0.332	(8.510, 11.370)	(8.079, 11.801)
Plateau stress (MPa)	32.69	2.12	(23.59, 41.79)	(20.85, 44.52)

4.2.3.5 Contour plots

Figure 4.12 and Figure 4.12 demonstrate the contour plot of the plateau stress and energy absorption capacity involving three different combinations of variables for diamond-reinforced porous Al composite including the influence of sintering time (90 min) as in Figure 4.12(a) and Figure 4.12 (a), compaction pressure (350 MPa) as in Figure 4.12(c) and Figure 4.12 (b), and sintering temperature (590 °C) as in Figure 4.12(c) and Figure 4.12 (c) on the plateau stress and energy absorption capacity. In combination with the parameters as shown in Figure 4.12 (a), the plateau stress was found to increase with increased in the sintering temperature and decreased on increasing the compaction pressure. Additionally, Figure 4.12 (b) illustrates that the maximum sintering temperature and time were found to influence the plateau strength, resulting in a sudden increment in the latter. However, Figure 4.12 (c) shows an increase in the plateau stress with increasing sintering time and medium compaction pressure. Meanwhile, Figure 4.12 (a) indicates a reduction in the plateau strength (-40 MPa) at a high sintering temperature and low compaction pressure.

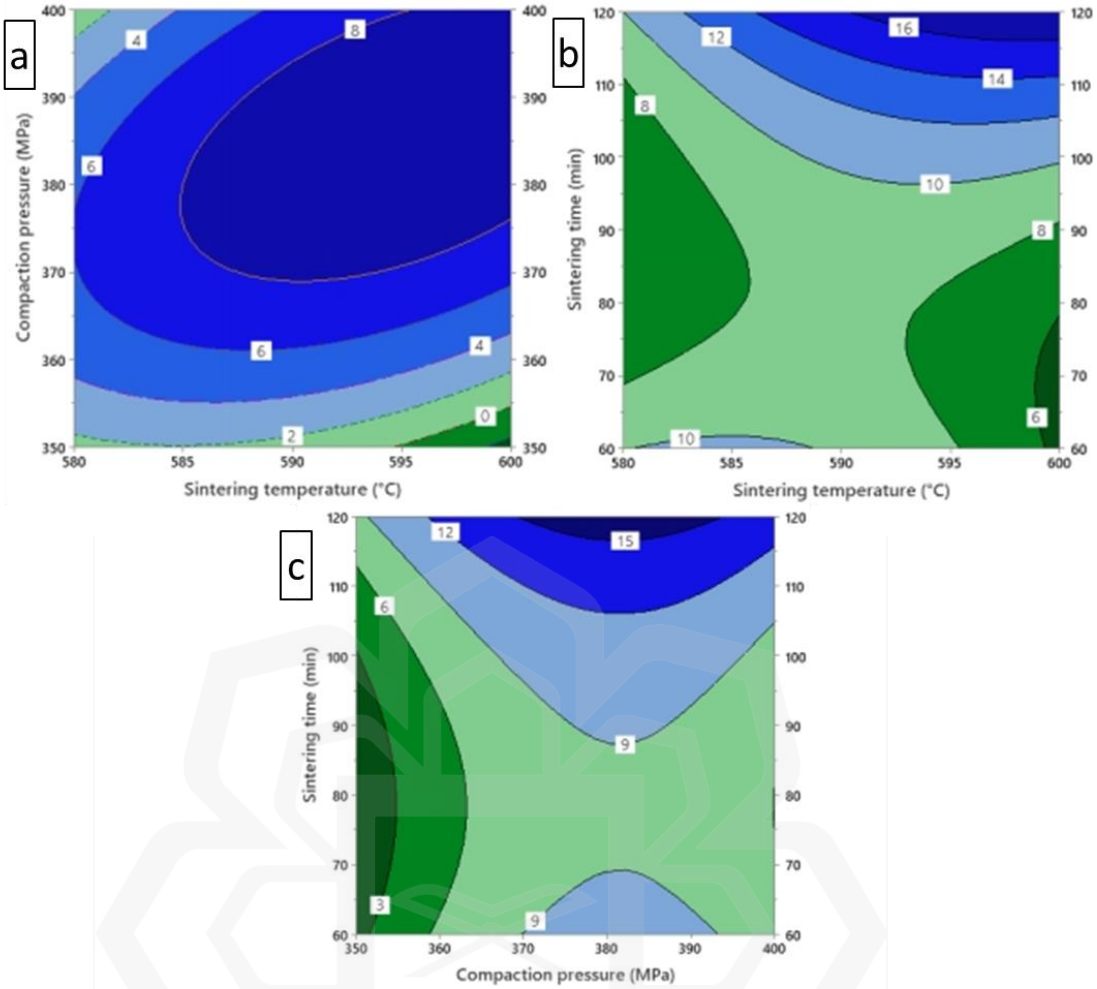

Figure 4.12 Contour plot of plateau stress in diamond-reinforced porous Al composite

A similar result was obtained for the energy absorption capacity as shown in Figure 4.12 (a). However, the energy absorption capacity was found to be higher as compared to the combined values of the sintering temperature and time as seen in Figure 4.12 (b). Moreover, Figure 4.12 (c) illustrates that the maximum energy absorption capacity was achieved at medium compaction pressure and maximum sintering time. Thus, the contour plots verified the impact of the selected parameters based on the changing of the response factors.

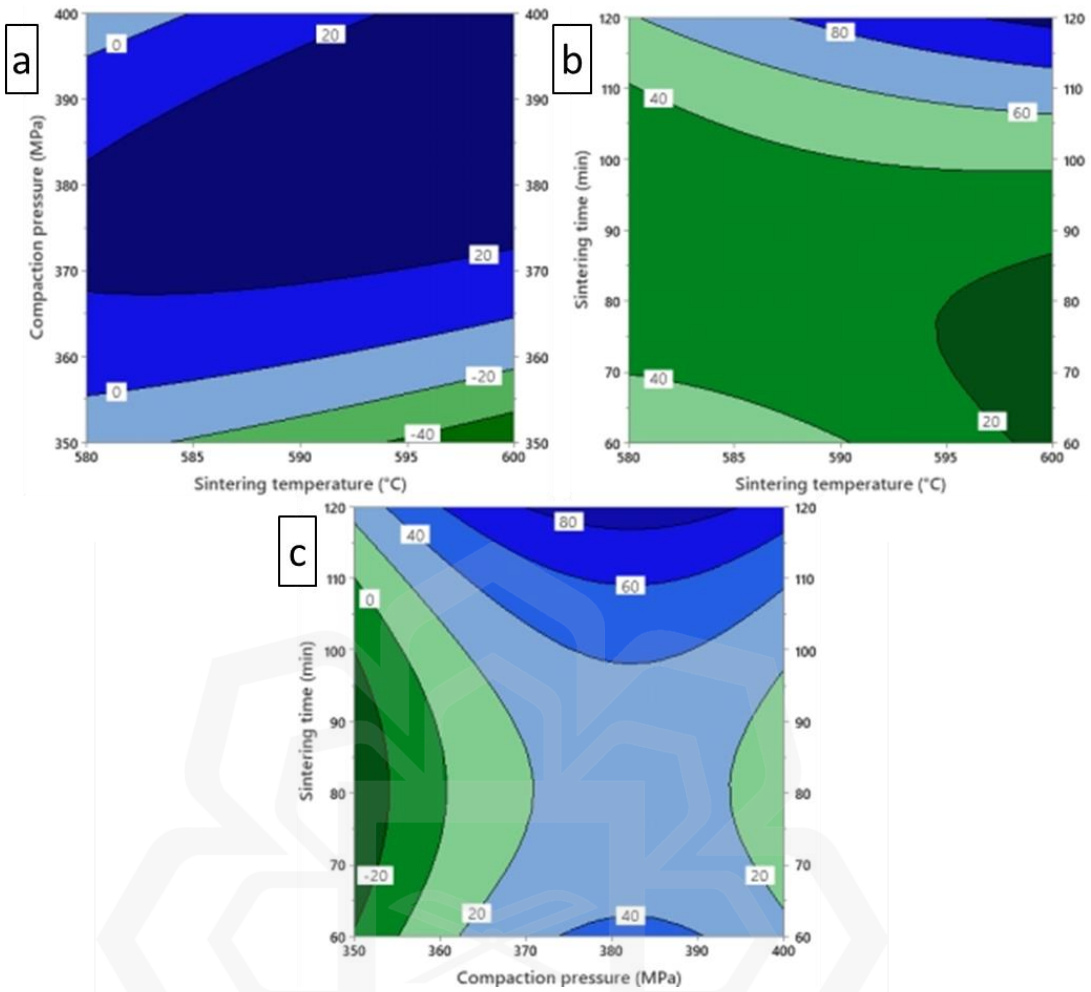

Figure 4.13 Contour plot of energy absorption capacity of diamond-reinforced porous Al composite

4.2.3.6 Confirmation test

Finally, the confirmation test based on the experimental approach is carried out after investigating the optimal test conditions based on the DOE approach. The confirmation test was executed by developing composite at optimum values of parameters including the sintering temperature of 590 °C, compaction pressure of 350 MPa, and sintering time of 90 min as obtained from Table 4.8. The porous Al composite was then compression tested to find the values of plateau strength and energy absorption capacity. Ultimately, the obtained results were contrasted with the anticipated outcomes, as seen in Figure 4.13, demonstrating the stress-strain diagrams of predicted and experimental results.

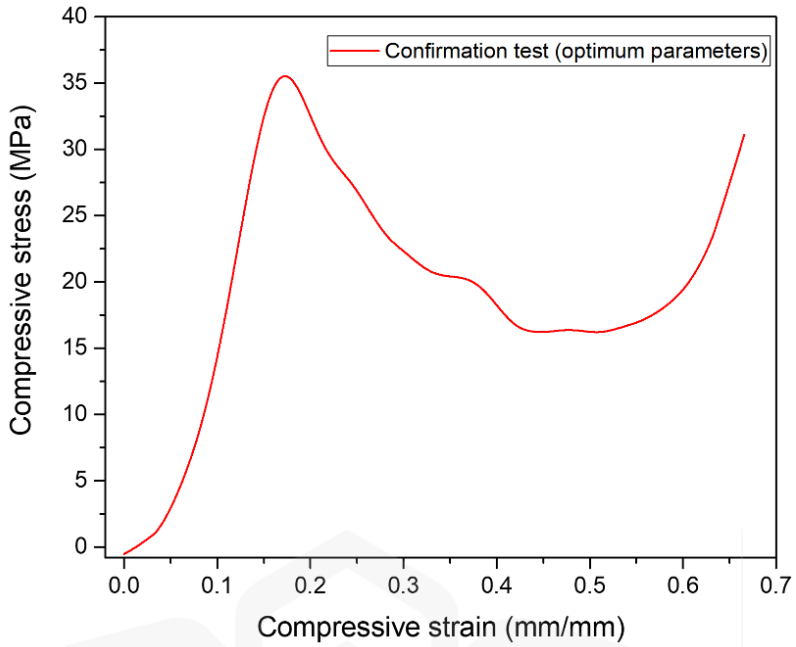

Figure 4.14 Compressive stress- strain diagram of confirmation test at optimum parameters

Furthermore, Table 4.9 demonstrates the comparative results that had been obtained from the optimum processing parameters. It can be seen that the experimental and predicted results were in reasonable agreement. However, percentage errors of -10.5% and -6.6% were observed for plateau strength and energy absorption capacity.

Table 4.9 Confirmation test comparisons with predicted values

Responses	**Prediction**	**Experimentation**	**Error (%)**
Plateau stress (MPa)	**32.69**	**36.12**	**-10.5**
Energy absorption capacity (MJ/m^3)	**9.94**	**10.6**	**-6.6**

The development of a porous Al composite with a well-defined porous structure through the use of powder metallurgy technique was made possible by parameter optimization, and this led to a notable improvement in the composite's compressive properties.

4.3 EFFECT OF DIAMOND CONTENT, PMMA CONTENT AND PMMA PARTICLE SIZE ON COMPRESSIVE PROPERTIES OF POROUS AL COMPOSITES

In this section, the effect of composition on the morphology, porosity and compressive properties of porous Al composites has been presented. The experimental plan was initiated to identify the critical factors and their interactions to attain the best compressive properties (plateau strength and energy absorption capacity). The experimental runs were planned by applying the Taguchi's L_9 orthogonal array where three input factors considered were the diamond content, PMMA particle size and PMMA particle content as shown in Table 4.10. The Taguchi model with three factors and three levels were chosen and thus orthogonal array L_9 with 9 rows and 3 columns were obtained. The run order together with the corresponding factors and levels are mentioned in Table 4.11. The porous composite was fabricated using PM technique at optimum conditions (acquired from Obj. 1) for 9 sets of combinations as per Taguchi orthogonal array and their compressive properties were recorded as shown in Table 4.10. The objective of this model was to obtain the highest compression properties (plateau stress and energy absorption capacity).

Table 4.10 Control factors (Process Parameters) and their levels

S.no	Diamond content (wt. %)	PMMA size (μm)	PMMA content (wt. %)	Plateau strength (MPa)	Energy absorption capacity (MJ/m^3)
1	**4**	**75**	**20**	**24.8**	**4.89**
2	**4**	**125**	**25**	**20.27**	**5.12**
3	**4**	**150**	**30**	**26.37**	**6.78**
4	**8**	**75**	**30**	**36.68**	**10.75**
5	**8**	**125**	**25**	**30.06**	**9.77**
6	**8**	**150**	**20**	**29.86**	**7.93**
7	**12**	**75**	**30**	**26.79**	**7.55**
8	**12**	**125**	**20**	**25.89**	**8.96**
9	**12**	**150**	**25**	**40.2**	**13.66**

Table 4.11 L_9 Orthogonal array layout with design factors

Factors	Symbol	Unit	Level 1	Level 2	Level 3
Diamond content	**A**	**wt.%**	**4**	**8**	**12**
PMMA size	**B**	**µm**	**75**	**125**	**150**
PMMA content	**C**	**wt.%**	**20**	**25**	**30**

4.3.1 Morphology of porous Al composites

The morphology of porous Al composite as shown in Figure 4.14 (a) exhibits two types of pore structures: macropores and micro-pores. Macro-pores are the desirable pores that were formed using PMMA particles as a space holder, which decomposes during sintering process leaving the pores behind (Jamal et al., 2016). These macro pores are spherical shaped and have almost similar size as that of PMMA particles as shown in Figure 4.14 (a). This indicates that PMMA particles can tailor the pore size and shape, thus controlling the porosities of porous composite. Moreover, it has been observed that the presence of irregular pores causes difficulty in prediction of mechanical properties (Goodall et al., 2007). The benefits of spherical shape pores as shown in Figure 4.14 (a), include homogeneous pores with regular shape and size, and easier prediction of mechanical properties theoretically. Similar findings were reported by (Bekoz and Oktay, 2012), used spherical carbamide particles as space holders resulting into better mechanical properties. Additionally, the presence of rounded corners in spherical porous structure often contributes to reducing stress concentration.

On the contrary, micro-pores are the unwanted pores that are formed during fabrication process and are mostly found in the macropore walls and struts fabrication (Bekoz & Oktay, 2014). In the current study, the resultant macropores have pores connectivity as observed in Figure 4.14 (c). As the space holder particles slide with each other during compaction, connected pores were formed after sintering. These connected pores were reported to aid in proper decomposition of the space holder during the sintering process (Anovitz & Cole, 2015).

Also, the EDX analysis of the cross section of porous composites Figure 4.15 (b) revealed the presence of all constituents added thus confirming their presence. These alloying elements have been found to improve the wetting action of Al matrix with diamond particle as shown in Figure 4.15 (d) well bonded diamond particle in Al alloy matrix.

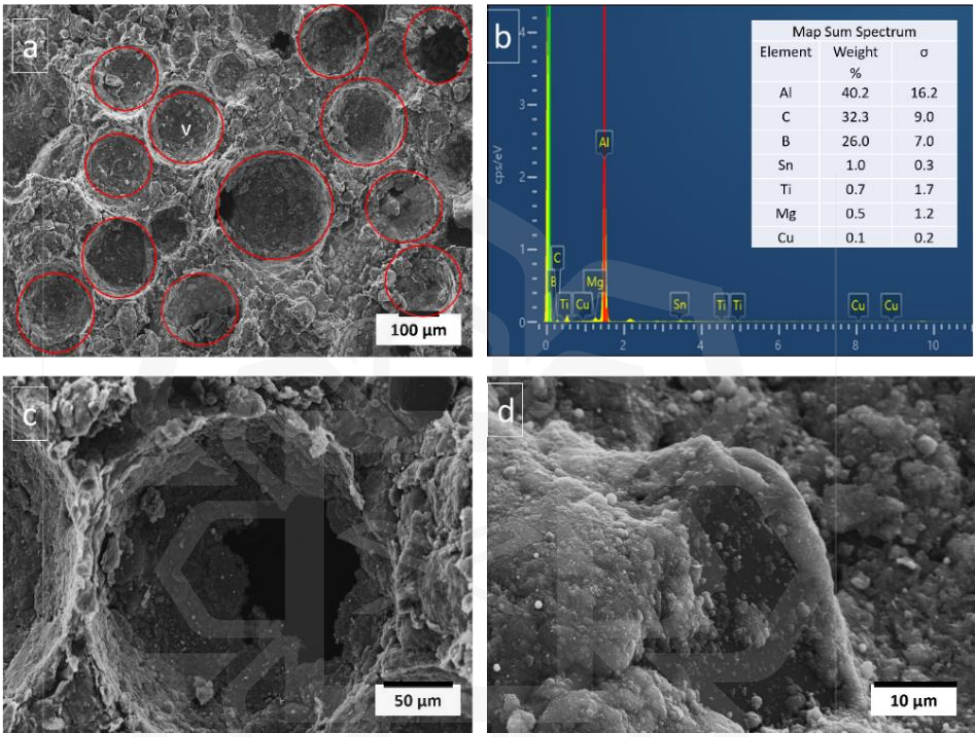

Figure 4.15 Microstructure of porous Al composite, (a) Pore distribution and shape, (b) EDX of composite cross section, (c) Pore cell and pore connectivity, and (d) Well bonded diamond particle

On the other hand, Table 4.12 presents the density and porosity percentage of the resultant porous Al composite at various Ti coated diamond content (4,8 and 12 wt.%), PMMA content (20, 25 and 30 wt.%) and PMMA particle size (75, 125 and 150µm). Initially, the overall density of the composite was found to insignificantly increased up to 25 wt.% of PMMA content followed by a decreased in the overall density with increasing PMMA particle content and size up to 30 wt. % and 150 µm at a constant diamond content of 4 wt. %.

Table 4.12 Densities and porosities of porous Al composite for 9 sets of parameters

S.no	1	2	3	4	5	6	7	8	9
Porosity (%)	**21**	**24**	**30**	**29**	**26**	**18**	**31**	**20**	**25**
Bulk density(g/cm^3)	**1.94**	**2.06**	**1.76**	**2.08**	**2**	**1.92**	**2**	**1.867**	**1.774**
Relative density (%)	**0.72**	**0.76**	**0.65**	**0.77**	**0.74**	**0.71**	**0.74**	**0.69**	**0.66**

In contrast, the overall percentage of porosity of the porous Al composite increased with increasing PMMA content. However, with the increase in diamond content increased from 4 wt. % to 12 wt. %, the overall densities decreased while the overall percentage of porosity increased, implying higher development of microporosity. This can be due to the insufficient filling of micropores formed by alloy metal as a result of higher Ti-coated diamond content (Chu et al., 2010). Nevertheless, an increased in the PMMA particle size from 75 µm to 150 µm was found to increase the overall densities whereas on the contrary the overall percentage of porosity was found to decrease.

4.3.2 Effect of varying composition (Experimental)

4.3.2.1 Effect of diamond particle content

The potential role and proper distribution of reinforcing particles in the matrix allow composite to exhibit higher strength as compared to monolithic materials (Mondal et al., 2014; Yu et al., 2008). The uniform distribution of reinforcement particles within the matrix cell wall is critical. The presence of diamond particles in the intact cell wall contributes to greater strength of cell walls as well as mechanical properties of the resultant porous metals and their composite.

As evident from Figure 4.15 the well bonded Ti- coated diamond particles are present in the cell walls, thereby increasing the overall plateau strength of porous Al composites as shown in Table 4.11. Further improvement was seen on increasing the Ti-coated diamond particle content from 4 wt. % to 12 wt. %. Similarly, the overall

energy absorption capacity of composite was also increased significantly with increasing content of Ti-coated diamond particle from 4 wt. % to 12 wt. %, respectively. These trends were significant for composite having the PMMA particle size of 150 µm. Porous Al composite with percentage of porosity between 20% to 30 % and Ti-coated diamond content of 4wt. % demonstrated plateau strength values ranging from 24.8 MPa to 26.37 MPa whereas in the case of 8 wt. % of Ti-coated diamond content, the plateau strength values were found to be in the range between 29.86 MPa to 36.68 MPa, respectively. However, the highest values of plateau strength were attained in the range of 26.78 MPa to 40.2 MPa with the addition of 12 wt. % of Ti-coated diamond content. Similarly, porous Al composite having percentage of porosity in the range of 20% to 30% with the addition of 4 wt. % of Ti coated diamond content displayed energy absorption capacity values between 4.88 MJ/m^3 to 6.78 MJ/m^3 while composite by the inclusion of 8 wt. % of Ti-coated diamond content presented energy absorption capacity values in the range of 7.93 MJ/m^3 to 10.75 MJ/m^3, respectively. The highest values of energy absorption capacity were recorded in the range 7.55 MJ/m^3 to 13.66 MJ/m^3 with the addition of 12 wt. % of Ti-coated diamond content.

The highest obtainable plateau strength and energy absorption capacity values of porous Al composite with the addition of 12 wt. % of Ti-coated coated diamond was due to the high stress resistance of Ti-coated diamond before reaching the critical stress as fracture occurred near or at the cell boundary during compression. Moreover, the presence of well bonded Ti-coated diamond particles in the cell walls was believed had increased the cell wall thickness thus greater bending resistance as shown in Figure 4.16Figure 4.15 (a, b). The strong bonding between Al alloy matrix and diamond particle is due to the improvement in wetting action between Al matrix and diamond particles by inclusion of allowing elements as well as the affinity of Ti coating with Al

matrix. The EDS analysis revealed that alloying elements are present in the sintered porous Al composites as shown in Figure 4.16 (c).

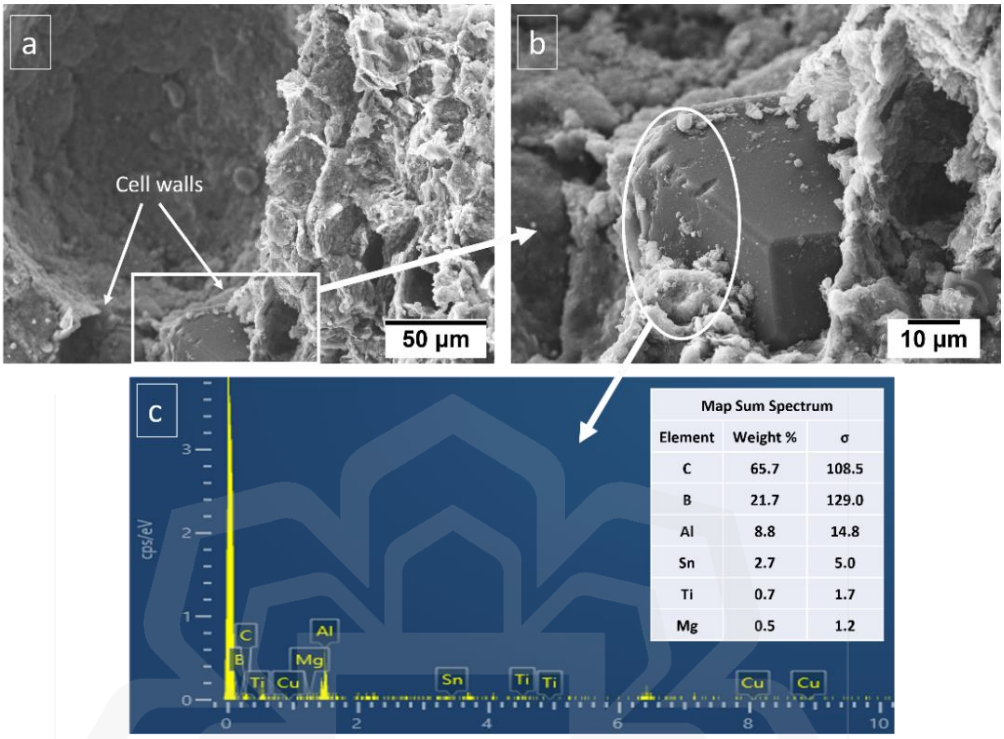

Figure 4.16 SEM images of (a, b) cell wall of sintered porous Al composite near the vicinity of diamond particle, and (c) EDX of the Al alloy matrix and Ti-coated diamond interface

4.3.2.2 Effect of PMMA particle size

The porous composite that replicated the shape and size of space holder materials are important in controlling the porosity and pore size (Tan et al., 2018). It allows the predictability and reproducibility of mechanical properties. The spherical structured cells (pores) and uniform distribution of the cell walls were obtained by adding the space holder particles of varying size resulting into pores of different size, as evident from Figure 4.17. Due to uniform pore distribution in the porous structure, the strength of porous Al composite was found to have improved.

Table 4.11 shows that the composites with PMMA particle size of 150 µm exhibited higher plateau strength values than composite with smaller PMMA

particle sizes (75 µm and 130 µm). The cell walls have a significant impact on the overall load capacity (Sun et al., 2021). The smaller pores size result into the formation of finer solid framework with smaller wall thickness while the larger pores size form thicker cell walls as shown in Figure 4.17. The thicker walls exhibit high compressibility thus better compressive properties. Moreover, pore size also allows to control the porosity as the pore size decreased, the number of pores increases hence resulting in a smaller thickness of edges of the cell. Furthermore, these cell edges cannot supply enough melt during sintering thus resulting in significant reduction in mechanical properties that eventually reducing the plateau strength. Similarly, these effects were also seen in the case of energy absorption capacity in which maximum values were acquired from the porous composite with 150 µm particle size of PMMA space holder.

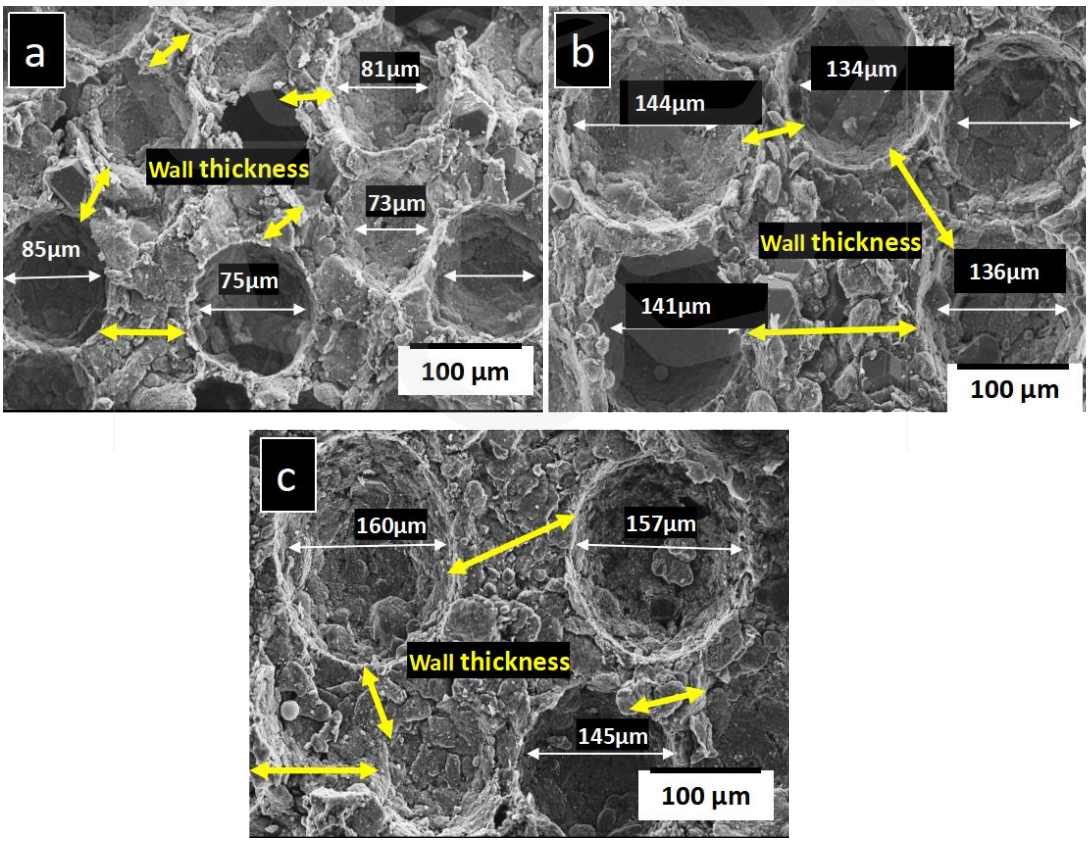

Figure 4.17 Pore size and wall thickness of pores in porous Al composite with varying PMMA particle size, (a) 75 µm, (b) 130 µm and (c) 150 µm

4.3.2.3 Effect of PMMA content

Porosity is known to influence the mechanical properties of porous composite and attaining uniform porosity dispersion could enhance the mechanical response (Bekoz & Oktay, 2013). The porosities can be easily controlled by proper selection of space holder's content. In this study, the porosities of the porous composite were varied using different contents of PMMA particles. The porosities in the porous Al composite were observed to be dependable on the PMMA content as tabulated in Table 4.11. The isolated pores were mostly found in composite containing 20 wt. % of PMMA particles in comparison to 25 wt. % and 30 wt. % of PMMA content as evident from Figure 4.16. Moreover, the interconnected pores were observed as the amount of PMMA particles increased. When PMMA content was increased from 20 wt. % to 30 wt. % the interconnected pore in the resultant composite also increased. These interconnected pores was reported to aid in the better decomposition of the space holder particles during sintering (Anovitz & Cole, 2015). The porous Al composite with 25 wt. % of PMMA content demonstrated well defined pores structure with minimal cracks as shown in Figure 4.16 (c, e, and h) and thus revealed greater compressive properties. The plateau strength and energy absorption capacity were recorded in the range of 20.27 MPa to 40.2 MPa and 5.12 MJ/m^3 to 13.66 MJ/m^3 respectively.

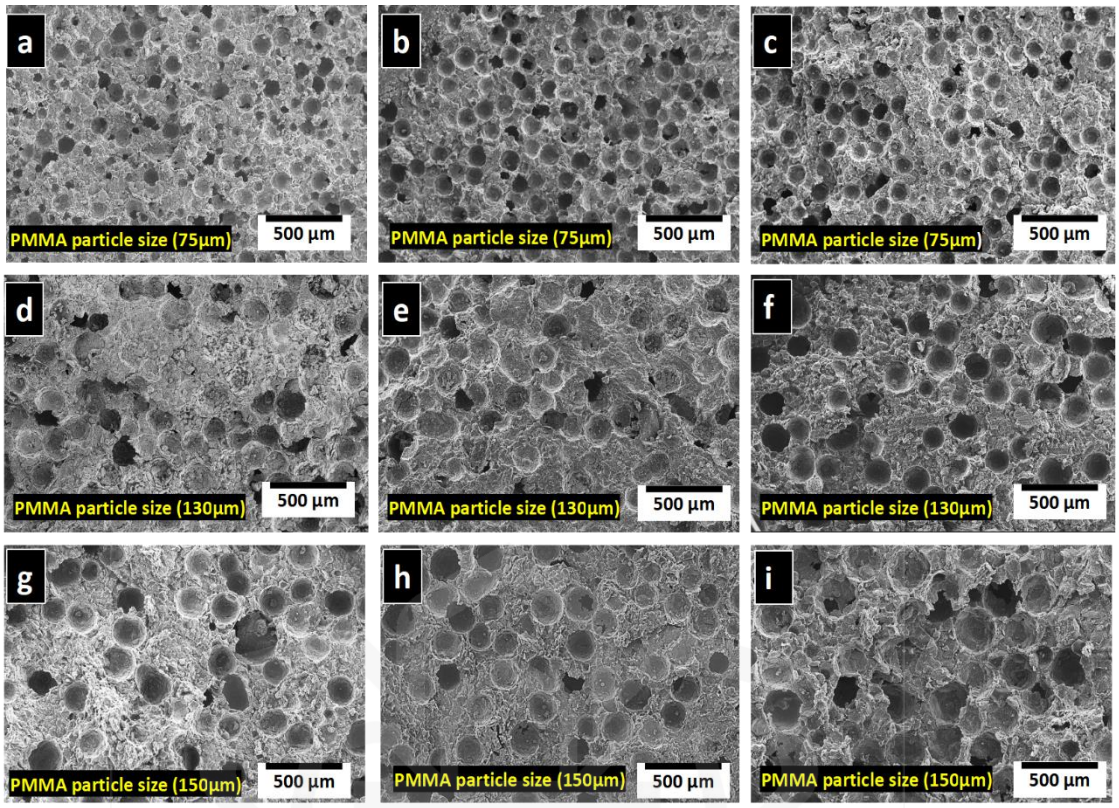

Figure 4.18 SEM microstructure of porous Al composite with varying PMMA particle content, (a, d, g) 20 wt.%, (b, e, h) 25 wt. %, and (c, f, i) 30 wt.%

4.3.3 Effect of varying composition (Analytic)

4.3.3.1 Analysis of Means

The plateau strength and energy absorption capacity were regarded as response variables to improve the compressive properties. To increase their applicability, the values of plateau strength and energy absorption capacity should be maximized. As a result, the signal-to-noise (S/N) ratio for the response factors was determined by keeping the option "larger the better". Figure 4.18 and Figure 4.19 demonstrate the main effect plot that explains the impact of input factors on the plateau strength and energy absorption capacity, respectively. The results of the compressive properties were analyzed using the MINITAB software, and the characteristic values were transformed to S/N ratio values. The mean of means and mean of S/N ratio graphs show that the

plateau strength increased with an increased in the diamond content up to 8 wt. % and then reduced insignificantly. However, in term of PMMA particle size, the maximum plateau strength values were obtained at level 1 (75 µm) and level 3 (150 µm) whereas in the case of PMMA content, the plateau strength was found to increase up to 25 wt. % in which on further addition the plateau strength continue to decrease. Similarly, from means of means graph of energy absorption capacity, it increased with an increase in the diamond content and maximum value was acquired at level 3(12 wt. %). On the other hand, in term of different size of PMMA particles, the energy absorption capacity increased and then decreased in which the maximum value was acquired at level 3(150 µm). In terms of PMMA content, the energy absorption capacity increased up to 25 wt.% in which beyond this, the energy absorption capacity decreased. Nevertheless, the value at level 3 (30 wt. %) was found to be higher in comparison to the lowest level 1 (20 wt. %) as evident from Figure 4.19.Figure 4.19

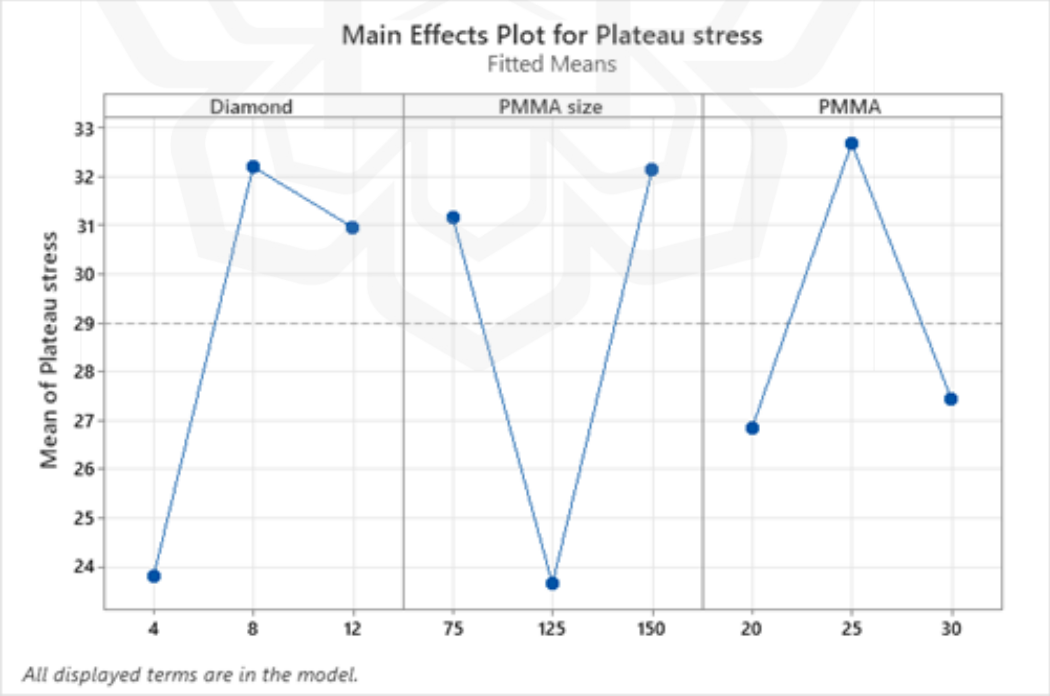

Figure 4.19 Mean response curve of plateau strength

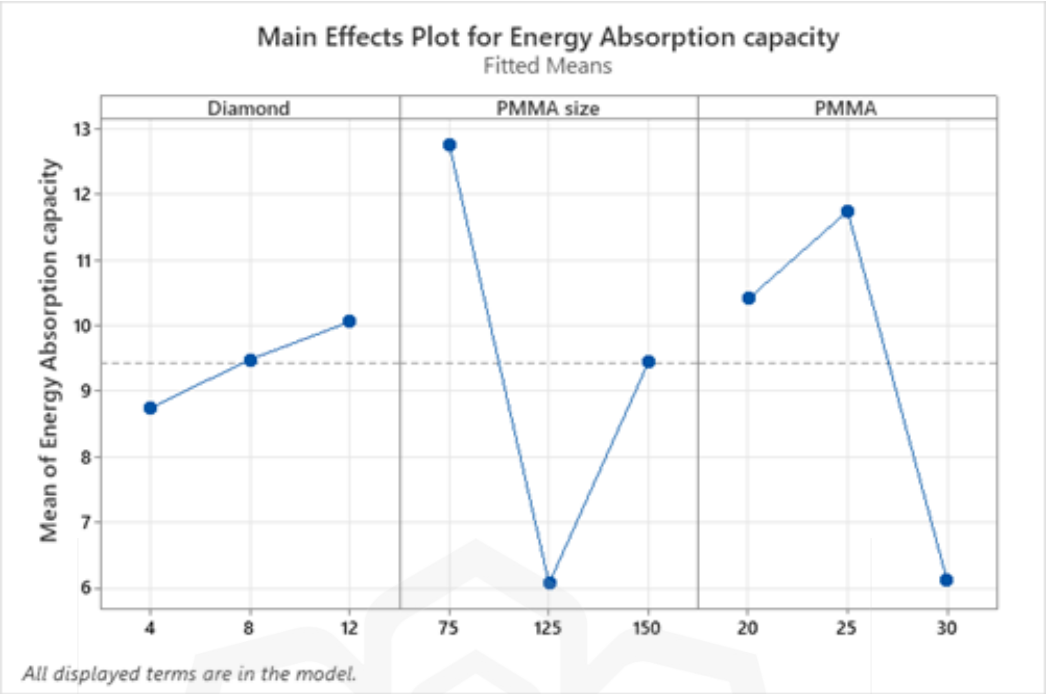

Figure 4.20 Mean response curve of energy absorption capacity

4.3.3.2 Analysis of variance

ANOVA serves to investigate the effect of parameters and their relationships by analyzing the mean square against response errors at predefined confidence levels. The ANOVA allows to find the effect of each factor on the overall variance of the results. The ANOVA results for the response factors including the plateau strength and energy absorption capacity, are presented in Table 4.13 and Table 4.14 respectively. The analysis was conducted at a 10% significance level, which corresponds to a 90% level of confidence. Each ANOVA table contains a percentage contribution to total variation for each factor's variable. The contribution of each factor that has a large impact on response factors (plateau strength and energy absorption capacity), as evident from Figure 4.21, is analyzed using the ANOVA table results. The diamond content shows the most significant (40.76%) effect on the plateau strength followed by PMMA size (22.85%) and PMMA content (14.41%), as evident from Table 4.13 and Figure 4.20 (a). Correspondingly, Table 4.14 and Figure 8b indicate that the diamond content highly

affects the energy absorption capacity (56.96%) followed by a PMMA content (13.52%) and a PMMA size (8.54%). This could be a reason for the diamond content to influence the plateau strength and energy absorption capacity significantly, which is around 40.76% and 56.96%, respectively.

As a result, the effect of diamond content on the plateau strength and energy absorption capacity of porous Al composite in the present study was maximum as compared to the effect of PMMA size and PMMA content. The influence of the PMMA content on the plateau strength was minimal (14.41%) whereas the effect of PMMA size on the energy absorption capacity was also found to be minimal (8.54%). It has been reported that the addition of diamond particles increased the load bearing capacity of porous Al composite (Liu et al., 2014). The authors added that as the modulus of the diamond particles was much greater than the matrix, the diamond particles bear the load directly by stress concentration. Moreover, during compression process, the additional stress concentration as a result of diamond particle jamming increased the particle's load-carrying capacity, thereby improving the compressive properties (Liu et al., 2014).

The linear polynomial model can be obtained from the ANOVA as it defines the plateau strength and energy absorption capacity as a function of diamond content, PMMA size, and PMMA content. The greatest R^2 predictions for plateau strength and energy absorption capacity were determined to be 94.49% and 99.18%, indicating that the model could predict new observations nearly as good as it matched the sample data. Furthermore, the regression equation adequately explained the current study.

Table 4.13 ANOVA Variance table for Plateau strength

Source	**DF**	**Seq SS**	**Contribution**	**Adj SS**	**Adj MS**	**F-Value**	**P-Value**
Diamond	2	122.95	40.76%	122.95	61.47	1.85	0.350
PMMA size	2	68.91	22.85%	91.66	45.83	1.38	0.420
PMMA	2	43.46	14.41%	43.46	21.73	0.66	0.604
Error	2	66.29	21.98%	66.29	33.14		
Total	8	301.61	100.00%				

Table 4.14 ANOVA Variance table for energy absorption capacity

Source	DF	Seq SS	Contribution	Adj SS	Adj MS	F-Value	P-Value
Diamond	2	35.326	56.96%	35.326	17.663	2.72	0.269
PMMA size	2	5.300	8.54%	6.047	3.024	0.46	0.683
PMMA	2	8.388	13.52%	8.388	4.194	0.64	0.608
Error	2	13.009	20.97%	13.009	6.504		
Total	8	62.023	100.00%				

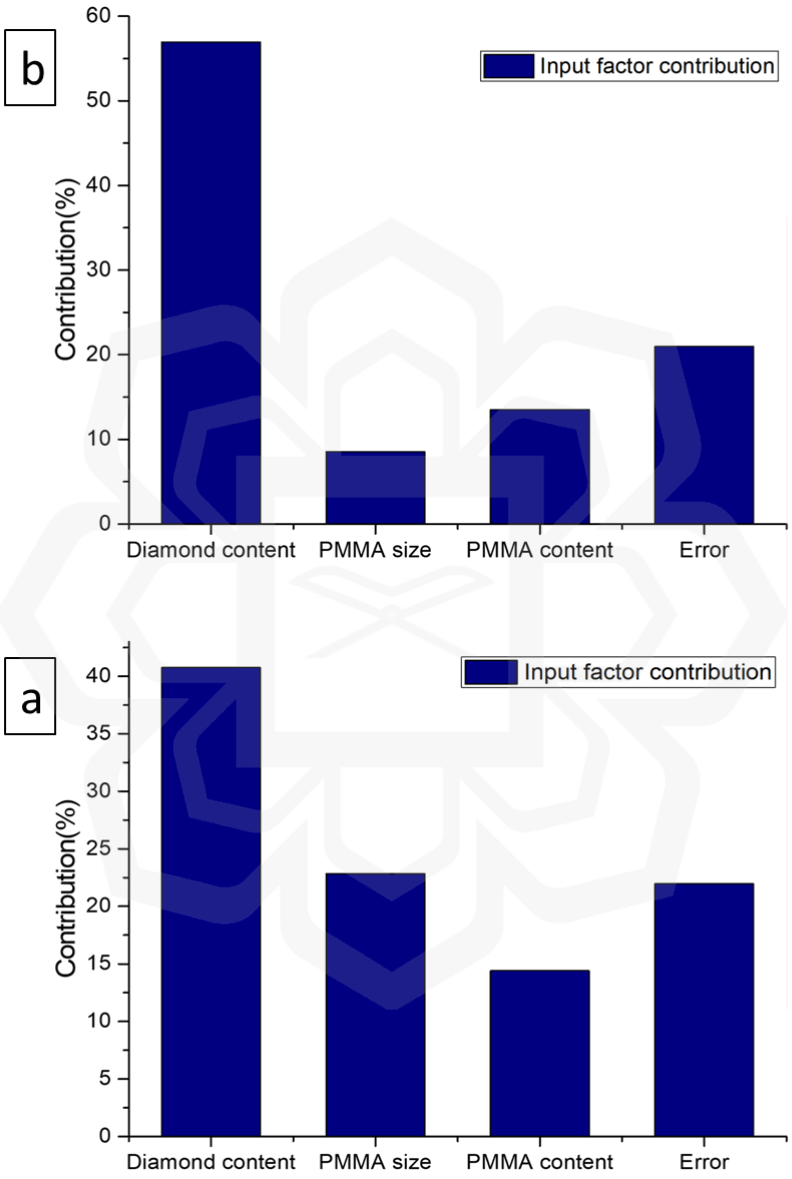

Figure 4.21 Percentage of the contribution of input factors on, (a) plateau strength, and (b) energy absorption capacity

4.3.3.3 Regression analysis

The statistical model based on linear regression equations was acquired applying L_9 orthogonal using MINITAB software. Based on each response factor, a regression equations (or linear polynomial model) for plateau strength and energy absorption capacity were derived as in Equation 4.4 and 4.5 and are presented as follows:

$$Plateau\ stress = 28.99 - 5.18D_1 + 3.21D_2 + 1.97D_3 + 2.18P_{s1} - 5.333P_{s2} + 3.15P_{s3} - 2.14P_{c1} + 3.69P_{c2} - 1.55P_{c3} \quad (4.4)$$

$$Energy\ absorption\ capacity = 8.379 - 2.78D_1 + 1.10D_2 + 1.68D_3 - 0.04P_{s1} - 1.03P_{s2} + 1.08P_{s3} - 1.12P_{c1} + 1.47P_{c2} - 0.35P_{c3} \quad (4.5)$$

where D is the diamond content, P_s is the PMMA particle size and P_c is the PMMA content.

The percentage deviations were obtained by calculating the response plateau strength and energy absorption values using linear regression Equation 4.4 and 4.5. The significant residual errors of each test, and the maximum errors of 1.12 and 1.39 (Table 4.15 and Table 4.16) were acquired for plateau strength and energy absorption capacity, to verify the discrepancy in the experimental and model fit values. The data for each experiment run is illustrated in Figure 4.21. A rate of change of plateau strength and energy absorption capacity were produced by the device errors and processing errors. In addition, experimentation also relies on other factors including mixing parameters and material compositions as the compressive properties also dependable on these factors.

Table 4.15 Fits and diagnostics for all observations for plateau strength

Obs	Plateau strength	Fit	SE Fit	Resid	Std Resid	Del Resid
1	24.80	23.85	5.50	0.95	0.55	0.43
2	20.27	22.17	4.62	-1.90	-0.55	-0.43
3	26.37	25.42	5.50	0.95	0.55	0.43
4	36.68	32.83	4.62	3.85	1.12	1.30
5	30.06	30.56	4.62	-0.50	-0.15	-0.10
6	29.86	33.21	5.08	-3.35	-1.23	-1.79
7	26.79	31.59	4.62	-4.80	-1.40	-6.62
8	25.89	23.49	5.50	2.40	1.40	6.62

Table 4.16 Fits and diagnostics for all observations for energy absorption capacity

Obs	Energy absorption capacity	Fit	SE Fit	Resid	Std Resid	DFITS
1	4.89	4.43	2.43	0.46	0.60	1.4955
2	5.12	6.03	2.05	-0.91	-0.60	-0.6289
3	6.78	6.32	2.43	0.46	0.60	1.4955
4	10.75	9.09	2.05	1.66	1.09	1.6322
5	9.77	9.92	2.05	-0.15	-0.10	-0.0922
6	7.93	9.44	2.25	-1.51	-1.26	-3.6402
7	7.55	9.66	2.05	-2.11	-1.39	-7.2209
8	8.96	7.90	2.43	1.06	1.39	17.1717
9	13.66	12.60	2.43	1.06	1.39	17.1717

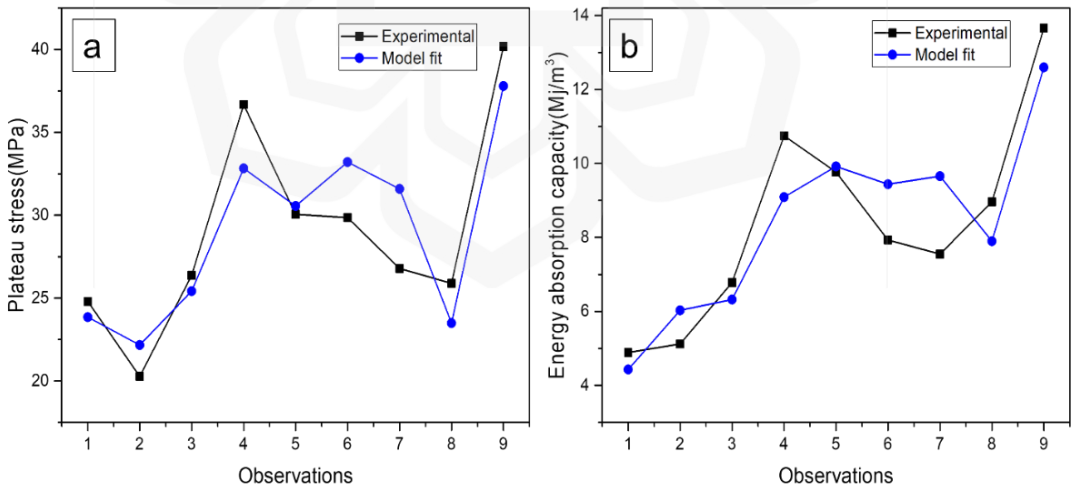

Figure 4.22 Evaluation of experimental and modal predicted (a) Plateau strength, and (b) Energy absorption capacity

4.3.3.4 Response optimization

The response optimization study was conducted to find the best results. The intention of conducting this study was to control the compressive properties of porous Al composite. In this study, the goal was to maximize the results to optimize the plateau strength and energy absorption capacity. As shown in Table 4.17 the lower value of plateau strength, which can be considered the predicted value. The target and lower values were observed to have maximum and minimum variations, but this is impractical. However, this discrepancy is due to the dependence of the compressive properties on other factors such as the alloy composition, crosshead speed during compression testing, and other factors. These may produce extremely high or low values. As a result, the fit values as mentioned in Table 4.17 can be considered a safe and reasonable value for plateau strength and energy absorption capacity in which can be attained with a combination of Ti-coated diamond content of 12 wt. %, PMMA particle size of 150 µm and PMMA particle content of 25 wt. %.

Table 4.17 Response optimization: composition and characteristics

Response	**Goal**	**Lower**	**Target**	**Upper**	**Weight**
Energy Absorption capacity	Maximum	4.89	13.66		1 1
Plateau strength	Maximum	20.27	40.20		1 1

Solution

Solution	Diamond	PMMA size	PMMA	Energy Absorption capacity Fit	Plateau strength Fit	Composite Desirability
1	12	150	25	12.6029	37.7998	0.879515

Variable Settings

Diamond	12
PMMA size	150
PMMA	25

Response	Fit	SE Fit	95% CI	95%PI	Fit

Energy Absorption capacity	12.60	2.43	(2.13, 23.08)	(-2.57, 27.77)
Plateau strength	37.80	5.50	(14.16, 61.44)	(3.56, 72.04)

4.3.3.5 Interaction plots

The diamond content and PMMA particle size interaction can be observed from the interaction plots of plateau strength as shown in Figure 4.23. At PMMA particle size of 75 µm and 125 µm, the plateau strength increased up to 8 wt. % of diamond in which further addition decreased the plateau strength. However, the plateau strength for PMMA size of 150 µm was found to increase with increasing diamond content from 4 wt. % to 12 wt. %, respectively. Similarly, the plateau strength values for 20 wt. % and 30 wt. % of PMMA content initially increased with increasing diamond content from 4 wt. % to 8 wt. % in which further addition of diamond content decreased the plateau strength value (diamond and PMMA content interaction plot). On the contrary, the plateau strength linearly increased with increasing diamond content from 4 wt. % to 12 wt. % in the case of PMMA particle size of 25 wt. %. Moreover, the interaction plot for PMMA size and PMMA content demonstrates that the plateau strength of porous Al composite increased (PMMA content of 20 wt. % and 25 wt. %) with increasing the PMMA particle size. However, the plateau strength decreased with maximum PMMA content of 30 wt. %.

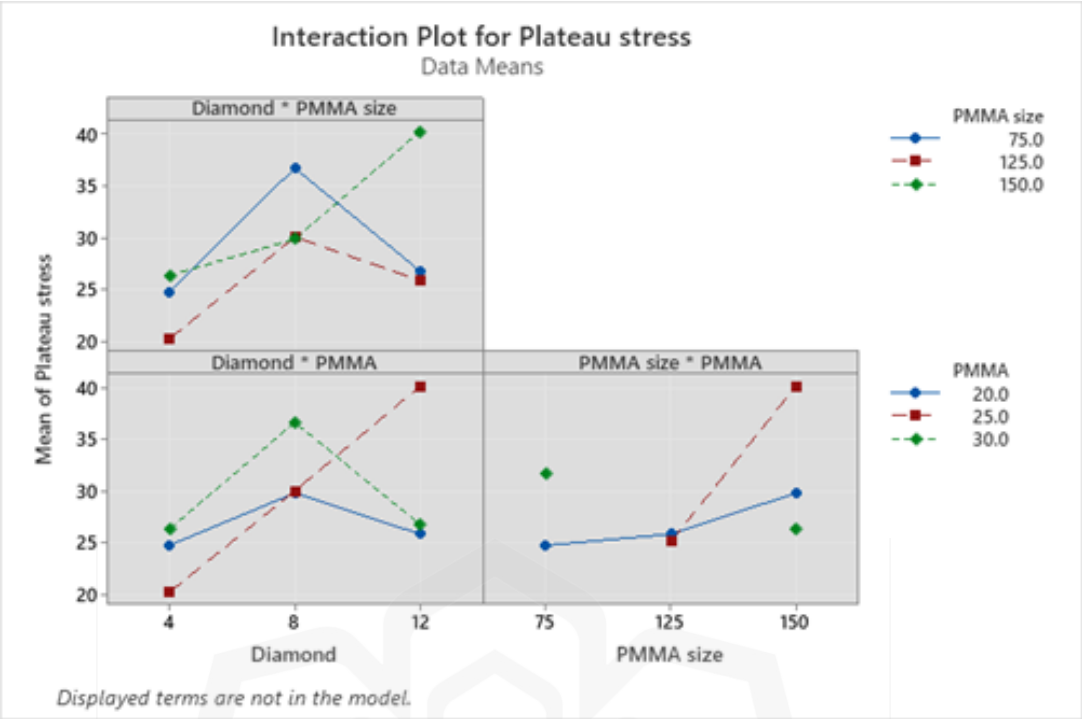

Figure 4.23 Interaction plots for plateau strength

The interaction plots for energy absorption capacity as shown in Figure 4.24 reveal the interaction plot for diamond content and PMMA particle size. The energy absorption capacity was found to initially increased from 4 wt. % to 8 wt. % of diamond content in which further addition of diamond content (12 wt. %), decreased the energy absorption capacity in the case of PMMA particle size of 75 µm and 125 µm. However, the energy absorption capacity increased with increasing diamond content from 4 wt. % to 12 wt. % as the PMMA particle size was maximized to150 µm. Similarly, for diamond and PMMA content interaction plot, the energy absorption capacity value for PMMA content of 30 wt. % was found to firstly increased with increasing diamond content from 4 wt. % to 8 wt. % (diamond content and PMMA content interaction plot) in which maximum addition of diamond content was found to decrease the energy absorption capacity. Although the energy absorption increased with increasing diamond content from 4 wt. % to 12 wt. % in the case of PMMA content ranging from 20 wt. % to 25 wt. %, the increasing pattern was found to be prominent

for PMMA content of 25 wt. %. Additionally, the energy absorption capacity for PMMA content of 25 wt. % increased with increasing PMMA content in which the energy absorption capacity for 20 wt. % and 30 wt. % of PMMA content decreased accordingly (PMMA particle size and PMMA content interaction plot).

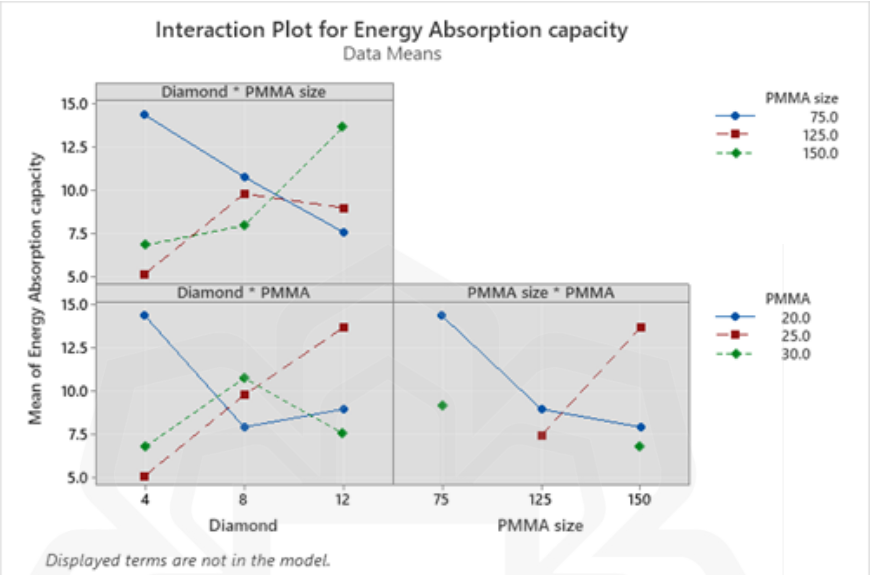

Figure 4.24 Interaction plots for energy absorption capacity

4.3.3.6 Contour plots

A comparison between the plateau strength and energy absorption capacity responses using contour plots. Figure 4.25 and Figure 4.26 display three contour plots including PMMA particle size versus diamond content, PMMA content contrasted with diamond content and PMMA content in competition with PMMA. The contour plot variations were expressed as color variation, with different ranges for the individual colors based on the intensity of the experimental results. The contour plots present the influence in rise or decline of plateau strength and energy absorption capacity at withhold value for PMMA content of 25 wt. % as shown in Figure 4.25 (a) and Figure 4.26 (a), PMMA particle size of 112.5 µm as reveals in Figure 4.25 (b) and Figure 4.26 (b), as well as diamond content of 8 wt. % as expresses in Figure 4.25 (c) and Figure 4.26 (c), respectively. In combination with the parameters as shown in Figure 4.25 (a), the

plateau strength increased with an increasing diamond content and the influence of the PMMA particle size revealed an increment pattern followed by a decrement pattern of plateau strength. Figure 4.25 (b) depicts that the plateau strength increased with increasing PMMA content. However, for increased diamond content, the plateau strength was found to have increased and then decreased accordingly. Moreover, the plateau strength increased with increasing PMMA content as seen in Figure 4.25 (c) whereas the plateau strength was found to decrease and then increased (maximum plateau strength) with increasing PMMA particle size. Furthermore, it can be observed from Figure 4.26 (a) that with increasing PMMA particle size, the energy absorption decreased whereas the energy absorption capacity increased with increasing diamond content.

Moreover, Figure 4.26 (b) reveals the energy absorption capacity increased by increasing size of PMMA particles as well as diamond content. However, the diamond content was found to have maximum influence thus providing higher value. A similar effect is seen in the contour plot of PMMA vs PMMA size in which the value of energy absorption capacity was found to be higher with the higher values of combined parameters (Figure 4.26 (c)). It can be said that an increase in the compressive properties of the resultant porous Al composite with increase in PMMA content as well as the size could be attributed to the presence of increased well-defined pores with unique cell wall thickness thereby consequently improving the compressive strength of the porous composite. In addition, the cell size as well as cell wall thickness increased with increasing PMMA size that eventually increasing the compressive properties. Therefore, these contour results successfully demonstrated that the selected inputs had effects on the changing response of the present work.

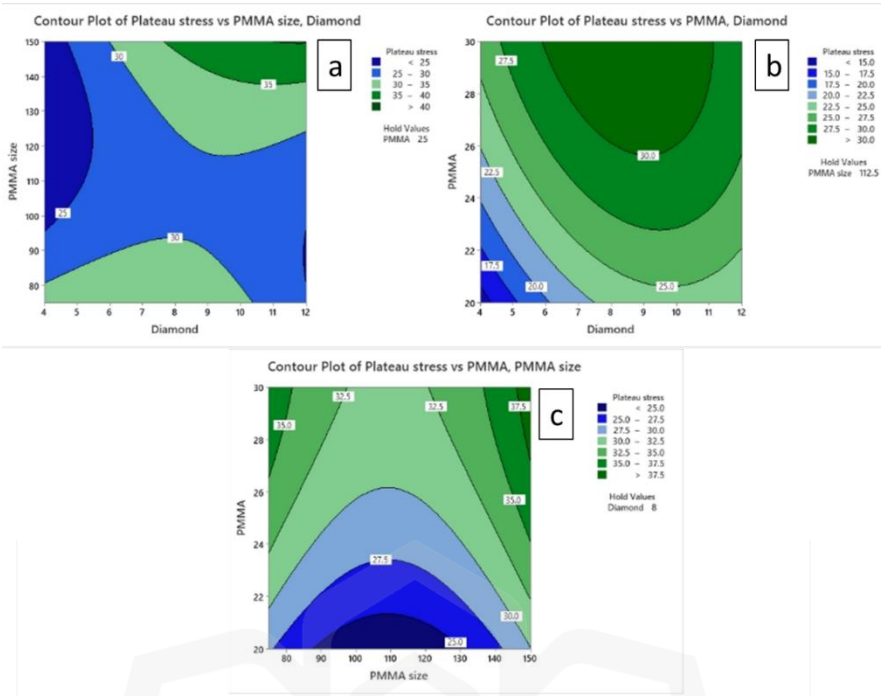

Figure 4.25 Contour plot of plateau strength for, (a) PMMA size vs diamond content (b) PMMA vs diamond content and (c) PMMA size vs PMMA content

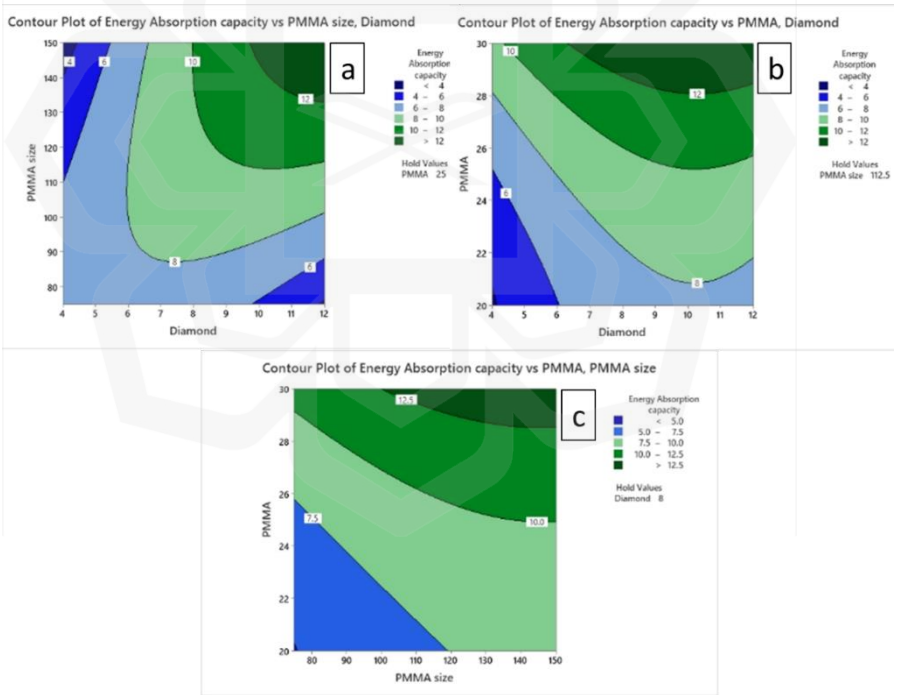

Figure 4.26 Contour plot of energy absorption capacity of, (a) PMMA size vs diamond content (b) PMMA vs diamond content and (c) PMMA size vs PMMA content

4.3.3.7 Confirmation test

Finally, the experimental confirmation for investigation of the optimal test conditions was performed. The confirmation test was carried out via experimental approach, based on the optimal level of factors including diamond content of 12 wt. %, PMMA particle size of 150 μm, and PMMA content 25 wt. %. Finally, the obtained results were compared with the predicted results. Figure 4.27 depicts the stress-strain diagram that shows the comparison between the confirmation test result and the highest value obtained from Taguchi L9 runs as demonstrated in Table 4.11. From Figure 4.27, the confirmation test results exhibited the highest plateau strength based on its higher stability as compared to the result obtained in the prior test.

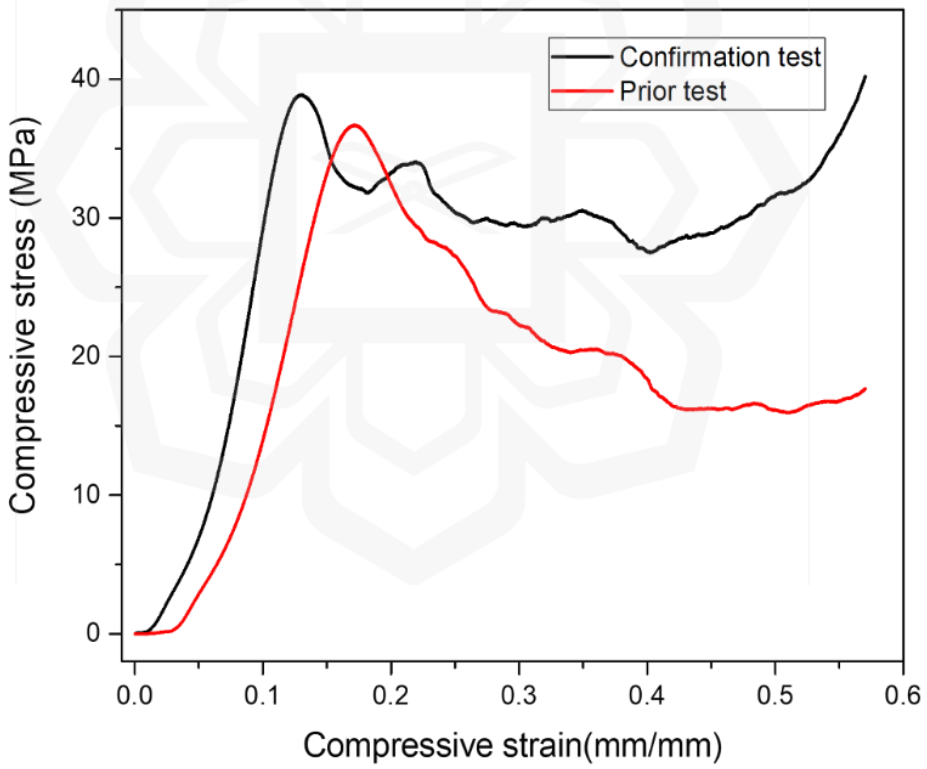

Figure 4.27 Comparison of confirmation test result at optimal input factors and maximum value obtained from Taguchi L_9 runs

Moreover, Table 4.18 tabulates the comparative results obtained for the best or optimal parameters. It was discovered that the experimental and predicted results were in close

agreement. However, an error of 6.4% and 11.1% was observed in plateau strength and energy absorption capacity, respectively.

Table 4.18 Comparison of confirmation test with predicted values

Responses	Prediction	Experimentation	Error (%)
Plateau strength (MPa)	**37.79**	**40.21**	**- 6.4**
Energy absorption capacity (MJ/m^3)	**12.60**	**11.20**	**11.1**

4.4 EFFECT OF UNCOATED AND COATED DIAMOND IN IMPROVING COMPRESSIVE PROPERTIES OF POROUS AL COMPOSITE

This section discusses the effects of uncoated and Ti-coated diamond particles as reinforcement materials on the microstructure, density, and compressive properties. Since in section 4.3, an improvement in the compressive properties was observed at higher Ti-coated diamond content and the effect only upto 12 wt.% was explored. Thus, to study the effect of further addition of diamond particles at optimum parameters, the uncoated and Ti-coated diamond content were varied at 0 wt. %, 6 wt. %, 9 wt. %, 12 wt. %, 15 wt. %, and 20 wt. %, respectively. The processing parameters employed to fabricate these porous Al composites were taken from the optimized results from section 4.2 (sintering temperature of 590℃, compaction pressure of 350 MPa and sintering time of 90 min). Furthermore, the content and the size of PMMA particles as a space holder material were taken from the optimized results of from section 4.3 (i.e., PMMA particle size of 150 μm and PMMA content of 25 wt. %).

4.4.1 Morphological analysis

4.4.1.1 Microstructure

Figure 4.28 (a, b) demonstrates the microstructure of the porous Al without any reinforcement as confirmed by EDX analysis Figure 4.28 (c). It shows a homogenous

distribution of closed macro-pore structure. These macro-pores were found to mimic the shape and size of the spherical PMMA particles. It is vital to obtain pores that imitate the morphology of the space holders, indicating that the pore structure can be tailored, depending on the space holder shape, size, and content. Moreover, these macro-pores were separated by a unique cell wall as observed in Figure 4.28 (a, b). However, the porous structure was not firm resulting in cracking of cell walls as evident from Figure 4.28 (a). This can be due to absence of reinforcement material that otherwise can impart firmness to the porous Al.

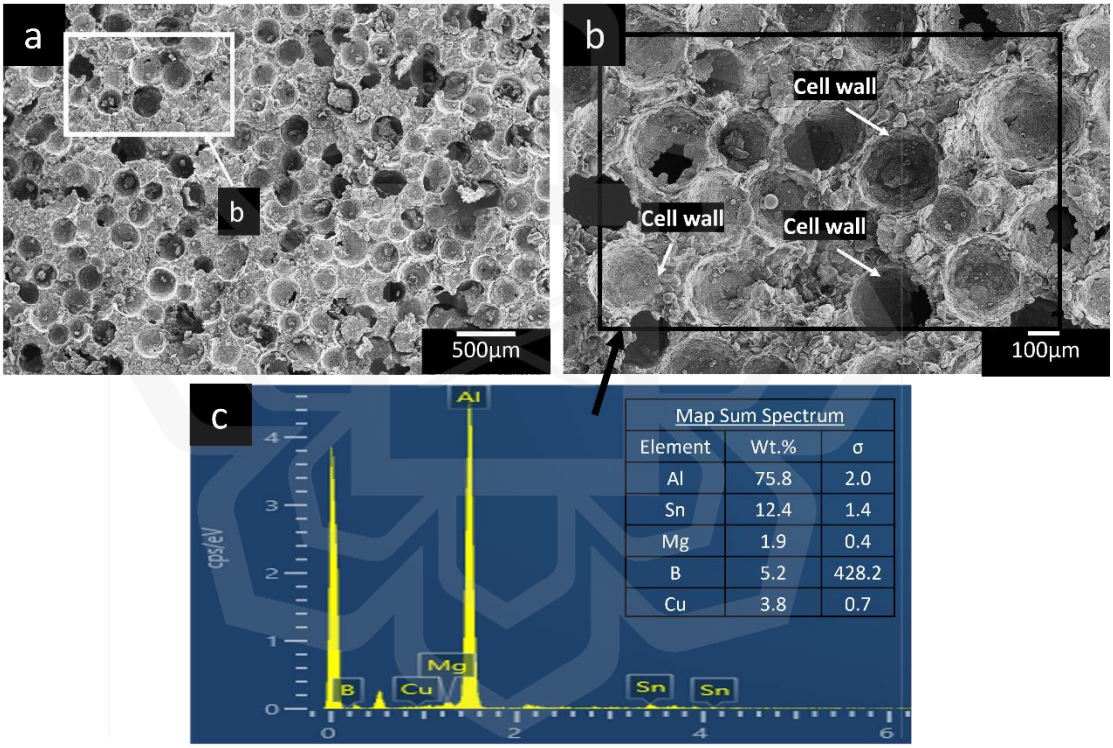

Figure 4.28 SEM micrography of porous Al with no reinforcement, (a) magnification of 33x, (b) magnification of 100x, and their (c) EDX

Further, the microstructure and EDX analysis of uncoated diamond reinforced porous Al composite are presented in Figure 4.29. The EDX analysis of composites reinforced with uncoated diamond (Figure 4.29 (f)) confirms the formation of carbides at the diamond and Al alloy matrix interface that resulted in weak adhesion between the diamond particles and matrix. This weak interfacial bonding caused gaps (empty

spaces) at the interfaces of Al alloy matrix and reinforcements as seen in Figure 4.29 (a-e). Moreover, the porosities were found to increase with increasing diamond content owing to the occurrence of more gaps (empty spaces) at the interfaces of Al alloy matrix and diamond particles (Figure 4.29(a-e)), resulting into poor wettability and weak bonding between Al alloy matrix and diamond reinforcement.

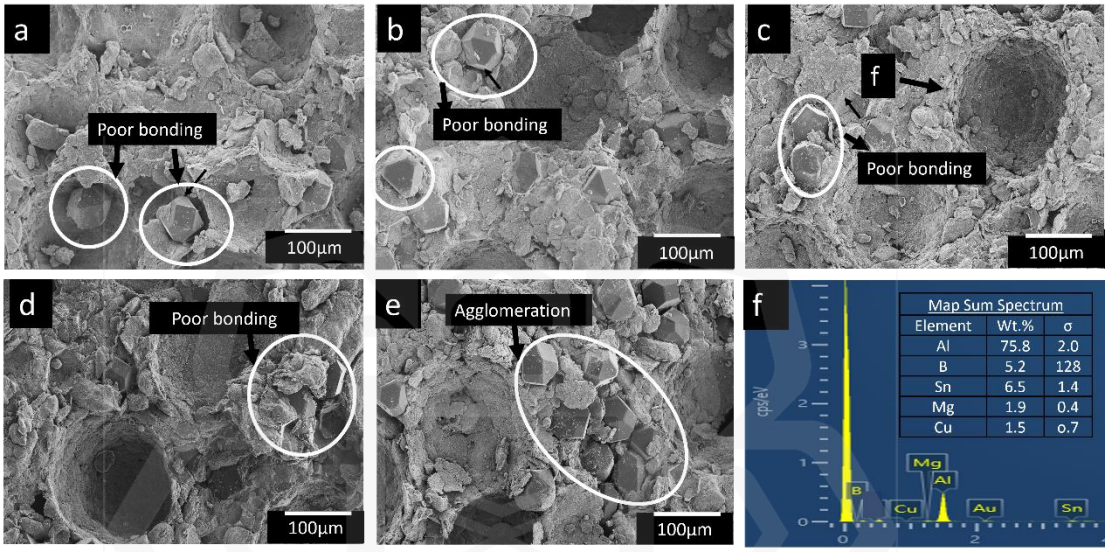

Figure 4.29 Morphology and elemental analysis of porous Al composite reinforced with, (a) 6 wt. %, (b) 9 wt. %, (c) 12 wt. %, (g) 15 wt. %, (e) 20 wt. % of uncoated diamond particles, and (f) EDX of porous Al composite

However, in case of porous Al composite reinforced with Ti-coated diamond, the interfacial interaction between diamond particles and Al alloy matrix was evidenced to improve as illustrated in Figure 4.30 (a-e). This could be due to the presence of Ti coating on the surface of diamond particles that significantly improved the wettability between the Al alloy matrix and diamond particles and thus increased their bonding strength. The EDX analysis as shown in Figure 4.30 (f) verifies the presence of alloying elements as well as Ti-coating element on the surface of diamond particles. However, at higher diamond content, the absence of sufficient matrix to wet the reinforcements lead to the agglomeration of these diamond particles on the boundaries of the Al alloy matrix hampered the diffusion bonding at the interface of Al alloy matrix and diamond

particles during sintering thus resulting in the formation of fracture initiation sources as proven in Figure 4.30 (e), thereby affecting the strength of the resultant porous Al composite.

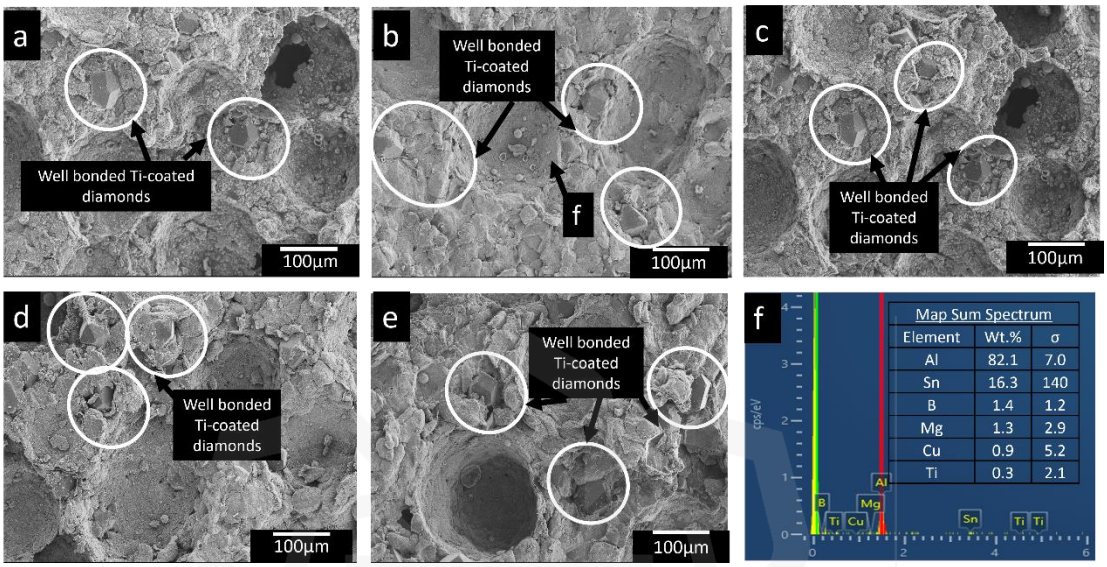

Figure 4.30 Morphology and elemental analysis of porous Al composite reinforced with, (a) 6, (a) 9, (a) 12, (a) 15, (a) 20 wt.% of Ti-coated diamond particles and (f) EDX of porous al composite

4.4.1.2 Porosity and Density

As per ASTM definitions, there are two types of porosity in composite: (1) engineered porosities that are intentionally designed and controlled for some specific performance or an engineered function. Such porosities typically possesses physical properties such as dimensions, size, shape, and architecture, which can be controlled during fabrication process and; (2) apparent porosities are unintentionally formed porous defects in the fabricated composite structure (Maharma et al., 2020). Therefore, the engineered porosities in the resultant porous Al composite were obtained using fixed PMMA content of 25 wt. %. However, from Figure 4.31 (a) the porosity values were found greater than 25 wt.%. This can be attributed to the formation of micropores and the few pores connectivity present in the cell walls of the porous composites.

Figure 4.31 reveals the percentage of porosity and relative densities porous Al composite at various uncoated and Ti-coated diamond content of 6 wt. %, 9 wt. %. 12 wt. %, 15 wt. % and 20 wt. %. The different percentage of porosity level indicated complete removal of PMMA particles during sintering. Moreover, the percentage of porosity was recorded to increase with increasing diamond content as shown in Figure 4.31 (a). On the contrary, the relative density was found to decrease with increasing diamond content as evidenced from Figure 4.31 (b). This could be probably due to the presence of cracks and voids between the interfaces of Al and diamond particles because of insufficient matrix filling the pores between the diamond particles owing to the densification difficulty with increasing Ti-coated diamond content as evident from Figure 4.30 (d, e), which was more pronounced in case of uncoated diamond reinforced porous Al composites.

Similar findings were also documented in the previous literature (Chung et al., 2014; Liu et al., 2017; Tatt et al., 2016; Zhang et al., 2016) Therefore, it can be concluded that the percentage of porosity and density of diamond reinforced composite in the current study not only depending on the PMMA content, but also on the interfacial bonding between the Al matrix and diamond reinforcement.

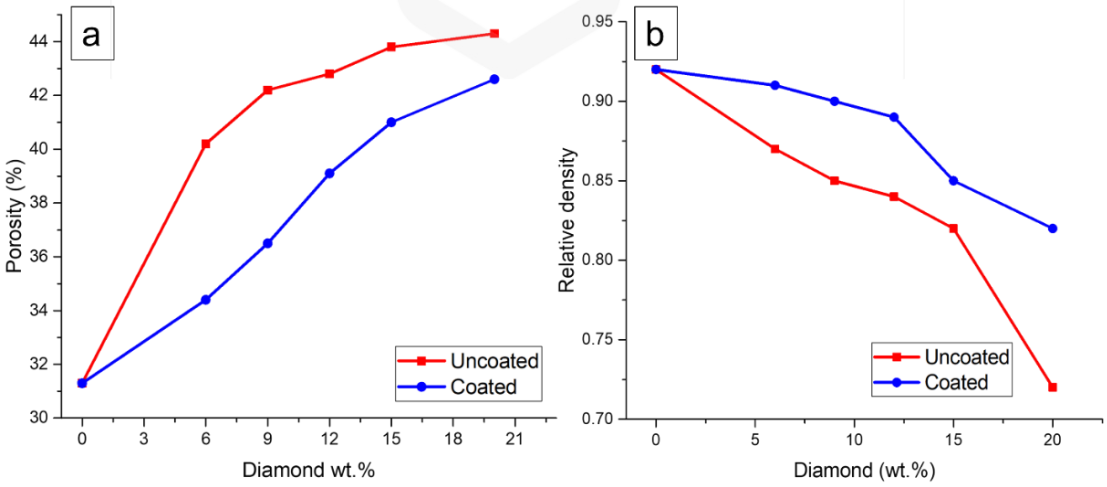

Figure 4.31 Percentage of (a) porosity and (b) relative densities of porous Al composite reinforced with uncoated and Ti-coated diamond

4.4.1.3 X-ray Diffraction analysis

The XRD patterns of the structural evolution of porous Al composite consisting of Al alloy matrix with uncoated and Ti-coated diamond particles as reinforcement as illustrated in Figure 4.28 and Figure 4.33, respectively. Both figures revealed the presence of the Al rich phase represented by the (111), (200), (220) and (311) diffraction peaks at 2θ of 38.54°, 44.78°, 65.11° and 78.28°, respectively. The main difference observed was a broadening of the Al peaks and a decrease in the intensities of their peaks. This is due to the reaction of Al with carbide in case of uncoated diamond reinforced composite and with Ti, in case of Ti-coated diamond reinforced composite during sintering process, thereby resulting in reducing crystallinity as evident from Figure 4.33 respectively. From Figure 4.28, the peak at 43.9° (111), and 75.6° (100) shows the presence of carbon from diamond particles. Similar peaks were observed by other researchers for carbon (Zhang et al., 2016, 2017b). Further, the crystalline diamond peaks were found to diminish initially, followed by its reappearance at high diamond content. The reason for this noticeable change in the XRD pattern is that the carbon atoms from the diamond particles get diffused into the Al-lattice resulting in the formation of Al–C solid solution alloy (Novak and Tschope, 2012; Tan et al., 2013). Moreover, with increase in diamond content the formation of Al_4C_3 (110) carbide phase increases as evident from Figure 4.28. The carbide formation often leads to the deterioration of the mechanical properties of the composite Similar results were obtained in a study during sintering of B_4C coated diamond reinforced composite between 30 min and 90 min (Sun et al., 2018).

However, in the case of porous Al composite with Ti-coated diamond particles, negligible or no traces of the diffraction peaks of Al_4C_3 carbide phase were observed, as evident from Figure 4.33. This implies that the Ti coating successfully inhibited the

reaction between Al and diamond particles during sintering. Where the diffusion of the carbon atoms from the diamond into the Ti-coated layer takes place, thereby occupying the Ti crystal at the octahedral interstitial positions of its lattices. Thus forming δ-TiC transition layer that combines with the diamond metallurgically, and the outer α-Ti layer later enabled wetting the Al matrix (Zhang et al., 2010a). Furthermore, the Al_2Ti peaks were also observed at 38.46° and 64.56° as shown in Figure 4.32 (Pal et al., 2016).

The peaks of XRD for Ti-coated diamond confirm the presence of Al_2Ti, Mg_2Sn, $AlB_{12,}$ Cu_5Sn_6, $Al_{12}Mg_{17}$ and MgB_2 phases in the resultant porous Al composite as shown in Figure 4.33. These phases were formed during sintering as a result of a partial reaction between the constituents. When Mg was added to Al matrix, the Al particle was primarily precipitated along the grain boundary in the form of $Al_{12}Mg_{17}$ phase. As the temperature rose above 120˚C, the $Al_{12}Mg_{17}$ phase began to soften. The $Al_{12}Mg_{17}$ phase could not then function as a pinning-grain boundary at high temperatures, resulting in a reduction of mechanical properties (Yang et al., 2016). This however could be improved by the addition of Sn element (Guan et al., 2018).

On the addition of Sn, Cu and Mg to Al, there occurred solid solubility of Sn in Mg and Sn in Cu that produce Mg_2Sn and Cu_5Sn_6 phases, respectively. The Mg_2Sn phase significantly contributed to fine-grain and precipitation strengthening (Guan et al., 2018). Not only that, Cu also having higher affinity for Sn in which Sn is known to initially melt and formed Cu-Sn phases in the vicinity of Cu. (Amore et al., 2008). Furthermore, the reaction between liquid Mg and free B also resulted into the formation of MgB_2 phase (Cafri, 2012). Moreover, B tended to enrich the interface due to pull of chemical bond forces that subsequently caused the interface-enriched B element to react spontaneously with the Al matrix to form AlB_{12} (Mei et al.,2021). The formation of the intermetallic element improve the properties of the composite (Ebhota & Jen, 2018).

These intermetallic phases act as hinderance to dislocation motion on application of load, thus enhances the strength of porous composites improved their performance.

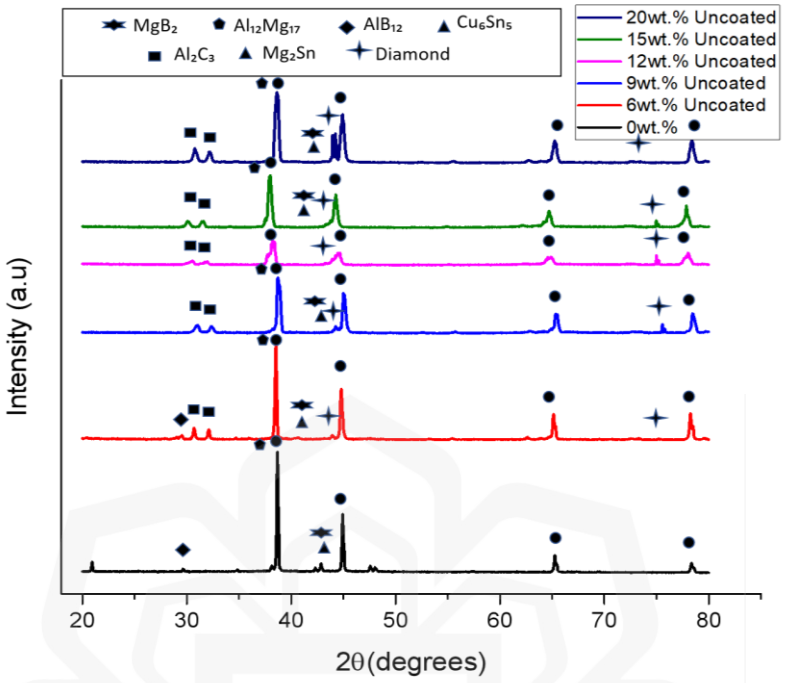

Figure 4.32 XRD patterns of porous Al composite reinforced with uncoated diamond

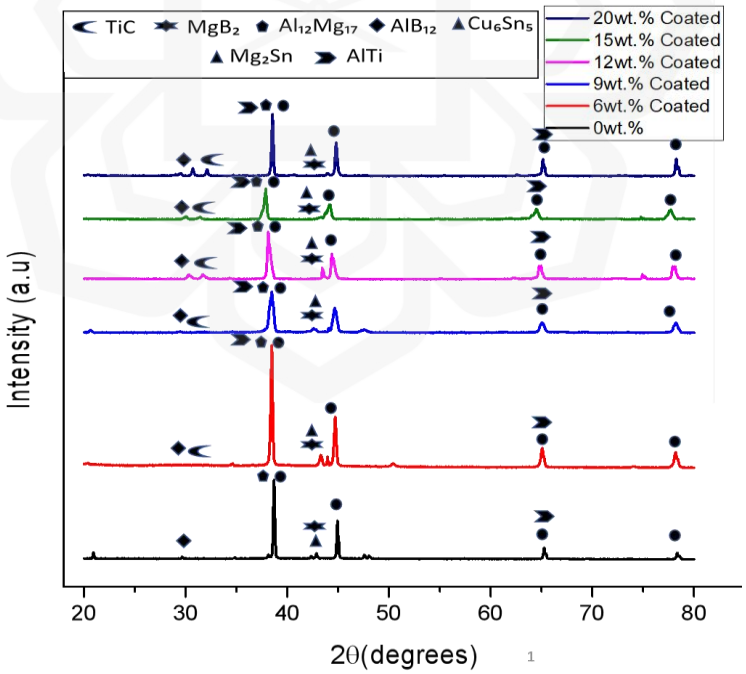

Figure 4.33 XRD patterns of porous Al composite reinforced with Ti-coated diamond particles

4.4.1.4 Compressive properties

The stress–strain curves of porous Al composite reinforced with uncoated and Ti-coated diamond under compression loading are displayed in Figure 4.34. The area under these curves represents the energy absorption capacities of the resultant composite. The compressive stress-strain curve of porous Al and its composites reinforced with uncoated and Ti-coated diamond displayed the typical three distinct regions of deformation that represents a linear elastic region, a plateau stage where the flow stress was nearly constant and a densification stage where all cells collapsed and flow stress increased rapidly (Jamal et al., 2016; Linul et al., 2017).

The longer plateau regions were exhibited by the porous composite reinforced with Ti-coated diamond. Also, the maximum values of plateau strength and energy absorption capacity in the range of (40-45 MPa) and (11.20-13.68 MJ/m^3) respectively were achieved for porous composite reinforced with 9-12 wt.% of Ti-coated diamond particles with an increment of 61-82% in plateau strength and 54-88% of energy absorption capacity as compared to the unreinforced porous Al as shown in Table 4.19.

Table 4.19 Compressive properties of uncoated and Ti-coated diamond composite

Diamond (wt.%)	**Plateau strength (MPa)**		**Energy absorption capacity (MJ/m^3)**	
	Coated	**Uncoated**	**Coated**	**Uncoated**
0	**24.77**	**24.77**	**7.27**	**7.27**
6	**35.23**	**16.81**	**9.17**	**4.87**
9	**45.12**	**17.50**	**13.68**	**3.57**
12	**40.51**	**15.24**	**11.20**	**3.40**
15	**27.92**	**14.13**	**6.07**	**3.36**
20	**20.42**	**11.40**	**4.25**	**2.38**

This can be attributed to the presence of well bonded Ti-coated diamond particles within the Al alloy matrix. Moreover, better bonding between Al matrix and diamond was achieved by the addition of alloying elements that promoted the wetting action. The well bonded Ti-coated diamond particles lead to an increase in cell wall strength as

evident from Figure 4.30. The stronger walls offer high resistance to compressive load during compression testing thereby enhancing their compressive properties. However, the plateau strength and energy absorption capacity declined sharply after 12 wt.% in both cases of uncoated as well as Ti-coated diamond reinforcements. This is due to insufficient availability of Al alloy matrix to wet the higher content of diamond particles. This weakens the interfacial bonding that acted as the load transfer between the diamond particles and Al matrix resulting in stress concentration. As a result, the porous composite with higher content of diamond resulted in higher porosities and lowest strength. In addition, the stress strain curves of porous Al composite with Ti-coated diamond reinforcement exhibited minimal variations as compared to uncoated diamond reinforcement. The presence of least variations implies a slight ductile behavior, and the significant variations are mainly due to the accumulation of localized stresses resulting in brittle behavior of porous composites.

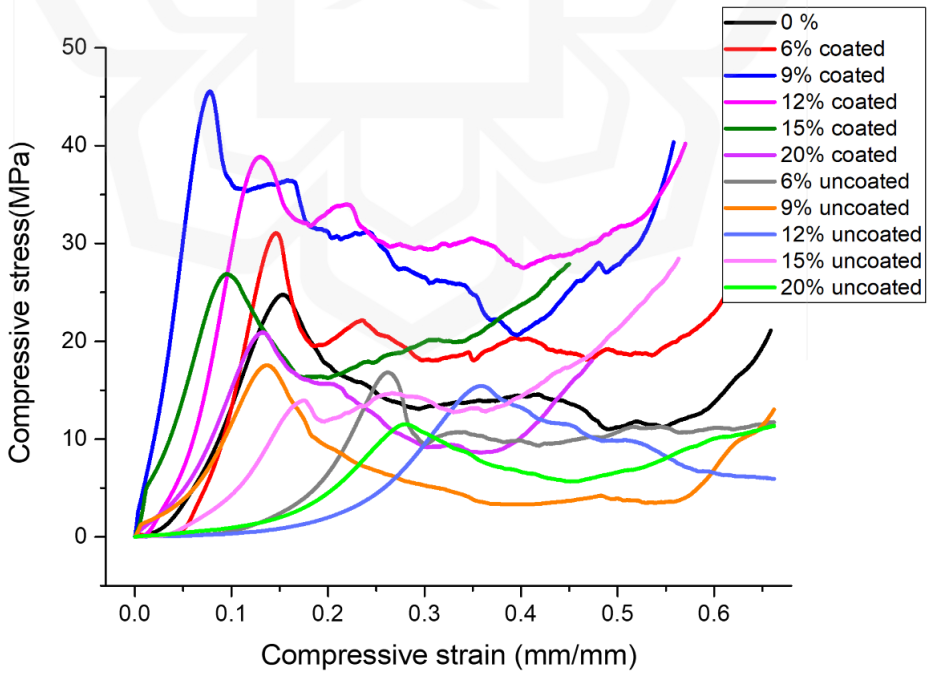

Figure 4.34 Compressive stress-strain diagram of Ti-coated and uncoated porous Al composite

4.4.1.5 Effect of alloying elements in improving strength

Changing the composition of the alloy matrix is one of the accepted strategies for processing composite materials at lower melting temperatures (Rajak et al., 2019). Previous research preferred binary alloys matrix for the preparation of porous Al composite via powder metallurgy (Yang et al., 2016). Even though binary Al alloy matrix demonstrated good foaming performance due to lower eutectic temperature points, an enhanced cellular structure is still required. In the current study, various alloying elements including Sn, Mg, Cu and B were introduced into the Al matrix to reduce the resultant melting temperature while improving the performance of the resultant Al alloy matrix.

In view of these, Mg element was constantly added to Al matrix to improve the wettability in the cellular structure (Asavavisithchai & Kennedy, 2006). The addition of Mg element reduces the wetting angle to assist the liquid phase sintering. During liquid-phase sintering, the liquid flows into the micropores via capillary action, resulting in high density porous composite. Similarly, Sn also assists the liquid phase sintering of composite, thereby providing a reliable porous structure stability. Nevertheless, melting of Sn element about Cu resulted in the forming of Cu–Sn phases due to the great affinity of Cu towards Sn element. Moreover, the liquid-solid partial reactions form Cu_5Sn_6 phase at lower sintering temperatures.

Another preferred active sintering additive is B element. The eutectic reaction between Al alloy matrix and boron occurs at temperatures higher than the eutectic transformation temperature, results in to liquid phase formation, which aids in the sintering of composite Similar observations were made on the addition of B element into stainless steel that consequently promoted liquid phase sintering (Ali et al., 2018; Kontis et al., 2016). B segregation at grain borders increased the strength and ductility

of composite (Abenojar et al., 2006). Thus, the addition of Mg, Sn, Cu, and B additives into the Al matrix could possibly enhance its mechanical properties by promoting the liquid phase sintering. Furthermore, the improvement in the mechanical properties could be due to the formation of many complex eutectic intermetallic phases such as $Al_{12}Mg_{17,}$ $AlB_{12,}$ MgB_2, Mg_2Sn, & Cu_6Sn_5 as evident in the current study from the XRD peaks (Figure 4.28 and Figure 4.33) with exception of Al_2Ti phase formation in the case of Ti-coated diamond reinforced porous Al composite. These intermetallic phases often contributed in enhancing the mechanical properties of the resultant composite due to their enhanced morphology, distribution and properties (Kaczmar et al., 2014; Parveez & Wani, 2021). These intermetallic phases act as a formidable barrier to the penetration of dislocations, resulting in a high work hardening rate that in turn improves the ductility and strength of porous composite. Therefore, it promotes effective load transfer from the Al matrix to the rigid phases. Additionally, they provide hindrance to crack propagations form by forming a network throughout the Al matrix thereby strengthening the Al alloy matrix.

4.4.1.6 Effect of Ti-coated diamond in improving strength

The porous composite can be further strengthened by dispersion strengthening and load sharing mechanisms (Yang et al., 2009). The dispersion strengthening occurs due to the incorporation of reinforcements in composites, that restricted the dislocation movements thereby enhancing their strength. Furthermore, these hard reinforcement particles share load when composite is subjected to loading thus increasing their load bearing capacity. However, reinforcement particles should be well bonded with the Al alloy matrix. There has been an appreciable increase in strength of the porous Al composite with Ti-coated diamond as reinforcement as compared to the unreinforced

alloy due to presence of well bonded Ti- coated diamond particles forming a strong bond with Al alloy matrix as evident from Figure 4.35(a-e). The presence of Ti coating on the diamond particles was found to restrict the reaction between the diamond particle and Al alloy matrix that prevented the formation of brittle intermetallic phase at the interface. This is further proven by the negligible carbide formations as seen in Figure 4.30. The Ti-coated layer comprises of two layers including the outer layer of α-Ti and the transition layer of δ-TiC that bond well with the diamond. Since titanium carbide (TiC) has lower formation free energy, it could easily form carbide in a short period of time and chemically bonded with the diamond. Moreover, the interface layer (α-Ti) served as a bridge connecting the Al alloy matrix and diamond reinforcement as shown in Figure 4.33. The resultant porous Al composite reinforced with Ti-coated diamond was found to exhibit the highest improvement in the plateau strength and energy absorption capacity as presented in Table 4.19.

On the other hand, the poor interface bonding of uncoated diamond with the Al alloy matrix as demonstrated in Figure 4.35 (f-j), declined the strength of resultant composites. In the case of uncoated diamond, the carbon from diamond reacts with Al matrix during sintering process resulting into formation of carbides (Al_2C_3) at the interface of uncoated diamond and Al alloy matrix. These carbides are formed because of the lower (0.052%) solid solubility of diamond (carbon) in Al (Edtmaier et al., 2018). This results in poor bonding as evident from Figure 4.29 and Figure 4.35 (f-j).

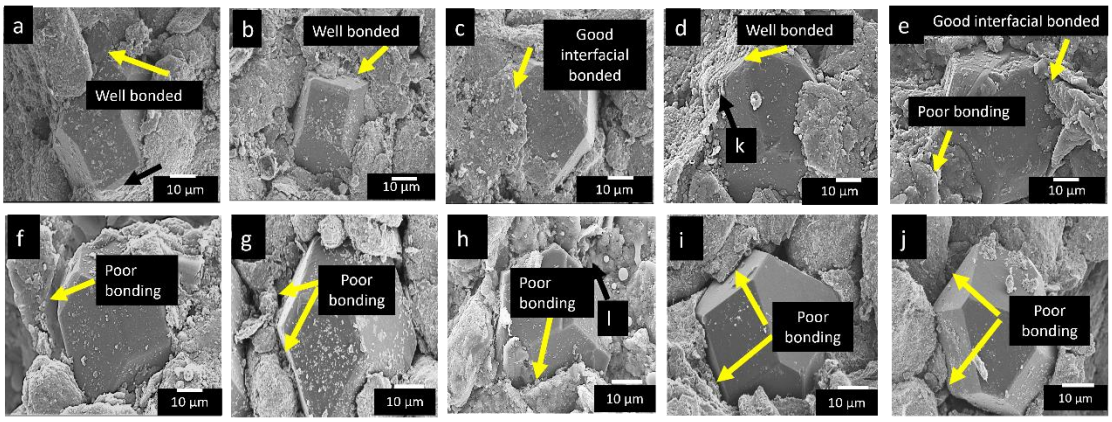

Figure 4.35 Morphology and elemental analysis of (a) 6 wt. %, (b) 9 wt. %, (c) 12 wt. %, (d) 15 wt. %, (e) 20 wt. % of uncoated and (f) 6 wt. %, (g) 9 wt. %, (h) 12 wt. %, (i) 15 wt. % and (j) 20 wt. % of Ti-coated diamond particle reinforced porous Al composite

4.5 SUMMARY

In this chapter, the effect of powder metallurgy processing parameters on the compressive properties of porous Al composite using experimental, numerical, and optimization methods were presented. The plateau stress and energy absorption test results on the other hand revealed the highest values of sintering temperature, compaction pressure and sintering time were obtained at 590 °C, 350 MPa, and 90 min, respectively. Besides that, statistical and regression analyses, model prediction, and contour plots were also examined. Finally, the response optimized results were validated by conducting the confirmation tests under these optimized conditions. The model was found to be reliable and significant based on the lowest percentage deviation with the marginal discrepancy values of -10.5% of plateau stress and -6.6% of energy absorption capacity. This disparity could be attributed to other factors than the existing parameters investigated. The other factors such as the composition of porous Al composites, space holder content and size might influence the compressive properties of the resultant porous Al composite. Therefore, it was critical to evaluate the effect of varying compositions such as Ti-coated diamond content as well as the PMMA content

and size on the compressive properties (plateau strength and energy absorption capacity) of the porous Al composite. It was also carried out experimentally, numerically, and using optimization technique. The higher values of plateau strength and energy absorption were obtained with the addition of diamond content of 12 wt. %, PMMA particle size of 150 μ m, and PMMA particle content of 25 wt. %. Followed by studying statistical and regression analyses, model prediction, contour, and surface plots. The response optimized results were finally obtained and validated by running the confirmation test under the optimal conditions. With the lowest percentage deviation, the model was found to be reliable and significant with the -6.4 % and 11.1 % marginal discrepancy in plateau strength and energy absorption capacity values, respectively.

In both cases, the morphology of the resultant composite was found to exhibit a spherical macro pores structure in which the Ti-coated diamond particles were uniformly distributed within the Al matrix alloy. Furthermore, the Ti-coated diamond particles were found to be well bonded with the Al matrix alloy, revealing improved wettability due to the coated diamond particles and the inclusion of sintering additives including Mg, Sn, Cu, and B that promoted liquid phase sintering. Moreover, the densities and porosities of composite were also affected by the parameter and compositional variations.

Finally, the effect of uncoated and Ti-coated diamond in strengthening porous Al composite were evaluated by means of morphological evaluation, elemental and compositional analysis, density and porosity determination and compression testing. The spherical and well-defined macro pores in the resultant composite were achieved using PMMA as a space holder material. In addition, the introduction of alloying elements was identified to influence the plateau strength of porous composite due to

the formation of intermetallic phases during sintering as confirmed by the XRD analysis. Moreover, the presence of Ti coating element on the diamond particles was found to significantly improve the interfacial bonding between the Al alloy matrix and diamond particle reinforcement thus improving the compressive properties. However, as the diamond content increased, micropores and cracks appeared on the cell wall due to insufficient wetting of diamond particles by the Al alloy matrix. Also, it was found that the Ti-coated diamond content ranging from 9-12 wt.% resulted in an increment of 61-82% in plateau strength and 54-88% of energy absorption capacity as compared to the unreinforced porous composite.

In the next chapter the outcome of the results and discussions have been elucidated to summarize the influence of the addition of alloying elements together with the inclusion of Ti-coated diamond reinforcement in enhancing the interfacial bonding between the Al matrix and diamond particles, thereby improving the overall properties of porous Al composite.

CHAPTER FIVE

CONCLUSION AND RECOMMENDATIONS

In the concluding chapter, the findings and some of the strengths and weaknesses of the approaches considered in this work are summarized. The contribution of the present work towards existing knowledge and few recommendations for the future work are also explored.

5.1 CONCLUSIONS

The current study was initiated to enhance the compressive properties of porous Al composite by the addition of alloying elements and using Ti-coated coating of diamond particles as reinforcement. Also, spherical PMMA particles were employed as space holders to form porosities. Further, the enhancement in the compressive properties were carried out by conducting parameter and compositional optimization. Where powder metallurgy processing parameters, reinforcement content, PMMA particle size, and PMMA content were considered as the input factors and plateau strength and energy absorption capacity as response factors. on the compressive properties of composite was studied using experimental and statistical analysis including DOE (Taguchi's L_9 orthogonal array) and ANOVA respectively. Finally, the effects of varying content of uncoated and Ti-coated diamond reinforcement in strengthening porous Al composite were evaluated by means of morphological evaluations, elemental and compositional analysis, density and porosity determination as well as compression analysis. The important observations made from the results obtained are summarized as follows:

1. The developed porous Al composite exhibited spherical macro pore structure as a result of addition of spherical PMMA particles as space holders. These

spherical porosities provided smooth edged cell walls thereby reducing surface roughness as well stress concentration in resultant composites. The PMMA particles also allowed the control over porosities (pore shape and pore size).

2. From parametric optimization, the maximum values of the plateau strength and energy absorption test were obtained at sintering temperature of 590 °C, compaction pressure of 350 MPa, and sintering time of 90 min. Moreover, the impact of sintering temperature and sintering time on the plateau strength and energy absorption was found to be predominant as compared to the compaction pressure. The confirmation tests found the model to be reliable and significant, with the lowest percentage deviation with marginal discrepancy of -10.5% in plateau strength and -6.6% in energy absorption capacity values.
3. In the case of compositional optimization, the highest values of plateau strength and energy absorption were obtained at diamond content of 12 wt. %, PMMA particle size of 150 μm, and PMMA content of 25 wt. %. The effects of diamond content and PMMA particle size on the plateau strength were found to be significant as compared to PMMA content whereas the effects of diamond content and PMMA content on the energy absorption capacity values were dominant as compared to PMMA particle size. The confirmation test validated the findings with the lowest percentage deviation in plateau strength and energy absorption capacity and the model utilized was found to be reliable and significant. The findings agreed well with the -6.4% and 11.1% marginal discrepancy in the values of plateau strength and energy absorption capacity.
4. At various contents of Ti-coated diamond and uncoated diamond in porous Al composites The Ti-coated diamond particles that were found to be uniformly distributed and well bonded with the Al matrix alloy thus revealing improved

wettability due to presence of the Ti-coating. Moreover, the inclusion of alloying elements including Mg, Sn, Cu, and B that promoted liquid phase sintering influenced the strength of porous Al composite by formation of intermetallic phases during sintering as revealed from the XRD analysis. On increasing the diamond content, pores and cracks were found to appear on the cell wall due to insufficient wetting of diamond particles by the Al alloy matrix. Their compressive properties were found to be improved by the addition of Ti-coated diamond particles as compared to uncoated diamond particles The maximum values of plateau strength and energy absorption capacity in the range of (40-45 MPa) and (11.20-13.68 MJ/m^3) respectively were achieved for porous composite reinforced with 9-12 wt.% of Ti-coated diamond particles with an increment of 61-82% in plateau strength and 54-88% of energy absorption capacity respectively, as compared to the unreinforced composites.

Thus, the addition of alloying elements together with the inclusion of Ti-coated diamond reinforcement could possibly promote the interfacial bonding between the Al matrix and diamond particles, thereby improving the compressive properties of porous Al composite.

5.2 CONTRIBUTIONS TO KNOWLEDGE

The main contribution of this research is to provide essential understanding on the enhancing the strength (compressive properties) of porous Al composites The specific contribution of this research work in porous material field are summarized as follows:

1. A significant improvement in the compressive properties of porous Al composite was achieved by inclusion of alloying elements in Al matrix and Ti-coated diamond as reinforcement material. The addition of Ti-coated diamond enabled the strengthening of Al alloy matrix using carbonaceous reinforcements

however prevented or minimized the formation of undesirable carbide phases that otherwise deteriorate the properties of resultant composites.

2. Optimization of various processing parameters of powder metallurgy technique was carried out for fabricating composite with improved properties. The influence of each parameter on the porous composite on the other hand, revealed the importance of processing parameters on the overall properties of the resultant porous Al composite.
3. Optimization of Ti-coated diamond content, PMMA content and PMMA particle size led to better control of porosity, strength, and microstructure of the resultant porous Al composite.
4. The most significant factors affecting the overall properties of the resultant composite were determined. The parameters including the sintering temperature and sintering time influenced the properties significantly as compared to compaction pressure. In addition, the reinforcement content and space holder content were identified to predominantly influence the overall properties in comparison to space holder particle size.
5. Prediction models such as surface plots, contour plots, interaction plots and graphs developed from optimization technique for each variable can be further utilized for various studies in to optimizing several properties of porous composite and thus widen their applications.

5.3 RECOMMENDATIONS

Several researchers have used various techniques and methods to improve the properties of porous composites. However, it still requires huge attention for better understanding of the mechanisms and methodologies that can be applied to

improve the strength of porous Al composites. Some of the recommendations are as follows:

1. The current work focused on usage of constant size of Ti-coated diamond particles. It will be interesting to investigate the effect of addition of various sizes of diamond particles on the microstructure, interfacial bonding strength between the reinforcement and Al alloy matrix and to find the optimum size.
2. As the formation of the intermetallic phases were identified using XRD analysis. It will be better to carry out their detailed microstructural analysis using transmission electron microscopy (TEM) and high-resolution electron microscopy (HR-TEM) to further study them on micro or nano levels.
3. The influence of powder metallurgy-based processing parameters on the microstructure and overall properties of porous Al composite were addressed and optimized in this study. The influence of processing parameters of other production techniques should be considered to evaluate their effect on improving properties of porous Al composites.
4. The porous structure acquired in the present study was found to enhance its compressive properties. However, the improvement in their compressive properties can be explored by impregnating resin in pores of porous Al composites.

REFERENCES

Abenojar, J., Martinez, M. A., & Velasco, F. (2006). Effect of the boron content in the aluminium/boron composite. *Journal of Alloys and Compounds*, *422*(1–2), 67–72.

Aboraia, M., Sharkawi, R., & Doheim, M. A. (2011). Production of aluminium foam and the effect of calcium carbonate as a foaming agent. *Journal of Engineering Sciences*, *39*(2), 441–451.

Aguirre-Perales, L. Y., Jung, I. H., & Drew, R. A. L. (2012). Foaming behavior of powder metallurgical Al-Sn foams. *Acta Materialia*, *60*(2), 759–769.

Aida, S. F., Hijrah, M. N., Amirah, A. H., Zuhailawati, H., & Anasyida, A. S. (2016). Effect of NaCl as a Space Holder in Producing Open Cell A356 Aluminium Foam by Gravity Die Casting Process. *Procedia Chemistry*, *19*, 234–240.

Aida, S. F., Zuhailawati, H., & Anasyida, A. S. (2017). The Effect of Space Holder Content and Sintering Temperature of Magnesium Foam on Microstructural and Properties Prepared by Sintering Dissolution Process (SDP) using Carbamide Space Holder. *Procedia Engineering*, *184*, 290–297.

Al-Maharma, A. Y., Patil, S. P., & Markert, B. (2020). Effects of porosity on the mechanical properties of additively manufactured components: a critical review. *Materials Research Express*, *7*(12).

Aldoshan, A., & Khanna, S. (2017). Effect of relative density on the dynamic compressive behavior of carbon nanotube reinforced aluminum foam. *Materials Science & Engineering A*, *689*(January), 17–24.

Alfonso, I., Figueroa, I. A., Béjar, L., Gutiérrez, H. M., González, G., Hernández, O., Aguilar, C., & Lara, G. (2017). Characterization of Al-Si-Cu-Mg foams manufactured in-situ. In *Journal of Alloys and Compounds* (Vol. 722). Elsevier B.V.

Ali, S., Rani, A. M. A., Altaf, K., & Baig, Z. (2018). Investigation of Boron addition and compaction pressure on the compactibility, densification and microhardness of

316L Stainless Steel. *IOP Conference Series: Materials Science and Engineering*, *344*(1).

Aliyi, I. M. (2019). *Metal matrix composites reinforced with diamond particles*. (Doctoral dissertation, Universidade de Coimbra).

Alizadeh, M., & Mirzaei-Aliabadi, M. (2012). Compressive properties and energy absorption behavior of Al-Al2O3 composite foam synthesized by space-holder technique. *Materials and Design*, *35*, 419–424.

Almomani, M. A., Shatnawi, A. M., & Alrashdan, M. K. (2014). Effect of sintering time on the density, porosity content and microstructure of copper – 1 wt. % silicon carbide composites. *Advanced Materials Research*, *1064*(December), 32–37.

Alrebdi, T. A., Gopinathan, R., Sunagar, P., Prabu, R. T., Kivade, R., Gous, M. Z., Alodhayb, A., & Tesemma, B. G. (2022). Optimization on Powder Metallurgy Process Parameters on Nano Boron Carbide and Micron Titanium Carbide Particles Reinforced AA 4015 Composites by Taguchi Technique. *Journal of Nanomaterials*, *2022*.

Amore, S., Ricci, E., Borzone, G., & Novakovic, R. (2008). Wetting behaviour of lead-free Sn-based alloys on Cu and Ni substrates. *Materials Science and Engineering A*, *495*(1–2), 108–112.

Anovitz, L. M., & Cole, D. R. (2015). Characterization and analysis of porosity and pore structures. *Pore Scale Geochemical Processes*, *November*, 61–164.

Arifvianto, B., & Zhou, J. (2014). Fabrication of metallic biomedical scaffolds with the space holder method: A review. *Materials*, *7*(5), 3588–3622.

Asavavisithchai, S., & Kennedy, A. R. (2006). The effect of Mg addition on the stability of Al-Al2O 3 foams made by a powder metallurgy route. *Scripta Materialia*, *54*(7), 1331–1334.

Atturan, U. A., Nandam, S. H., Murty, B. S., & Sankaran, S. (2016). Processing and characterization of in-situ TiB2 stabilized closed cell aluminium alloy composite foams. *Materials and Design*, *101*, 245–253.

B.Novak, K.Tschope, A. P. R. and T. G. (2012). Fundamentals of aluminium carbide formation. *Light Metals 2012*, *2*, 1–1407.

Bafti, H., & Habibolahzadeh, A. (2010). Production of aluminum foam by spherical carbamide space holder technique-processing parameters. *Materials and Design*, *31*(9), 4122–4129.

Banhart. (2010). From fundamental research to applications. *Europhysics News*, *41*(6), 3.

Banhart, J. (2007). Metal Foams—from Fundamental Research to Applications. *Frontiers in the Design of Materials*, 279–289.

Banhart, J. (2013). Light-metal foams - History of innovation and technological challenges. *Advanced Engineering Materials*, *15*(3), 82–111.

Banhart, J. (2014). Metal Foams — from Fundamental Research to Applications. *Frontiers in the Design of Materials, May*, 279–289.

Baroutaji, A., Sajjia, M., & Olabi, A. G. (2017). On the crashworthiness performance of thin-walled energy absorbers: Recent advances and future developments. *Thin-Walled Structures*, *118*(November 2016), 137–163.

Begum, Y., Bharath, K. N., Doddamani, S., Rajesh, A. M., & Kaleemulla, K. M. (2020). Optimization of Process Parameters of Fracture Toughness Using Simulation Technique Considering Aluminum–Graphite Composites. *Transactions of the Indian Institute of Metals*, *73*(12), 3095–3103.

Behymer, N., & Morsi, K. (2023). Review: Closed-Cell Metallic Foams Produced via Powder Metallurgy. *Metals*, *13*(5).

Bekoz, N., & Oktay, E. (2012). Effects of carbamide shape and content on processing and properties of steel foams. *Journal of Materials Processing Technology*, *212*(10), 2109–2116.

Bekoz, N., & Oktay, E. (2013). Mechanical properties of low alloy steel foams: Dependency on porosity and pore size. *Materials Science and Engineering A*, *576*, 82–90.

Bekoz, N., & Oktay, E. (2014). The role of pore wall microstructure and micropores on the mechanical properties of Cu-Ni-Mo based steel foams. *Materials Science and Engineering A*, *612*, 387–397.

Bi, Y., Zheng, Y., & Li, Y. (2015). Microstructure and mechanical properties of sintered porous magnesium using polymethyl methacrylate as the space holder. *Materials Letters*, *161*, 583–586.

Byakova, A., Bezim'yanny, Y., Gnyloskurenko, S., & Nakamura, T. (2014). Fabrication method for closed-cell aluminium foam with improved sound absorption ability. *Procedia Materials Science*, *4*, 9–14.

C. Salvo, C. Aguilar, S. Lascano, L. Pérez, M. López, R. V. M. (2018). The effect of alumina particles on the microstructural and mechanical properties of copper foams fabricated by space-holder method. *Materials Research Express*, *29*(27), 1–19.

Čapek, J., & Vojtěch, D. (2014). Microstructural and mechanical characteristics of porous iron prepared by powder metallurgy. *Materials Science and Engineering C*, *43*, 494–501.

Čapek, J., Vojtěch, D., & Oborná, A. (2015). Microstructural and mechanical properties of biodegradable iron foam prepared by powder metallurgy. *Materials and Design*, *83*, 468–482.

Casati, R., & Vedani, M. (2014). Metal matrix composites reinforced by Nano-Particles—A review. *Metals*, *4*(1), 65–83.

Che, Z., Zhang, Y., Li, J., Zhang, H., Wang, X., Sun, C., Wang, J., & Kim, M. J. (2016). Nucleation and growth mechanisms of interfacial Al4C3 in Al/diamond composites. *Journal of Alloys and Compounds*, *657*, 81–89.

Chen, Z., Gu, M., & Peng, D. (2010). Heat transfer performance analysis of a solar flat-plate collector with an integrated metal foam porous structure filled with paraffin. *Applied Thermal Engineering*, *30*(14–15), 1967–1973.

Choudhary, M., Sharma, A., Raj, S. A., Sultan, M. T. H., Hui, D., & Md Shah, A. U.

(2022). Contemporary review on carbon nanotube (CNT) composites and their impact on multifarious applications. *Nanotechnology Reviews*, *11*(1), 2632–2660.

Chu, K., Jia, C. C., Liang, X. B., & Chen, H. (2010). Effect of sintering temperature on the microstructure and thermal conductivity of Al/diamond composites prepared by spark plasma sintering. *International Journal of Minerals, Metallurgy and Materials*, *17*(2), 234–240.

Chung, C. Y., Chu, C. H., Lee, M. T., Lin, C. M., & Lin, S. J. (2014). Effect of titanium addition on the thermal properties of diamond/Cu-Ti composites fabricated by pressureless liquid-phase sintering technique. *The Scientific World Journal*, *2014*, 1–8.

Damanik, F. S., Damanik, M. S. F., & Lange, P. G. (2019). Effect of Nickel Coated of Carbon Fiber on Distribution of Carbon Fiber Reinforced Aluminium (AlSi7) Foam Composite by Powder Metallurgy. *International Conference on Innovative Technologies*, 9–13.

Daoud, A. (2009). Compressive response and energy absorption of foamed A359–Al2O3 particle composites. *Journal of Alloys and Compounds*, *486*(1), 597–605.

Daoud, A., Abou El-Khair, M. T., Fairouz, F., Mohamed, E., & Lotfy, A. (2021). Effect of Processing Parameters on 7075 Al–Silica Particle Waste Composite Foams Produced with Recycled Aluminum Cans. *Physics of Metals and Metallography*, *122*(13), 1326–1337.

Das, S., Rajak, D. K., Khanna, S., & Mondal, D. P. (2020). Energy Absorption Behavior of Al-SiC-Graphene Composite Foam under a High Strain Rate. *Materials 2020*, *13*(783), 1–13.

Dixit, M., & Srivastava, R. (2019). The effect of copper granules on interfacial bonding and properties of the copper-graphite composite prepared by flake powder metallurgy. *Advanced Powder Technology*, *30*(12), 3067–3078.

Duarte, I., Ventura, E., Olhero, S., & Ferreira, J. M. F. (2015). An effective approach to reinforced closed-cell Al-alloy foams with multiwalled carbon nanotubes. *Carbon*,

95, 589–600.

Ebhota, W. S., & Jen, T.-C. (2018). Intermetallics Formation and Their Effect on Mechanical Properties of Al-Si-X Alloys. In *Intermetallic Compounds - Formation and Applications* (pp. 21–44).

Edtmaier, C., Segl, J., Rosenberg, E., Liedl, G., Pospichal, R., & Steiger-Thirsfeld, A. (2018). Microstructural characterization and quantitative analysis of the interfacial carbides in Al(Si)/diamond composites. *Journal of Materials Science*, *53*(22), 15514–15529.

Esen, Z., & Bor, Ş. (2011). Characterization of Ti-6Al-4V alloy foams synthesized by space holder technique. *Materials Science and Engineering A*, *528*(7–8), 3200–3209.

Everett, R. (2012). *Metal matrix composites: processing and interfaces. Academic press.*

Farahani, M. R., Rezaei Ashtiani, H. R., & Elahi, S. H. (2022). Effect of Zinc Content on the Mechanical Properties of Closed-Cell Aluminum Foams. *International Journal of Metalcasting*, *16*(2), 713–722.

French, A. D. (2014). Idealized powder diffraction patterns for cellulose polymorphs. *Cellulose*, *21*(2), 885–896.

García-Moreno, F., Radtke, L. A., Neu, T. R., Kamm, P. H., Klaus, M., Schlepütz, C. M., & Banhart, J. (2020). The influence of alloy composition and liquid phase on foaming of Al–Si–Mg alloys. *Metals*, *10*(2).

Ghafarian, M., Mohebbi-Kalhori, D., & Sadeghi, J. (2013). Analysis of heat transfer in oscillating flow through a channel filled with metal foam using computational fluid dynamics. *International Journal of Thermal Sciences*, *66*, 42–50.

Goodall, R., Marmottant, A., Salvo, L., & Mortensen, A. (2007). Spherical pore replicated microcellular aluminium: Processing and influence on properties. *Materials Science and Engineering A*, *465*(1–2), 124–135.

Guan, M., Hu, Y., Zheng, T., Zhao, T., & Pan, F. (2018). Composition optimization and

mechanical properties of Mg-Al-Sn-Mn alloys by orthogonal design. *Materials*, *11*(8).

Guden, M., & Yüksel, S. (2006). SiC-particulate aluminum composite foams produced from powder compacts: foaming and compression behavior. *Journal of Materials Science*, *41*(13), 4075–4084.

Guo, Z., Ma, D., Yuan, X., & Dong, X. (2016). Effect of Mg addition on the foaming behaviour of AlSi7 based alloy prepared by powder metallurgy method. *Xiyou Jinshu Cailiao Yu Gongcheng/Rare Metal Materials and Engineering*, *45*(12), 3068–3073.

H-JA Lukaszewicz, D. (2014). Automotive Composite Structures for Crashworthiness. *Advanced Composite Materials for Automotive Applications: Structural Integrity and Crashworthiness*, 99–125.

Hamdi, A. A. (2018). *Effect of magnesium and tin as sintering additives on microstructure and compressive properties of porous aluminum* (Issue August).

Hassan, Z. K. (2019). *Production of metal foams by using powder metallurgy method*. *020004*(July).

Hassani, A., Bagherpour, E., & Qods, F. (2014). Influence of pores on workability of porous Al/SiC composites fabricated through powder metallurgy + mechanical alloying. *Journal of Alloys and Compounds*, *591*, 132–142.

Huang, L., Wang, H., Yang, D., Ye, F., & Lu, Z. P. (2012). Effects of scandium additions on mechanical properties of cellular Al-based foams. *Intermetallics*, *28*, 71–76.

Huang, L., Yang, D. H., Wang, H., Ye, F., & Lu, Z. P. (2013). Effects of Scandium on Corrosion Resistance and Mechanical Properties of Cellular Al-Based Foams. *High Performance Structure Materials*, *747*, 93–100.

Islam, M. A., Kader, M. A., Hazell, P. J., Brown, A. D., Saadatfar, M., Quadir, M. Z., & Escobedo, J. P. (2016). Investigation of microstructural and mechanical properties of cell walls of closed-cell aluminium alloy foams. *Materials Science and Engineering A*, *666*, 245–256.

J. Vairamuthu, A. S. K., Stalin, B., & Ravichandran, M. (2010). Optimization of powder metallurgy parameters of TiC and B4C reinforced aluminium composites by Taguchi method. *Transactions of the Canadian Society for Mechanical Engineering*, *45*(2), 249–261.

Jamal, A., Tan, W., & Anuar, H. (2016). Fabrication and Compressive Properties of Low to Using PMMA Space Holder Technique. *Www.Mdpi.Com/Journal/Materials*, 1–13.

Jamal, N A, Maizatul, O., Anuar, H., Yusof, F., Nor, Y. A., Khalid, K., & Zakaria, M. N. (2018). Preliminary development of porous aluminum via powder metallurgy technique. *Materialwiss. Werkstofftech*, *49*, 460–466.

Jamal, Nur Ayuni, Tan, A. W., Yusof, F., Katsuyoshi, K., Hisashi, I., Singh, S., & Anuar, H. (2016). Fabrication and compressive properties of low to medium porosity closed-cell porous Aluminum using PMMA space holder technique. *Materials*, *9*(4), 1–13.

Jamal, Nur Ayuni, Yusof, F., Nor, Y. A., Othman, M., Khalid, K., & Zakaria, M. N. (2018). The role of tin and magnesium in assisting liquid phase sintering of aluminum (Al). *IOP Conference Series: Materials Science and Engineering*, *290*(1).

Jankovic, A., Chaudhary, G., & Goia, F. (2021). Designing the design of experiments (DOE) – An investigation on the influence of different factorial designs on the characterization of complex systems. *Energy and Buildings*, *250*, 111298.

Jiang, B., Wang, Z., & Zhao, N. (2007). Effect of pore size and relative density on the mechanical properties of open cell aluminum foams. *Scripta Materialia*, *56*(2), 169–172.

Jiang, L., Li, Z., Fan, G., Cao, L., & Zhang, D. (2012). The use of flake powder metallurgy to produce carbon nanotube (CNT)/aluminum composites with a homogenous CNT distribution. *Carbon*, *50*(5), 1993–1998.

Kaczmar, J. W., Naplocha, K., & Morgiel, J. (2014). Microstructure and strength of Al2O3

and carbon fiber reinforced 2024 aluminum alloy composites. *Journal of Materials Engineering and Performance*, *23*(8), 2801–2808.

Kamath, P. M., Balaji, C., & Venkateshan, S. P. (2013). Convection heat transfer from aluminium and copper foams in a vertical channel - An experimental study. *International Journal of Thermal Sciences*, *64*, 1–10.

Kang, B., Kong, T., Dan, N. H., Phuong, D. D., Ryu, H. J., & Hong, S. H. (2021). Effect of boron addition on the microstructure and mechanical properties of refractory Al0.1CrNbVMo high-entropy alloy. *International Journal of Refractory Metals and Hard Materials*, *100*, 105636.

Kennedy, A. (2012). Porous Metals and Metal Foams Made from Powders. In *Powder Metallurgy* (Issue August, pp. 31–46).

Kontis, P., Yusof, H. A. M., Pedrazzini, S., Danaie, M., Moore, K. L., Bagot, P. A. J., Moody, M. P., Grovenor, C. R. M., & Reed, R. C. (2016). On the effect of boron on grain boundary character in a new polycrystalline superalloy. *Acta Materialia*, *103*(November), 688–699.

Küçük, Ö., Elfarah, T. T. K., Islak, S., & Özorak, C. (2017). Optimization by using taguchi method of the production of magnesium-matrix carbide reinforced composites by powder metallurgy method. *Metals*, *7*(9), 1–12.

Kumar, N., Soren, S., Prasad, R., Singh, Y., Nautiyal, H., Sharma, A., Tiang, S. S., & Lim, W. H. (2023). Optimization of Sintering Process Parameters by Taguchi Method for Developing Al-CNT-Reinforced Powder Composites. *Crystals*, *13*(9), 1352.

Kumar, S., Kumar, S., Nagpal, P. K., Gawade, S. R., Salunkhe, S., Chandrasekhar, U., & Davim, J. P. (2023). Development of the Al12SiCuFe Alloy Foam Composites with ZrSiO4 Reinforcements at Different Foaming Temperatures. *Metals*, *13*(4).

Lafdi, K., Mesalhy, O., & Shaikh, S. (2007). Experimental study on the influence of foam porosity and pore size on the melting of phase change materials. *Journal of Applied Physics*, *102*(8).

Li, B. Q., Wang, C. Y., & Lu, X. (2013). Effect of pore structure on the compressive

property of porous Ti produced by powder metallurgy technique. *Materials and Design*, *50*, 613–619.

Li, A. Bin, Xu, H. Y., Geng, L., Li, B. L., Tan, Z. Bin, & Ren, W. (2012). Preparation and characterization of SiC p/2024Al composite foams by powder metallurgy. *Transactions of Nonferrous Metals Society of China (English Edition)*, *22*(SUPPL. 1), s33–s38.

Li, J. W., Shan, C. F., Teng, Y. L., & Gai, Z. C. (2019). Development of Low Cost Lightweight Aluminum Foam for Railway Transportation. *IOP Conference Series: Materials Science and Engineering*, *649*(1).

Li, X., Liu, Y., Ye, J., An, X., & Ran, H. (2018). Multifunctional foaming agent to prepare aluminum foam with enhanced mechanical properties. *Materials Research Express*, *5*(3), 36529.

Lin, Y., Zhang, Q., Chang, J., Wang, H., Feng, X., & Wang, J. (2019). Microstructural characterization and compression mechanical response of glass hollow spheres/Al syntactic foams with different Mg additions. *Materials Science and Engineering A*, *766*(July), 138338.

Linul, E., Şerban, D. A., Marsavina, L., & Kovacik, J. (2017). Low-cycle fatigue behaviour of ductile closed-cell aluminium alloy foams. *Fatigue and Fracture of Engineering Materials and Structures*, *40*(4), 597–604.

Liu, B., Huang, W., Wang, H., Wang, M., & Li, X. (2014). Study on the load partition behaviors of high particle content B 4C/Al composites in compression. *Journal of Composite Materials*, *48*(3), 355–364.

Liu, X., Zhang, J., Fang, Q., Wu, H., & Zhang, Y. (2017). Response of closed-cell aluminum foams under static and impact loading: Experimental and mesoscopic numerical analysis. *International Journal of Impact Engineering*, *110*, 382–394.

Luo, H., Zhao, J., Du, H., Yin, W., & Qu, Y. (2022). Effect of Mg Powder's Particle Size on Structure and Mechanical Properties of Ti Foam Synthesized by Space Holder Technique. *Materials*, *15*(24).

Luo, Y., Yu, S., Liu, J., Zhu, X., & Luo, Y. (2010). Compressive property and energy absorption characteristic of open-cell SiCp/AlSi9Mg composite foams. *Journal of Alloys and Compounds*, *499*(2), 227–230.

Ma, Y., Yang, X., He, C., Yang, K., Xu, J., Sha, J., Shi, C., Li, J., & Zhao, N. (2018). Fabrication of in-situ grown carbon nanotubes reinforced aluminum alloy matrix composite foams based on powder metallurgy method. *Materials Letters*, *233*, 351–354.

Madgule, M., Sreenivasa, C. G., & Borgaonkar, A. V. (2022). Effect of influencing parameters on developing aluminium metal foam by using powder metallurgy technique with a foaming agent as a wax powder. *Journal of Porous Materials*, 1–25.

Maiorano, L. P., Castillo, R., & Molina, J. M. (2023). Al/Gf composite foams with SiC-engineered interfaces for the next generation of active heat dissipation materials. *Composites Part A: Applied Science and Manufacturing*, *166*(February 2022), 107367.

Manohar, G., Pandey, K. M., & Ranjan Maity, S. (2020). Effect of compaction pressure on mechanical properties of AA7075/B4C/graphite hybrid composite fabricated by powder metallurgy techniques. *Materials Today: Proceedings*, *38*(June), 2157–2161.

Manonukul, A., Muenya, N., Léaux, F., & Amaranan, S. (2010). Effects of replacing metal powder with powder space holder on metal foam produced by metal injection moulding. *Journal of Materials Processing Technology*, *210*(3), 529–535.

Matan Cafri, N. F. (2012). *Boron carbide / magnesium alloys composites : Processing , microstructure and properties* (Issue October). Ben-Gurion University of the Negev.

Michailidis, N., Tsouknidas, A., Lefebvre, L. P., Hipke, T., & Kanetake, N. (2014). Production, characterization, and applications of porous materials. *Advances in Materials Science and Engineering*, *2014*, 2–4.

Mohd Razali, R. N., Abdullah, B., Ismail, M. H., Ahmad, U. K., Idham, M. F., & Rasmli, A. (2013a). Mechanical properties of aluminium foam by conventional casting combined with NaCL space holder. *Applied Mechanics and Materials*, *393*(January 2015), 156–160.

Mohd Razali, R. N., Abdullah, B., Ismail, M. H., Ahmad, U. K., Idham, M. F., & Rasmli, A. (2013b). Mechanical properties of aluminium foam by conventional casting combined with NaCL space holder. *Applied Mechanics and Materials*, *393*(September), 156–160.

Mondal, D. P., Goel, M. D., Bagde, N., Jha, N., Sahu, S., & Barnwal, A. K. (2014). Closed cell ZA27-SiC foam made through stir-casting technique. *Materials and Design*, *57*, 315–324.

Mondal, D. P., Goel, M. D., & Das, S. (2009). Compressive deformation and energy absorption characteristics of closed cell aluminum-fly ash particle composite foam. *Materials Science and Engineering A*, *507*(1–2), 102–109.

Moradi, M. R., Moloodi, A., & Habibolahzadeh, A. (2015). Fabrication of Nano-composite Al-B4C Foam via Powder Metallurgy-space Holder Technique. *Procedia Materials Science*, *11*(2000), 553–559.

Mu, Y., Yao, G., Cao, Z., Luo, H., & Zu, G. (2011). Strain-rate effects on the compressive response of closed-cell copper-coated carbon fiber/aluminum composite foam. *Scripta Materialia*, *64*(1), 61–64.

Mukherjee, M., García-Moreno, F., Jiménez, C., Rack, A., & Banhart, J. (2017). Microporosity in aluminium foams. *Acta Materialia*, *131*, 156–168.

Nakamura, T., Gnyloskurenko, S. V., Sakamoto, K., Byakova, A. V., & Ishikawa, R. (2002). Development of new foaming agent for metal foam. *Materials Transactions*, *43*(5), 1191–1196.

Navacerrada, M. A., Fernández, P., Díaz, C., & Pedrero, A. (2013). Thermal and acoustic properties of aluminium foams manufactured by the infiltration process. *Applied Acoustics*, *74*(4), 496–501.

Pal, U., Sandoval, A., Madrid, S. I. U., Corro, G., Sharma, V., & Mohanty, P. (2016). Mixed titanium, silicon, and aluminum oxide nanostructures as novel adsorbent for removal of rhodamine 6G and methylene blue as cationic dyes from aqueous solution. *Chemosphere*, *163*, 142–152.

Parveez, B., & Wani, M. F. (2021). Tribological behaviour of nano-zirconia reinforced iron-based self-lubricating composites for bearing applications. *Tribology International*, *159*(February).

Paulin, I. (2014). Synthesis and characterization of al foams produced by powder metallurgy route using dolomite and titanium hydride as a foaming agents. *Materiali in Tehnologije*, *48*(6), 943–947.

Prabhu, B., Suryanarayana, C., An, L., & Vaidyanathan, R. (2006). Synthesis and characterization of high volume fraction Al-Al2O3 nanocomposite powders by high-energy milling. *Materials Science and Engineering A*, *425*(1–2), 192–200.

Rahimian, M., Ehsani, N., Parvin, N., & Baharvandi, H. reza. (2009). The effect of particle size, sintering temperature and sintering time on the properties of Al-Al2O3 composites, made by powder metallurgy. *Journal of Materials Processing Technology*, *209*(14), 5387–5393.

Rajak, D. K., Pagar, D. D., Kumar, R., & Pruncu, C. I. (2019). Recent progress of reinforcement materials: A comprehensive overview of composite materials. *Journal of Materials Research and Technology*, *8*(6), 6354–6374.

Ramasamy Karuppasamy, & Milon Selvam Dennison, M. P. (2018). Preparation and Characterization of Aluminium Foam Prepared Through Melt Route Method. *International Research Journal of Engineering and Technology*, *5*(3), 190–195.

Ravi Kumar, N. V., Gokhale, H., & Gokhale, A. A. (2012). Role of SiCP on processing and physical characteristics of Al-Si- Mg/SiCP composite foams. *Materials Science Forum*, *710*, 383–388.

Ravi Kumar, N. V., Ramachandra Rao, N., Sudhakar, B., & Gokhale, A. A. (2010). Foaming experiments on LM25 alloy reinforced with SiC particulates. *Materials*

Science and Engineering A, *527*(21–22), 6082–6090.

Rodriguez-Contreras, A., Punset, M., Calero, J. A., Gil, F. J., Ruperez, E., & Manero, J. M. (2021). Powder metallurgy with space holder for porous titanium implants: A review. *Journal of Materials Science and Technology*, *76*, 129–149.

Salehi, A., Babakhani, A., & Zebarjad, S. M. (2015). Microstructural and mechanical properties of Al-SiO2 nanocomposite foams produced by an ultrasonic technique. *Materials Science and Engineering A*, *638*, 54–59.

Schäffler, P., Hanko, G., Mitterer, H., & Zach, P. (2008). Alulight metal foam products. *Proceedings of the 5th International Conference on Porous Metals and Metallic Foams:Metfoam*, 7–10.

Shang, X. L., Zhang, B., Han, E. H., & Ke, W. (2012). The effect of 0.4 wt.% Mn addition on the localized corrosion behaviour of zinc in a long-term experiment. *Electrochimica Acta*, *65*, 294–304.

Showaiter, N., & Youseffi, M. (2008). Compaction, sintering and mechanical properties of elemental 6061 Al powder with and without sintering aids. *Materials and Design*, *29*(4), 752–762.

Shunmugasamy, V. C., & Mansoor, B. (2015). *Cellular Magnesium Matrix Foam Composites for Mechanical Damping Applications*. *October*.

Stöbener, K., & Rausch, G. (2009). Aluminium foam-polymer composites: Processing and characteristics. *Journal of Materials Science*, *44*(6), 1506–1511.

Sun, L., Wang, Y., Wang, L., Wang, F., Xu, H., Huang, W., & You, X. (2021). Preparation and properties of controllable aluminum foam. *Materials Research Express*, *8*(2).

Sun, Y., Zhang, C., He, L., Meng, Q., Liu, B. C., Gao, K., & Wu, J. (2018). Enhanced bending strength and thermal conductivity in diamond/Al composites with B4C coating. *Scientific Reports*, *8*(1), 1–12.

Surace, R., De Filippis, L. A. C., Ludovico, A. D., & Boghetich, G. (2009a). Influence of processing parameters on aluminium foam produced by space holder technique.

Materials and Design, *30*(6), 1878–1885.

Surace, R., De Filippis, L. A. C., Ludovico, A. D., & Boghetich, G. (2009b). Influence of processing parameters on aluminium foam produced by space holder technique. *Materials and Design*, *30*(6), 1878–1885.

Tan, P. P., Mohamad, H., & Anasyida, A. S. (2018). Properties of Porous Magnesium Using Polymethyl Methacrylate (PMMA) as a Space Holder. *Journal of Physics: Conference Series*, *1082*(1).

Tan, Z., Li, Z., Fan, G., Kai, X., Ji, G., Zhang, L., & Zhang, D. (2013). Diamond/aluminum composites processed by vacuum hot pressing: Microstructure characteristics and thermal properties. *Diamond and Related Materials*, *31*, 1–5. https://doi.org/10.1016/j.diamond.2012.10.008

Tatt, T. K., Muhamad, N., Muchtar, A., Sulong, A. B., & Cherng, N. M. (2016). Influence of sintering parameters on the compressive yield strength of stainless steel foams produced by the space holder method. *Sains Malaysiana*, *45*(4), 653–658.

Tatt, T. K., Muhamad, N., Muchtar, A., Sulong, A. B., & Shia, K. Y. (2021). Production of porous stainless steel using the space holder method. *Sains Malaysiana*, *50*(2), 507–514. https://doi.org/10.17576/jsm-2021-5002-21

Tjong, S. C. (2013). Recent progress in the development and properties of novel metal matrix nanocomposites reinforced with carbon nanotubes and graphene nanosheets. *Materials Science and Engineering R: Reports*, *74*(10), 281–350. https://doi.org/10.1016/j.mser.2013.08.001

Torres, Y., Rodríguez, J. A., Arias, S., Echeverry, M., Robledo, S., Amigo, V., & Pavón, J. J. (2012). Processing, characterization and biological testing of porous titanium obtained by space-holder technique. *Journal of Materials Science*, *47*(18), 6565–6576. https://doi.org/10.1007/s10853-012-6586-9

Vicario, I., Crespo, I., Plaza, L. M., Caballero, P., & Idoiaga, I. K. (2016). Aluminium foam and magnesium compound casting produced by high-pressure die casting. *Metals*, *6*(1). https://doi.org/10.3390/met6010024

Wang, J., Yang, X., Zhang, M., Li, J., Shi, C., Zhao, N., & Zou, T. (2015). A novel approach to obtain in-situ growth carbon nanotube reinforced aluminum foams with enhanced properties. *Materials Letters*, *161*, 763–766.

Wang, P., Liu, D. Y., & Xu, C. (2013). Numerical study of heat transfer enhancement in the receiver tube of direct steam generation with parabolic trough by inserting metal foams. *Applied Energy*, *102*, 449–460.

Wang, Z., Shen, J., Lu, G., & Zhao, L. (2011). Compressive behavior of closed-cell aluminum alloy foams at medium strain rates. *Materials Science and Engineering A*, *528*(6), 2326–2330.

Weissman, S. A., & Anderson, N. G. (2015). Design of Experiments (DoE) and Process Optimization. A Review of Recent Publications. *Organic Process Research and Development*, *19*(11), 1605–1633.

Wu, J., Zhang, H., Zhang, Y., Li, J., & Wang, X. (2012). Effect of copper content on the thermal conductivity and thermal expansion of Al-Cu/diamond composites. *Materials and Design*, *39*, 87–92.

Xia, X. C., Chen, X. W., Zhang, Z., Chen, X., Zhao, W. M., Liao, B., & Hur, B. (2013). Effects of porosity and pore size on the compressive properties of closed-cell Mg alloy foam. *Journal of Magnesium and Alloys*, *1*(4), 330–335.

Xun Li, Ying Liu, Jinwen Ye, X. A. R. (2018). Multifunctional foaming agent to prepare aluminum foam with enhanced mechanical properties. *Materials Research Express*, *29*(27), 1–11.

Yang, B., Yu, J. kang, & Chen, C. (2009). Microstructure and thermal expansion of Ti coated diamond/Al composites. *Transactions of Nonferrous Metals Society of China (English Edition)*, *19*(5), 1167–1173.

Yang, D., Hu, Z., Chen, W., Lu, J., Chen, J., Wang, H., Wang, L., Jiang, J., & Ma, A. (2016). Fabrication of Mg-Al alloy foam with close-cell structure by powder metallurgy approach and its mechanical properties. *Journal of Manufacturing Processes*, *22*, 290–296.

Yang, K., Yang, X., He, C., Liu, E., Shi, C., Ma, L., Li, Q., Li, J., & Zhao, N. (2017). Damping characteristics of Al matrix composite foams reinforced by in-situ grown carbon nanotubes. *Materials Letters*, *209*, 68–70.

Yang, X., Hu, Q., Du, J., Song, H., Zou, T., Sha, J., He, C., & Zhao, N. (2019). Compression fatigue properties of open-cell aluminum foams fabricated by space-holder method. *International Journal of Fatigue*, *121*(November 2018), 272–280.

Yang, X., Hu, Q., Li, W., Song, H., Zou, T., Zong, R., Sha, J., He, C., & Zhao, N. (2020). Compression-compression fatigue performance of aluminium matrix composite foams reinforced by carbon nanotubes. *Fatigue and Fracture of Engineering Materials and Structures*, *43*(4), 744–756.

Yang, X., Shi, C., He, C., Liu, E., Li, J., & Zhao, N. (2011). Synthesis of uniformly dispersed carbon nanotube reinforcement in Al powder for preparing reinforced Al composites. *Composites Part A: Applied Science and Manufacturing*, *42*(11), 1833–1839.

Yin, S., Xie, Y., Cizek, J., Ekoi, E. J., Hussain, T., Dowling, D. P., & Lupoi, R. (2017). Advanced diamond-reinforced metal matrix composites via cold spray: Properties and deposition mechanism. *Composites Part B: Engineering*, *113*, 44–54.

Yong Mei, Boyu Ju, Wenshu Yang, F. H. & G. W. (2021). Microstructure Evolution of B4C/Al Interface: A First-Principle Study. *Journal of Materials Engineering and Performance*, *30*, 9326–9332.

Yu, S., Luo, Y., & Liu, J. (2008). Effects of strain rate and SiC particle on the compressive property of SiCp/AlSi9Mg composite foams. *Materials Science and Engineering: A*, *487*(1), 394–399.

Yuan, W., Tang, Y., Yang, X., & Wan, Z. (2012). Porous metal materials for polymer electrolyte membrane fuel cells - A review. *Applied Energy*, *94*, 309–329.

Zhang, C., Cai, Z., Wang, R., Peng, C., & Feng, Y. (2017a). Enhancing densification capacity and properties of Al/diamond composites by partial liquid hot pressing. *Surface and Coatings Technology*, *313*(November), 347–354.

Zhang, C., Cai, Z., Wang, R., Peng, C., & Feng, Y. (2017b). Enhancing densification capacity and properties of Al/diamond composites by partial liquid hot pressing. *Surface and Coatings Technology*, *313*(November), 347–354.

Zhang, C., Cai, Z., Wang, R., Peng, C., Qiu, K., & Wang, N. (2016). Microstructure and thermal properties of Al/W-coated diamond composites prepared by powder metallurgy. *Materials and Design*, *95*, 39–47.

Zhang, Y., Wang, X., Jiang, S., & Wu, J. (2010). Thermo-physical properties of Ti-coated diamond/Al composites prepared by pressure infiltration. *Materials Science Forum*, *654–656*(June), 2572–2575.

PUBLICATIONS AND CONFERENCES

Journal Articles

1. **Parveez, B.,** Jamal, N. A., Maleque, A., Yusof, F., Jamadon, N. H., & Adzila, S. (2021). Review on advances in porous Al composite and the possible way forward. *Journal of Materials Research and Technology*, *14*, 2017-2038. **(ISI-Q1 Impact Factor-6.267)**
2. **Parveez, B.,** Jamal, N. A., Anuar, H., Ahmad, Y., Aabid, A., & Baig, M. (2022). Microstructure and mechanical properties of metal foams fabricated via melt foaming and powder metallurgy technique: A review. *Materials*, *15*(15), 5302. **(ISI-Q1 Impact Factor-3.601)**
3. **Parveez, B.,** Jamal, N. A., Aabid, A., Baig, M., & Yusof, F. (2023). Experimental analysis and parametric optimization on compressive properties of diamond-reinforced porous al composite. *Materials*, *16*(1), 91. **(ISI-Q1 Impact Factor-3.601)**
4. **Parveez, B.,** Jamal, N. A., Maleque, M. A., Rozhan, A. N., Aabid, A., & Baig, M. (2023). Optimizing the compressive properties of porous aluminum composite by varying diamond content, space holder size and content. *Materials*, *16*(3), 921. **(ISI-Q1 Impact Factor-3.601)**
5. **Parveez, B.,** Jamal, N., Azhar. A. Z. A., Zaki, H.H.H., Aabid, A., Baig, M., & Maleque, M.A., (2023). Improvement in effectiveness of diamond in strengthening the porous Aluminium composite. *Journal of Materials Research and Technology*. **(ISI-Q1 Impact Factor-6.267)**
6. **Parveez, B.,** Jamal, N. A., Muhammad, R., (2023). Effect of uncoated and coated diamond on the compressive properties of porous aluminium

composite. *Material Science and Engineering Technology*. **(ISI-Q3 Impact Factor-1.034)**

7. **Parveez, B.,** Jamal, N. A., Aabid, A., & Baig, M., & Maleque, M.A., (2023). Microstructure and strengthening effect of coated diamond particles on the porous aluminium composite**.** *Materials*. **(ISI-Q1 Impact Factor-3.601)**

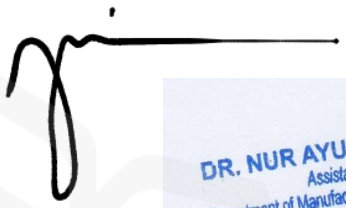

ARTICLES IN PEER-REVIEWED CONFERENCES

1. **Parveez, B.,** Jamal, N. A., Zaki, H.H.H., Azhar. A. Z. A. (2022). Microstructure and mechanical properties of porous aluminium composite reinforced with diamond particles. Presented at the *International Conference on Advances in Manufacturing and Materials Engineering, (ICAMME).* Held at International Islamic University Malaysia, Kuala Lumpur, Malaysia. 9th-10th August, Paper ID: 11 **(Scopus indexed)**
2. **Parveez, B.,** Jamal, N. A., Muhammad, R. (2022). Investigation of morphology and compressive properties of diamond reinforced porous aluminium composite. Presented at the *3rd International Multidisciplinary Conference on Education, Engineering and Social Sciences, (IMCEES).* Held virtually at Kuala Lumpur, Malaysia. 19th November Paper ID: IMCEES2022: 020-015. **(Scopus indexed)**
3. **Parveez, B.,** Jamal, N. A., Muhammad, R. (2022). Compressive properties of coated diamond reinforced porous aluminium composite. Presented at the *The 8th International Conference on Mechanical, Manufacturing and Plant Engineering, (ICMMPE).* Held at Berjaya Times Square, Kuala Lumpur, Malaysia. 24th November, Paper ID: mmp22489. **(Scopus indexed)**

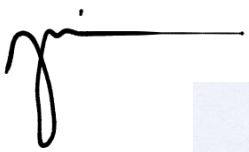

DR. NUR AYUNI BINTI JAMAL
Assistant Professor
Department of Manufacturing & Materials Engineering
Kulliyyah of Engineering
International Islamic University Malaysia

ACHIEVEMENT AND AWARDS

1. Presently serving as a President in “Postgraduate Student Association (PGSA 2022-2023), Kulliyyah of Engineering, International Islamic University Malaysia, Kuala Lumpur, Malaysia.
2. Received “Bronze medal” in Kulliyyah of Engineering Research, Innovation and Commercialization Exhibition (KERICE) 2022, held at KAED and organized by Kulliyyah of Engineering, International Islamic University Malaysia, Kuala Lumpur, Malaysia.
3. Received “IIUM Sejahtera award” for Semester 2 (2021-2022) and Semester 1 (2022-2023), Centre for Postgraduate Studies, International Islamic University Malaysia, Kuala Lumpur, Malaysia.
4. Presented and received certification of appreciation in a research video competition 2022 for title “Porous Aluminium Composite: Fabrication and Analysis”, organized by Kulliyyah of Engineering, International Islamic University Malaysia, Kuala Lumpur, Malaysia.
5. Received best 3MT presentation award for the title “Strengthening of porous Aluminium Foam Composite” 3MT 2022, International Islamic University Malaysia, Kuala Lumpur, Malaysia.
6. Presented and received certification of appreciation for being a Vice-President in “Postgraduate Student Association (PGSA 2020-2021), Kulliyyah of Engineering, International Islamic University Malaysia, Kuala Lumpur, Malaysia.